DISSERTATION

INVESTIGATIONS TO IMPROVE CDTE-BASED SOLAR CELL OPEN CIRCUIT VOLTAGE AND EFFICIENCY USING A PASSIVATION AND SELECTIVITY THEORETICAL FRAMEWORK

Submitted by

Carey Reich

Department of Mechanical Engineering

In partial fulfillment of the requirements

For the degree of Doctor of Philosophy

Colorado State University

Fort Collins, Colorado

Fall 2022

Doctoral Committee:

Advisor: Walajabad S. Sampath

James R. Sites
Darius Kuciauskas
Zachary C. Holman

ABSTRACT

INVESTIGATIONS TO IMPROVE IN CDTE-BASED SOLAR CELL OPEN CIRCUIT VOLTAGE AND EFFICIENCY USING A PASSIVATION AND SELECTIVITY THEORETICAL FRAMEWORK

The voltage of CdTe-based solar cells has remained conspicuously low despite years of efforts focused directly on its improvement. The efforts here have been primarily in increasing the equilibrium carrier concentration of the CdTe or its alloys which are used to absorb the light. This direction has been guided by a theory of solar cells that views the cell only as a single p/n junction. The modelling which has been used to confirm this as an appropriate direction indicated that with a moderate carrier lifetime, relatively small front interface recombination velocity, and large equilibrium carrier concentration in the absorber, efficiencies greater than the current record of 22.1% will be possible with open circuit voltages reaching over 1V. However, cells with these properties have been measured and increases in Voc and efficiency have not been attained.

In the c-Si community, notably, the “passivation – selectivity” framework has been developed. In particular, it rejects the view that a singular p/n junction is responsible for the function of a solar cell. Instead, this framework operates with the understanding that the potential in the cell which can be turned into useful electrical energy and an increase in open circuit voltage comes only from the excess carriers generated by sunlight forcing a deviation from the equilibrium condition. As such there are two main components: 1) passivation – which refers to the recombination behavior in the cell and development of a large internal potential difference and 2) selectivity – which refers to the asymmetry of conduction in the cell that allows for production of

a unidirectional current and an external voltage approaching that within the cell. This framework tends to break the cell into 3, sometimes overlapping, regions: an absorber region that is used to produce as large a potential difference as possible, and two contact regions in which the transport properties are modified to prefer transport of one carrier or the other. Here this framework is applied to CdTe-based solar cells to determine what limits current cells and how to overcome these limitations.

In the investigation of passivation, first the electron contact interface is evaluated, resulting in the determination that this interface is not currently limiting the recombination in the cell. As a result, the current baseline is compared to structures hypothesized to provide improvement in the recombination behavior. It is found that cells with CdSeTe as the only material in the bulk exhibit more ideal recombination behavior when compared to a CdSeTe/CdTe structure as is currently used. This comparison demonstrates a pathway for cells to overcome their current limitation due to recombination, with the possibility of reaching up to 25% efficiency and 970 mV Voc with the material that currently is produced at CSU. A native oxide of TeOx is found to passivate the surface, reducing the rate non-radiative recombination, and forms during dry air exposure, providing a pathway to passivate contacts that would be ideal if not for the recombination at the interface.

In the investigation related to selectivity, the electron contact is evaluated and it is demonstrated that MgZnO is appropriately selective when deposited with the correct conditions. It therefore is expected that hole selectivity is the primary loss to open circuit voltage in structures determined to have longer excess carrier lifetimes and large radiative efficiencies. Efforts to investigate novel routes to hole selectivity by use of heterojunction contacts are presented. Such routes did not yield improvements in cell Voc and efficiency, and through this work it was determined that

a major source of selectivity losses in these cells is the high resistance to hole transport through the bulk semiconductor. Increasing hole concentration or thinning the absorber provide pathways to overcome this specific limitation, but it is modelled that such cells will require structures with hole selective materials that internally cause a reduction of electron current to see improvement in V_{oc} and efficiency.

ACKNOWLEDGEMENTS

I would first like to thank Dr. Sampath for allowing me to pursue research in his laboratory starting very early in my undergraduate studies and continuing through all of my degrees. Without his generosity, guidance, and discussions this would not have been possible. Next, I would like to thank Dr. Holman and Dr. Onno for effectively allowing me to be a part of their group as well despite there being no direct need. It has been their guidance through this theoretical framework which has led directly and indirectly to the understanding of solar cells I have today. Dr. Sites has also been essential in my studies, providing alternative viewpoints to consider during my learning process as well as allowing use of his laboratory for numerous essential measurements in the research. Additionally, Dr. Kuciauskas has provided many hours of discussion and training on carrier dynamics and measurements thereof, as well as introducing me to more complex optical topics essential to these measurements. I would also like to thank Dr. Swanson for his role in my education, as my first mentor in the lab and the person most directly responsible for pulling me into research when I was doing basic cell finishing and other mundane tasks as an undergraduate job. Without his efforts and willingness to discuss complex topics ranging from basic solar cell function to the syntax in the constitution, I certainly never would have had the opportunities that I have since then. I would also like to thank my colleague Adam Danielson for being my partner in the lab, insisting on using best practices in the research, and being willing to keep an open mind to and engage in discussions about the theoretical framework we were learning simultaneously. Dr. Drayton has also played an essential role in my education, teaching me fundamentals in both processing and measurement of our cells. She, along with Drew, were the first to support my research efforts. I would also like to thank my

colleagues at NREL and CSM for their collaborative efforts which have resulted in some of the most interesting results related to the MgZnO contact. Finally, I would like to thank all of the members of the Sampath, Sites, and Holman labs not yet mentioned. The lab ecosystem is not complete without everyone who has put in efforts to keep everything running, engaged in discussion, deposited layers, and further provided numerous learning opportunities for me.

This material is based upon work supported by the U.S. Department of Energy's Office of Energy Efficiency and Renewable Energy (EERE) under the Solar Energy Technologies Office Award Number DE-EE0008552 and DEEE0008557. This work is partly funded by National Science Foundation I/UCRC (Award Number – 1540007 and 1821526). The author would like to thank the NSF I/UCRC Industrial Advisory Board for their guidance and support. Some of the deposition materials used in this work were provided by 5N Plus Inc. as in-kind support.

TABLE OF CONTENTS

LIST OF FIGURES

CHAPTER 1: INTRODUCTION

1.1) Climate Change

Following their accelerating development of novel technologies which gave them competitive advantages in nearly every naturally environment on earth, the homo sapiens has proliferated and spread across the planet. This explosion of technology and the subsequent use by an ever increasing population required and continues to require the conversion of vast amounts of energy in to useful work. While initially, machines predating this period used relatively renewable sources – for example, the conversion of gravitational potential energy to kinetic energy from the flow of water in a stream – this was not sufficient. To meet the needs of the population, an energy source with higher energy density and the ability to be used irrespective of location on earth was required. This came in the form of first coal, then oil and later natural gas, extracted from reserves in the ground. Release of some energy in the chemical bonds of these substances through combustion allowed humans to put that energy to use through the evaporation and expansion of hot water vapor. Effectively, this process converted chemical energy to thermal energy, then from thermal energy to so-called "PV work" where the change in pressure and volume of a substance with temperature is harnessed to accomplish a physical task the humans desired [1]. This boom started in the late 1800s and has continued to this day. Humans have benefitted in the short term, with the quality of life increasing dramatically around the world as the technologies that use this work or have been enabled by its use spreads to ever more centers of population. However, this great easing of the human condition was accompanied by a hidden but insidious problem, the release of carbon-based molecules into the atmosphere at a growing rate. After a period of relative stability lasting the last 9,000 years or so, humans have instigated

dramatic changes in climate which are occurring and will continue to occur in a very short period of geologic time.

At the simplest point of view, a heat balance can be created for the earth as a system. The system itself would be the earth and its atmosphere. To make the analysis easier, the transfer of heat into and out of the bounds of the system by conduction and convection are negligible as the environment that surrounds earth's atmosphere is a near perfect natural vacuum. This leaves only heat transfer by radiation through the boundaries in our energy balance. Although there is work being done within the system (rotation of the planet, etc.) this is relatively constant and thus will have little to no effect on the transient heating and cooling. Similarly, the sun's irradiance is quite constant on biological time spans, with dramatic changes taking billions of years. In fact, the variation in the solar output over the last 150 years has only accounted for 0.1 °C, while the average warming reached 1 °C in 2017 [2,3]. Thus, the energy input and generation (energetic "sources") sum to a nominally constant value, dominated by energy from the solar radiation.

The constant impinging energy from solar radiation is that which the vast majority of life on earth uses to sustain itself in some form [4]. In addition to providing the energy for the vast majority of known life of this planet, the energy from the sun keeps the planet habitable, keeping the temperature of the planet above a critical low point, that of the freezing point of water, which marks the lower bound of the "goldilocks zone" of habitability [5]. However, the heating of the surface is reversed by the thermal radiation of the earth itself into space [6].

Earth, currently, radiates analogous to a ~300K black body emitter, producing the thermal radiation in near accordance with the law described by Planck in 1901 [7]. However, some of this radiation is absorbed before reaching and passing through the boundary of the system. This is due to absorption from the atmosphere, preventing that energy in the thermal photons from

leaving the system. Earth's atmosphere is composed of primarily N_2, CO_2, and O_2. As it turns out, the CO_2 is the primary driver for reduction of this radiative cooling mechanism, as it is a near perfect match for the peak emission from the earth's thermal emission as seen in figure 1 [6].

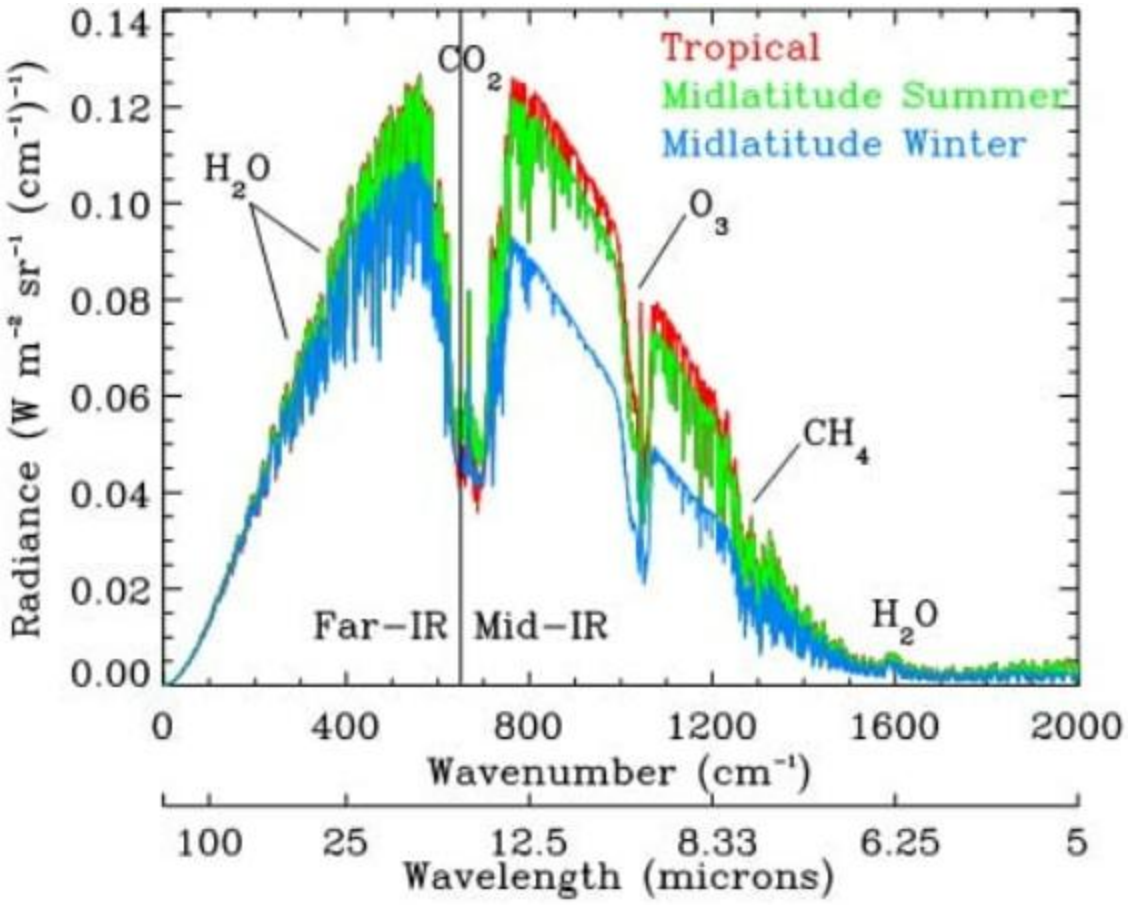

Figure 1: Modelled IR emission from the earth as would be detected from low earth orbit. Retrieved from IEEE Earthzine [6].

Unlike the "sources" of energy in the system we are analyzing, the concentration of CO_2 fluctuates over time in the atmosphere, leading to the variation of the energetic "sink" as seen in figure 2. Historically, these fluctuations occurred over long periods of geologic time due to naturally occurring processes [9]. If the analysis is correct, the global temperatures will have

varied with the CO_2 concentration through time. In fact, this is very apparent in the collected data, as seen in figure 2.

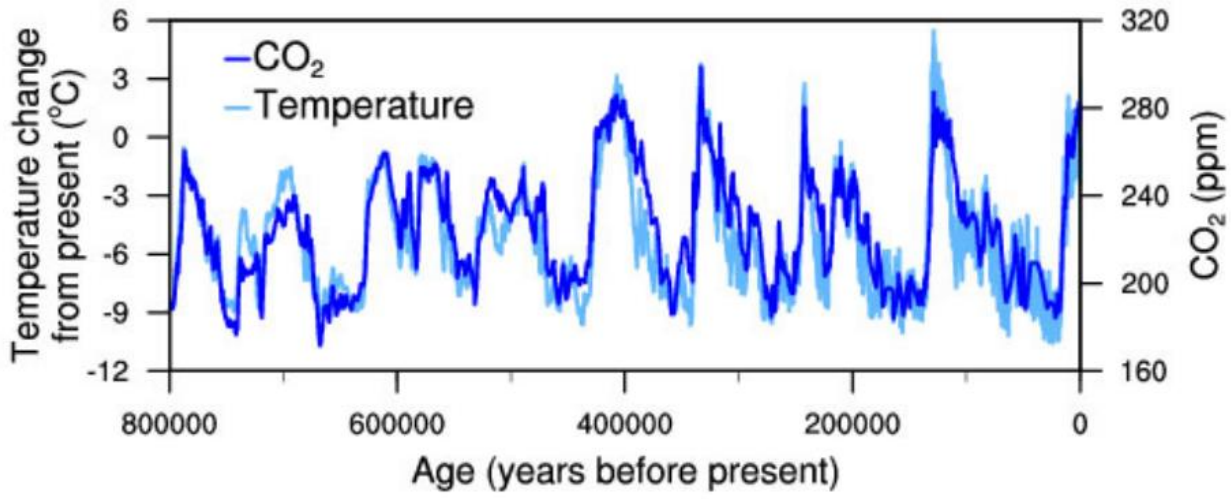

Figure 2: Historic CO_2 concentrations and global temperatures showing a clear dependance, retrieved from NOAA [8]

This relationship between Carbon in the atmosphere and global temperature being well understood let's return to humans and their use of fossil fuels. As previously noted, the manner in which they have harnessed the stored energy of fossil fuels is through combustion. The idealized combustion reaction between these fossil fuel molecules, consisting of carbon and hydrogen, and oxygen gas, results in CO_2 and H_2O. Burning large numbers of these fossil fuel molecules generally results in the release of an even larger number of CO_2 molecules. This is easily demonstrated by balancing the chemical reaction for the combustion of octane, the primary component of gasoline used to fuel many vehicles, as an example in equation 1. It is clear here that combustion of two molecules of octane produces sixteen molecules of CO_2. In equation 2 we also balance the combustion reaction with methane for demonstration of the only hydrocarbon combustion reaction that produces an equal number of CO_2 molecules as the

number of input molecules containing carbon. It is clear that combustion of carbon containing molecules releases CO_2 in vast quantities.

$$25O_2 + 2C_8H_{18} \leftrightarrow 18H_2O + 16CO_2 \qquad (1)$$

$$4O_2 + CH_4 \leftrightarrow 2H_2O + CO_2 \qquad (2)$$

In this manner, humans have released CO_2 into the atmosphere at an alarming rate, and it is demonstrated in figure 3 that this recent release of CO_2 has indeed been significant enough to dramatically increase the concentration in the atmosphere. In fact, CO_2 in the past 150 years has increased from fluctuating around 225 PPM, with the 100 PPM difference between the maximum and minimum being large enough be correlated with fluctuations in global temperature of about 15 degrees Celsius over the last 800,000 years, to greater than 400 PPM as shown in figure 3C [8]. Such a large increase in such a short span is bound to increase the temperature of earth quite quickly relative to any previous changes following the historical correlation, the simple heat balance, and is supported by numerous models [9]. It should be noted here that while this increase in global average temperature will be quick relative to the previous fluctuations, it will be slow to see the full effect on the scale of a human life due to the incredibly large thermal mass in the system of the earth. This however, does not make it less dire, or immediate of a problem to solve. It is clear in figure 3b that the current increase in CO_2 is already producing some increase in global average temperature, with a clear relationship between the two in the current data. While the full extent of negative impacts this will have on the earth's meta-ecosystem are unknown, it is clear that the changes which have already begun will be dramatic and tragic [13].

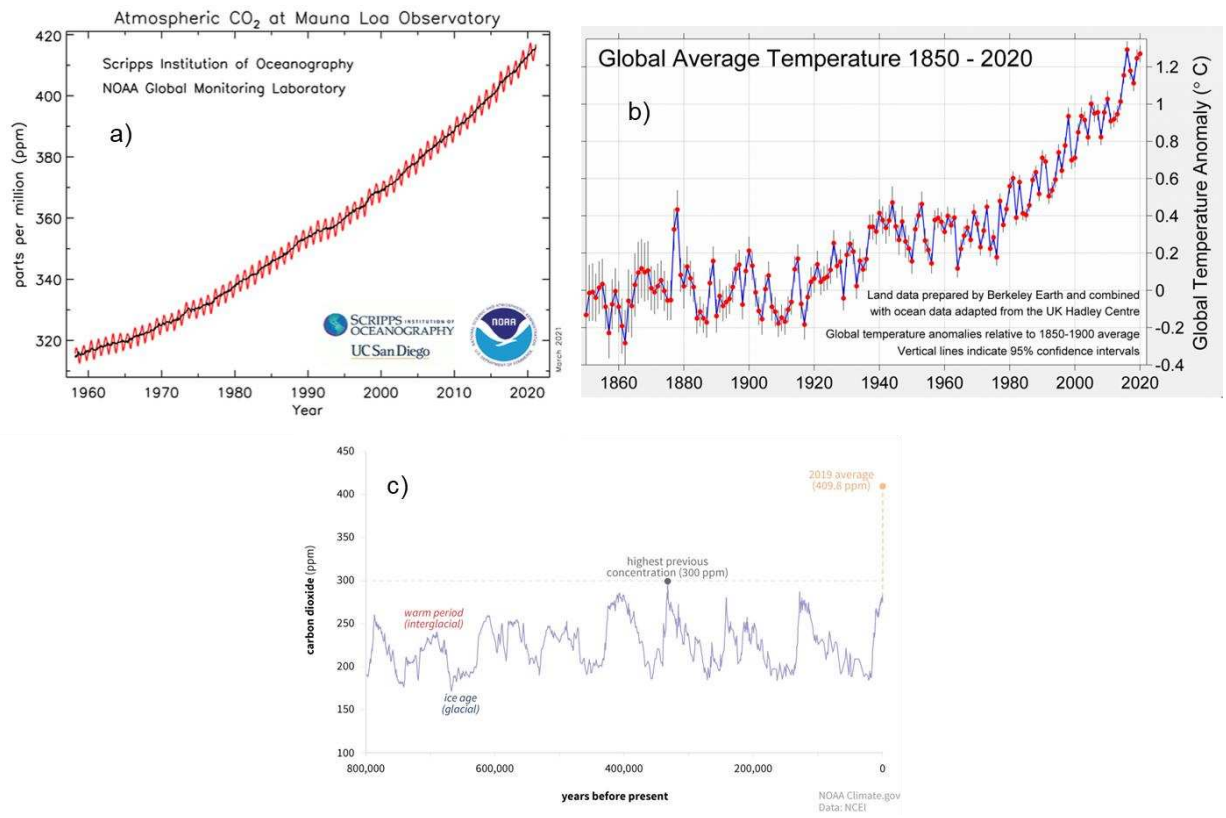

Figure 3: a) Global CO_2 concentrations since the start of the industrial revolution Retrieved from [11]. b) Global average temperature anomaly. Retrieved from [12] c) Atmospheric CO_2 over the past 800,000 years showing relative stability abruptly interrupted in recent years [10].

Aside from large-scale ecosystem alterations, acute climatic changes will inevitably impact humanity. Larger and more deadly natural disasters will be prevalent and are already being manifested in more severe fire seasons around the globe and longer and more severe tropical storm and cyclone seasons, costing billions or trillions of USD [13]. Sea level rise from land-bound ice melting into the oceans will put cities under water, forcing mass migration of billions of people, with the possible loss of annual arctic ice formation [13]. Droughts and heat waves are already becoming more common and can possibly lead to dramatic famines and other adverse effects [13]. These are among many possibilities, each sounding more catastrophic than the last.

It is clear that humanity needs to become less dependent on the combustion of fossil fuels for their energy needs to prevent further worsening of these impacts [9].

1.2) Paths away from increasing climate catastrophe

There is one additional legacy that fossil fuels leave which is positive: the advancement of science through technology. This advancement has allowed us to find new ways of harnessing energy gradients to produce useful work which do not involve combustion of fossilized hydrocarbons. Some of these methods are the oldest methods of harnessing energy from seemingly unending sources, but modernized to produce vast amounts of useful energy, such as hydro and wind energy. Others are brand new to human utilization like nuclear, albeit with its own set of concerns. However, if appropriately harnessed, some combination of their use would allow for humanity to continue their current use of energy for their benefit without continued emission of CO_2 into the atmosphere.

Estimation of how much energy is available through non-fossil conversion methods and comparison to the reserves of fossilized energy as well as the current consumption of energy by humans has been carried out with clear results, found in figure 4 [14]. Solar energy impinging on the earth in the form of radiation is by far the most plentiful, and in fact, it is the origin of the second most plentiful renewable energy resource: wind [14, 15]. This puts an immediate cap on how much energy is available in the wind. At the level that wind energy is extractable to humans, it is driven by variations in surface temperature, and while a large amount of total energy is available in the wind, it represents a small portion of the energy in the heat from the sun that drives it as it goes through multiple changes in form before it drives the movement of the wind [15].

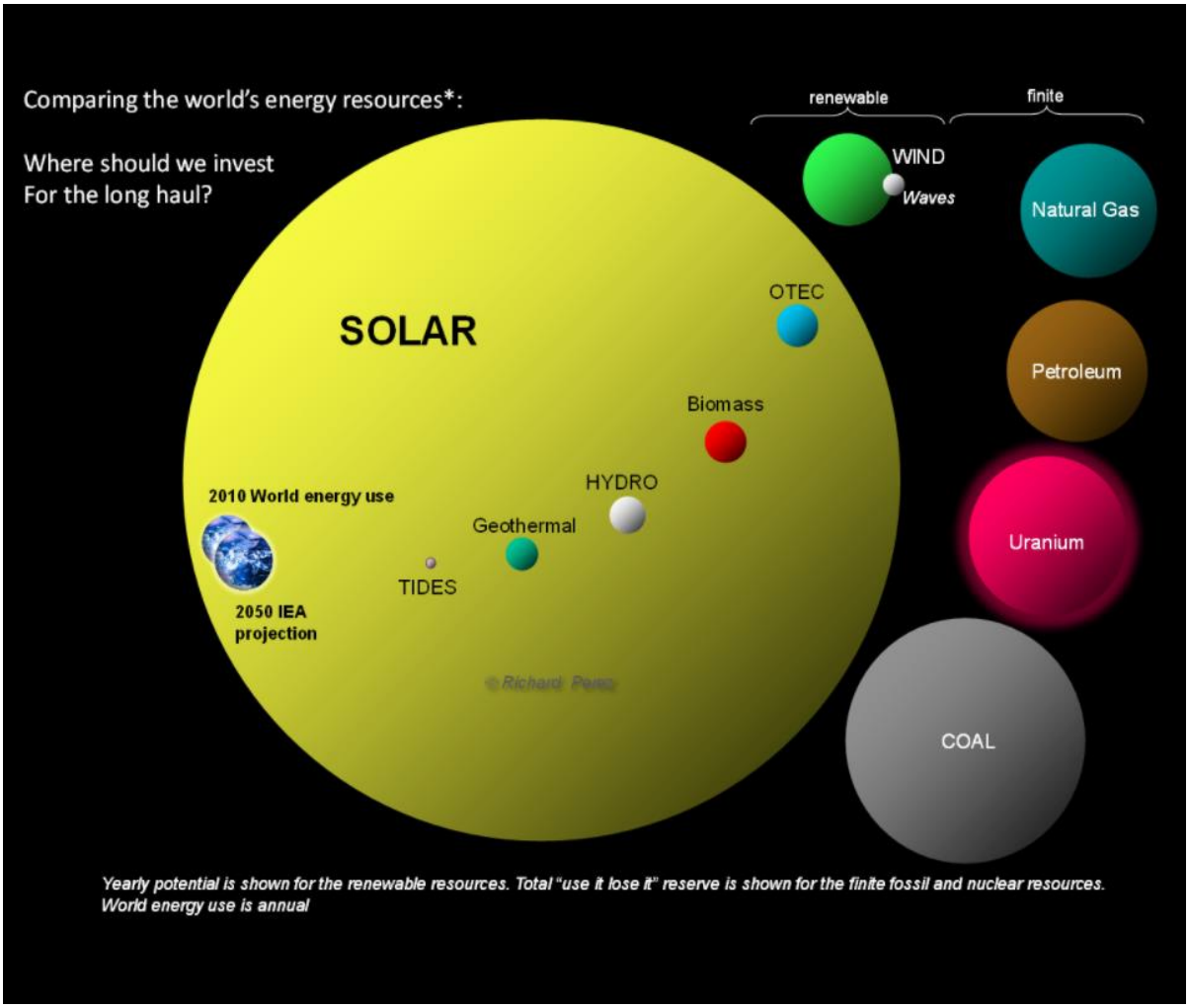

Figure 4: Energy resources on earth, represented by size of the corresponding circle. Renewables show annual availability and non-renewables show total known reserve. Retrieved from SUNY Albany Prof. Richard Perez [14]

In addition to the wind there is hydraulic energy extraction. This is directly driven by the conversion of gravitational potential energy being converted to kinetic energy, then to electrical energy. However, this too is driven by the sun, as the most common method is putting turbines inside dams on rivers fueled by rain and snowfall at higher elevations [16]. As such, the creation of gravitational potential energy is initiated by the evaporation of water due primarily to solar heat. There are two issues with this non-fossil source of energy for humans: 1) the most ideal

places to implement such energy extraction are already in use and as such, most additional production in this manner would be retrofitting current irrigation dams and 2) the practice of damming rivers to implement the turbines has been shown to cause excessive and yet to be fully understood ecological harm [17, 18]. Yet other hydro-energy like tidal extraction leverages the gravitational potential energy from the moon or energy within waves driven by wind. This energy is difficult to extract, and especially that from the waves, is a relatively small portion of available energy for human conversion as seen in figure 4.

Something common about all of the conversion techniques discussed thus far is their intermittent availability. The sun only shines during the day and can be shielded from the ground by cloud cover, the wind does not always blow (impacting wave energy extraction as well), and tidal energy can only be extracted between high and low tides. Often, nuclear energy is cited as a solution to this problem. Harnessing the energy of an atom does seem like a great solution, as the energy density is greater than any other source. However, humans also consume an extremely large amount of energy, for example the US used 3.8 trillion kWh in 2020 by electricity alone [19]. As is commonly known, the waste from nuclear powerplants is radioactive, which can pose harm to any living thing exposed to it. While 90% of the waste is low level, and generally safe to be around for short durations, the high level waste is extremely dangerous, typically the remains of the fuel rods used to produce electricity [120]. Using a reasonable estimate for the amount of waste from a fuel rod per electrical energy produced, producing all of the electricity the US used in 2020 would generate $6x10^5$ kg of highly radioactive waste (about 30 cubic meters) [21]. While this is not a huge amount, it remains dangerous for an exceptionally long time, up to a thousand years to decay to the levels of radiation of the original ore and would pile up quickly requiring vast amount of long term storage if this is to be viable [20]. Additionally, while the uranium

resource for energy production is relatively large compared with other non-renewable energy sources as seen in figure 4, it is clearly a finite source with total availability dwarfed by the annual solar resource, and fast advancement of energy storage technologies enables intermittent sources which produce excess energy the ability to provide uninterrupted power.

Solar energy is the most plentiful resource on earth and drives most other sources of energy extraction. The energy contained in fossil fuels is, in fact, solar energy stored by ancient organisms [22]. Although solar energy is only available to a location when the sun is illuminating it, the amount of energy incident on that area is incredibly large, approximated around $1kW/m^2$ although the actual power density depends on a number of factors such as season, latitude, and elevation [23].

In addition to the abundance and origination of most useful energy on earth, the sun is a consistent source of energy. It has been stable for the past 4.5 billion years, and will only run out of hydrogen fuel in an estimated 6.5 billion years [24, 25]. While it is possible our descendants will still be alive, the earth is expected to become inhospitable to life when the solar luminosity increases 10% in about 1.1 billion years [25]. Thus, the entire period of earth's residence in the habitable zone of the solar system will have the sun as a constant source of power, demonstrating its long term viability. Solar energy is typically converted to electrical energy through two means: solar thermal and solar photovoltaic (PV). Solar thermal production uses radiation from the sun to heat a substance for direct use or to drive a turbine, similar to how fossil fuels are used. Advances in solar thermal power come in geometry and design of concentrators and working fluids. Solar PV on the other hand converts light energy directly to electrical energy, and will be the focus of the remainder of this document.

CHAPTER 2: SOLAR PHOTOVOLTAICS

2.1) Energy from the Sun

PV is intended to convert energy in the form of radiation to useful energy for human use in the form of electricity, so it is appropriate to start with the energy contained within sunlight. At its most basic level, the sun is a thermal emitter of radiation, and as such it follows the Planck law of thermal emission found in equation 3 where $\Phi_{BB}(\lambda)$ is the photon flux emitted at a given wavelength, λ is the wavelength of light (inversely related to the energy contained by a single photon), c is the speed of light in a vacuum, h is the Planck constant, k_B is the Boltzmann constant, and T is the temperature in K [7]. Examples of this are plotted in figure 5. It is a good approximation of the spectrum to eliminate the "-1" grouped with the exponent at low temperatures or large photon energies when the exponent is much greater than 1. This approximation is generally considered valid when $hc/\lambda > 3k_bT$.

$$\Phi_{BB}(\lambda) = \frac{2\pi c}{\lambda^4 \left[\exp\left(\frac{hc}{\lambda k_B T}\right) - 1\right]} \qquad (3)$$

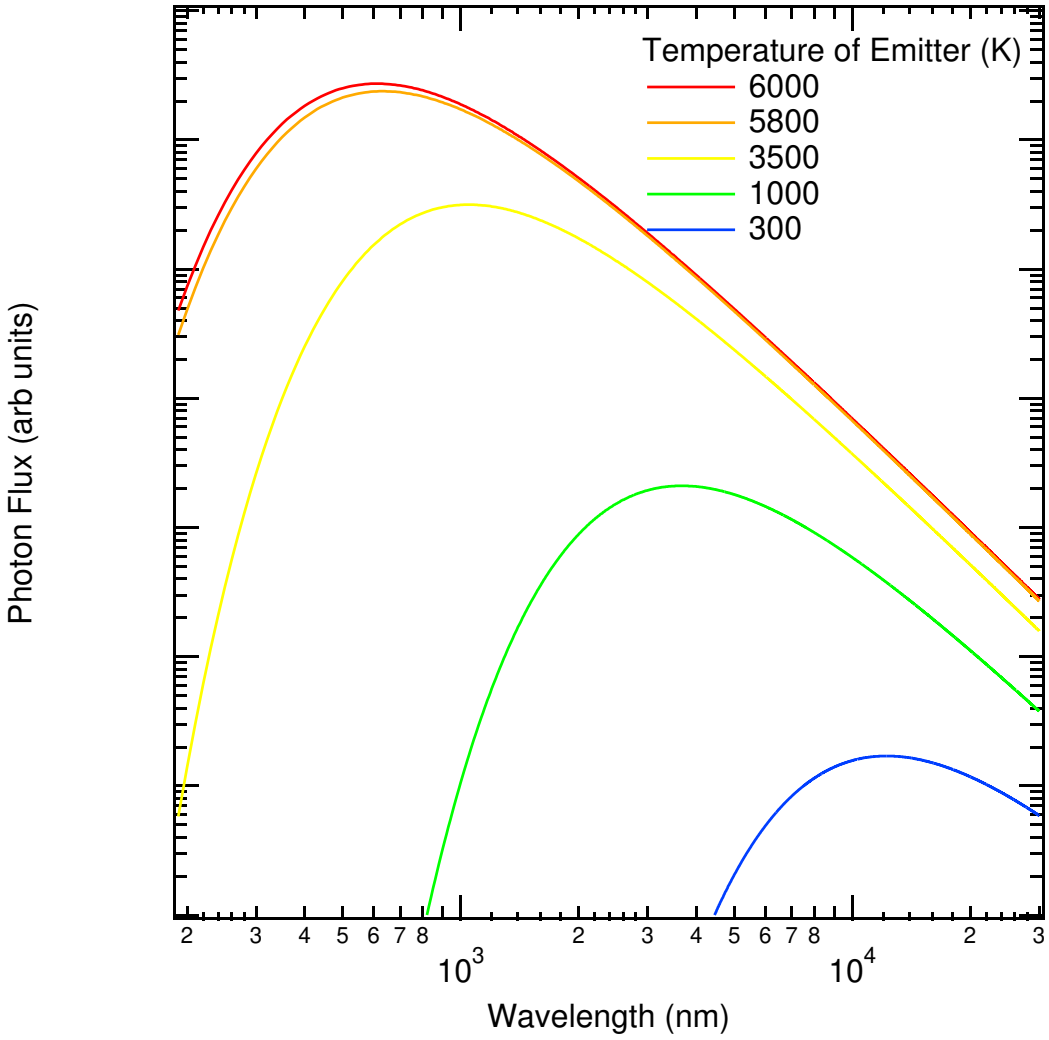

Figure 5: Black Body Spectra for emitters at various temperatures showing relative intensity and peak location

As the thermal spectrum is defined, it shows greater number of light particles, or photons, and a shift in the peak emission of those photons toward shorter wavelengths the hotter the emitter is. In fact, the sun is roughly a 5800-6000K emitter, which has a peak photon emission between 500-600 nm [26, 27]. It is by this mechanism that our sun provides a significant energetic flux in the form of the thermal photons – a photon's energy is related to its wavelength by hc/λ showing

photons with shorter wavelength at higher energy, and with the peak squarely in the visible there is a large flux of high energy photons.

The actual solar spectrum as it arrives at the earth is somewhat altered, as atoms and compounds in the solar atmosphere, namely hydrogen and helium, are strongly absorbing in the UV and thus cause a reduction of the shortest wavelength photons emitted, well before they enter the vacuum between the sun and the earth [27]. Additionally, the sun is emitting this flux of energy spherically in all directions, and as such most of the photons are not directed toward the earth. This leads to a much diminished flux of energy at the earth's atmosphere relative to the total energy emitted from the sun by radiation, although still quite large at ~1300 W/m^2 [26, 27].

Finally, for terrestrial applications, the light energy that reaches the ground is again partially diminished by the same mechanism as the UV loss at the sun: absorption of energy from the atmosphere, although the difference in the atmospheric composition causes many bands of absorption at different wavelengths rather than a small band near the shortest wavelengths. The greatest contributors to earth's atmospheric absorption are H_2O and CO_2 in the infrared wavelengths and Ozone in the UV, with smaller but non-negligible contributions from other species such as methane and nitrous oxides [29]. Despite all of this, a significant amount of solar energy in the form of light still reaches the ground. The total energy hitting the ground at any instant is dependent on the path length of the photons through the atmosphere as the longer atmospheric path length, the more interactions with absorbing chemicals and the greater the absorption probability [26, 27, 29, 30]. A standard in solar cell testing corresponds to a path length of 1.5 times the smallest thickness of the atmosphere (AM1.5) which corresponds to the condition of 40 degrees north or south, solar noon on the equinoxes, and at sea level [26, 27, 29, 30]. The corresponding incident power from the sun is 1 kW/m^2, now in power units because the

energy is supplied continuously under illumination, losing about 300 W through atmospheric absorption [26, 27, 29, 30]. This incident power spectrum – showing losses progressively – is displayed in terms of incident photon flux as resolved by both wavelength in figure 6, where the difference between AM0 and AM1.5G (red and black) demonstrates the loss of incident photons to atmospheric absorption.

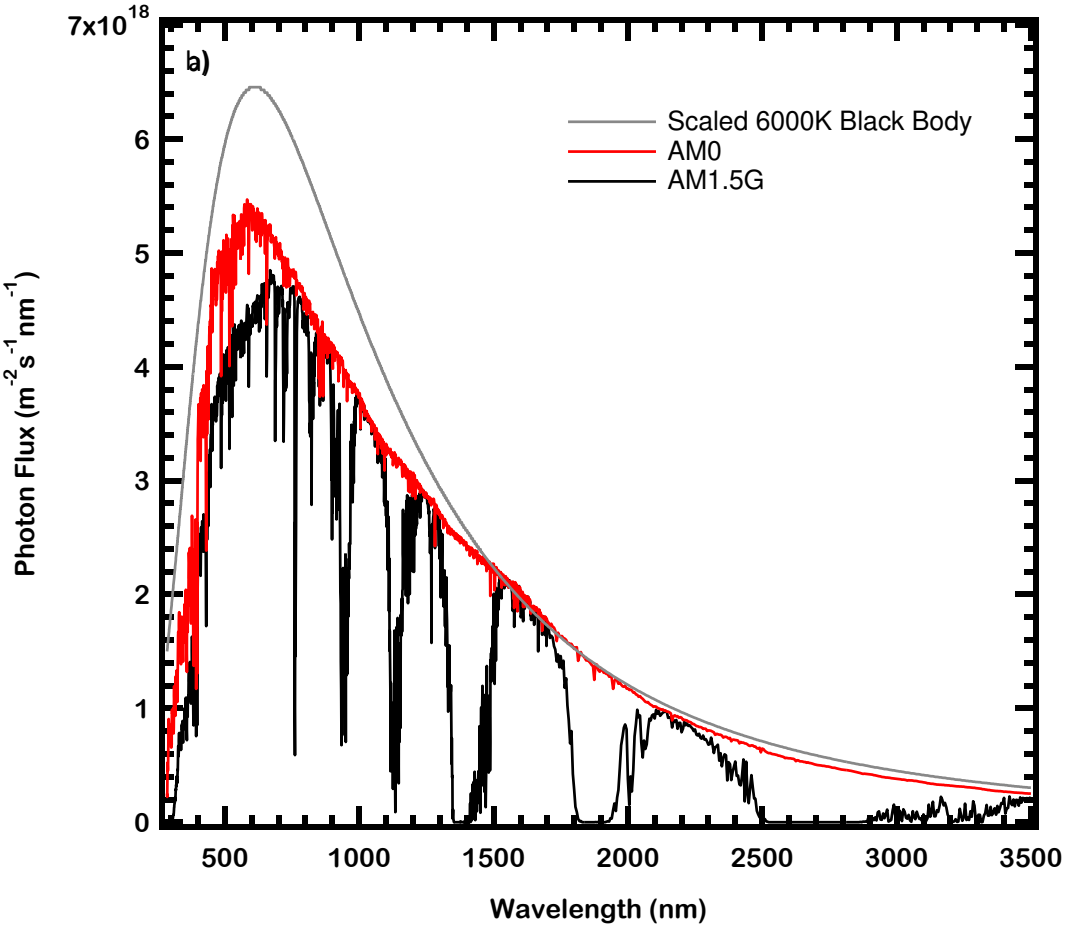

Figure 6: Comparisons of the Solar Spectra from space and under AM1.5G to the 6000K black body spectrum [27]

Solar PV is then designed to convert this power into electrical power. As any basic electronics and circuitry class will teach you, the very simple relation of P = IV where P is electrical power, I is current, and V is the voltage is governing. As such, the requirement of PV is to directly

convert the power impinging on the cell in the form of light into an electrical current and voltage for the power to be useful to humans. In order for this to happen, the energy of photons needs to be donated directly to carriers of electrical charge in the cell, and further, the donation of that energy needs to be in a manner that allows for the carriers to leave the absorber and traverse a photo-induced potential through an external circuit.

2.2) Design of a Solar Cell

2.2.1) Light Absorber

The first important aspect of the solar cell is the absorber. The required property here is that the donation of energy from a photon generates a pair of charge carriers – one positive (called a hole) and an electron, energetically separated within the material [26, 27, 31]. There are many materials which can accomplish this, but the most common material used, and that in this document, are traditional semiconductors [26, 27, 31, 32].

Semiconductors are quite unique in their match for absorbing the solar spectrum in a manner that is optimal to best harness the impinging energy, arising from a property called a bandgap. In basic chemistry, we are taught that electrons exist about a central nucleus in distinct “orbitals” corresponding to some distinct set of quanta, with the most important here being energy [33]. This is certainly true of a single stand-alone atom. However, atoms rarely stand alone, and because of this, atoms interact in ways that cause the behavior of electrons to deviate from the idealized single atom case [27].

When atoms are in proximity their outermost orbitals start to interact, and many electrons would like to exist at the same quantum state. However, the Pauli exclusion principle forbids this, leading to an energetic rearrangement of the electrons in the orbitals, slightly altering the energy

at which electrons exist [27]. Semiconductors are crystals and as such they are solids with ~10^{22}-10^{23} atoms per cubic centimeter [34, 35, 36, 37]. This large density of atoms leads to some equilibrium of atomic arrangement and spacing, forming a continuum-like band of allowed states as the orbitals interact [27]. This band of energy states corresponding to the outer, and typically filled, orbital is known as the valence band [27]. In addition to the valence band, a band of allowed states at higher energy, currently unfilled, known as the conduction band. The band forms at some distinct energy greater than the valence band, with ideally no states that electrons can occupy between the two energy levels [26, 27]. This gap in allowed states is called the bandgap and is the property of semiconductors that is finely tuned to the solar spectrum. This is all demonstrated in figure 7 for Si, with the single orbital energies on the far right of the diagram and the formation of bands moving left, forming the equilibrium bandgap at the lattice spacing a_0 for that condition.

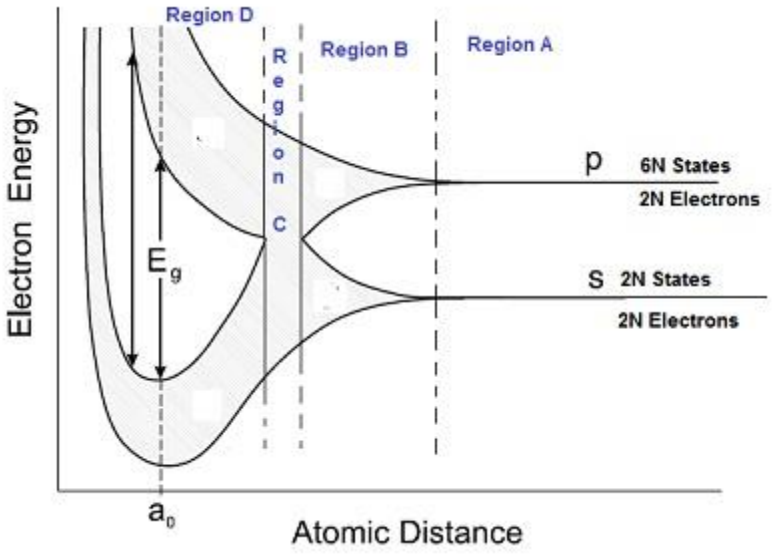

Figure 7: Structure of the Valence and Conduction bands based on the orbitals and atomic spacing Retrieved from [38]

To understand how this allows for generation of energetic charge carriers let's bring back a photon. When this photon interacts with an electron in the valence band, there are two possible outcomes – the photon is high enough energy that it will annihilate in the interaction, transferring the energy to the electron, or the photon energy is too low and it continues through the material [26, 27, 31]. The defining factor for if the energy of the photon is too high or too low is if there is an empty allowed state energetically separate at the precise energy of the photon [26, 27, 31]. Because there is a distribution of states in both valence and conduction bands separated by some energy as shown for CdTe in figure 8, these two bands define the absorption. The higher the energy of photon – the higher the probability that there is an empty state separated by the proper energy and thus the more likely to be absorbed. As the photon energy decreases the probability is diminished until the difference between the maximal energy of the valence band and the minimum energy of the conduction band. After this point, the energy of photons is too small to excite the electron to any available states, and the photon is unaffected by its traversal of the material [26, 27, 31]. This typically this is written as absorption occurs when $E_{ph} \geq E_g$, and might lead you to anticipate a step-like absorption profile. However, the probabilistic nature of these interactions means that only an infinitely thick slab of material would have this perfect step absorption, since photons of energy close to but at or greater than the bandgap often traverse significant portions of the material without being absorbed. When the interaction between a photon and an electron results in excitation, the electron leaves behind a vacant state, which effectively becomes a positive charge carrier particle, the previously discussed "hole" [26, 27, 31].

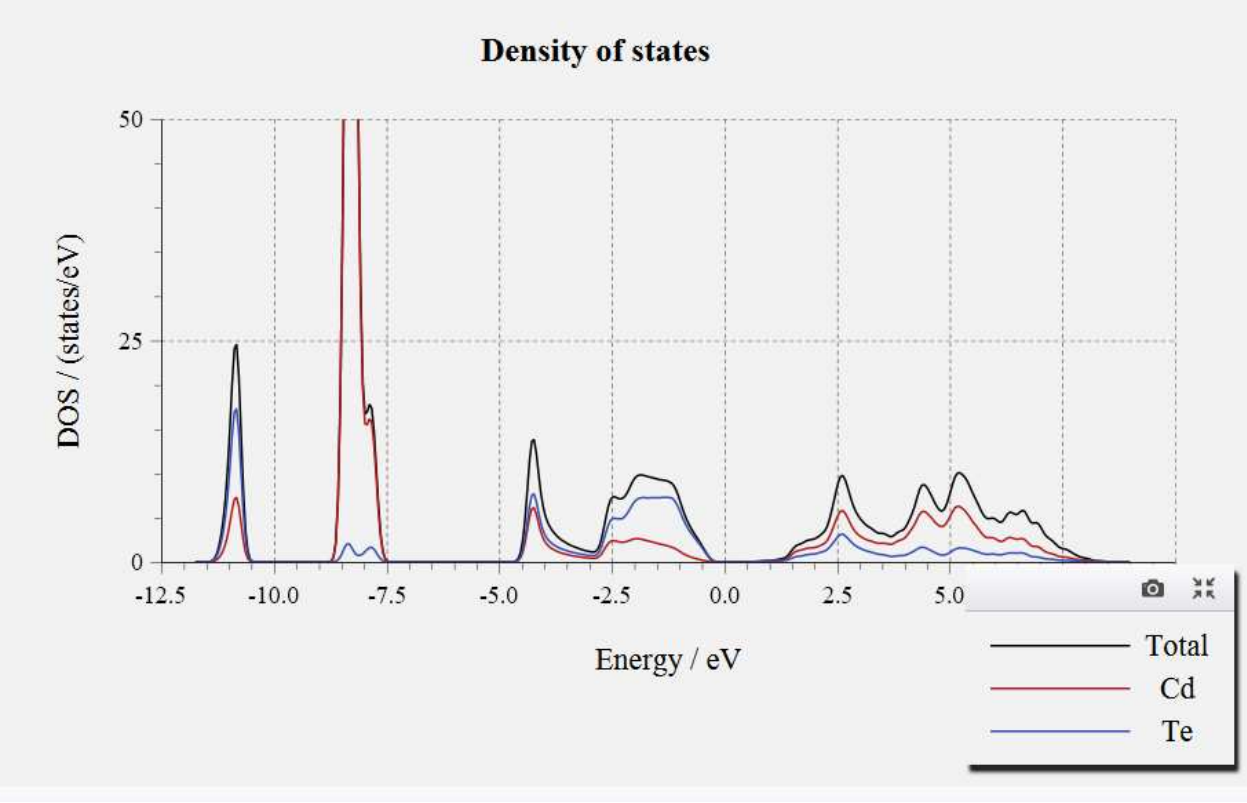

Figure 8: Density of states in CdTe as a function of energy relative to the fermi energy in the bandgap. It is apparent that a larger combined density of states is available for higher energy transitions. Retrieved from [39].

Through this process, we now have satisfied our first property required in the absorber – generation of an energetically separated set of positive and negative charge carriers by absorption of light, as excited electrons exist in the conduction band and the excited holes exist in the valence band. However, a single carrier will provide a very small amount of energy. Luckily, we have continuous illumination from a large flux of photons from the sun, and many of them have energy high enough to be absorbed. This produces electron hole pairs continuously, allowing for a large quantity of electrical charge carriers of opposite charge to be energetically separated within the absorbing material.

In parallel to this generation, there also exists pathways for these carriers to lose their energy without traversing the external circuit, which is how humans would make use of it [26, 27, 40]. This process is called recombination, and ideally this occurs in the reversible process from generation – the emission of a photon, so-called radiative recombination [26, 27, 40]. Radiative recombination is most common when an electron and hole in the different bands recombine (although due to the principle of reciprocity, any recombination between any set of states sufficiently separated to cause absorption of a photon can emit a photon), and the emission of the photon follows energy conservation – it matches the energy that was lost to the charge carriers in the annihilation of the electron-hole pair [26, 27, 40]. This process is ideal because it sets the lower limit for recombination rate, and thus the upper limit for how long carriers can exist in the semiconductor before they lose their energy [26, 27, 40]. This recombination rate is dictated by the material itself and the density of all carriers in the conduction and valence bands [26, 27, 40]. Aside from radiative recombination however, there is defect-assisted recombination, both in the bulk and at surfaces, which disperses the energy of the annihilation of the electron-hole pair in the form of a phonon [26, 27, 40]. This recombination is dictated by the density of the defects, the range across which they can capture a carrier, and the density of carriers that can be captured by the defect [26, 27, 40]. This is the most insidious form of recombination, as rates tend to be quite high due to the difficulty of eliminating defects in real crystals and as such it can act as a large sink to the number of photogenerated carriers, and thus loss of their energy for use. Finally, the remaining pathway for recombination is the donation of the energy to another carrier in the same band, allowing it to annihilate with the opposite charged particle from the other band [26, 27, 40]. The newly excited carrier will thermalize, also producing a phonon and losing the energy for electrical power production [26, 27, 40]. A simplified schematic of such processes is

shown in figure 9. Through these processes the number of excess carriers – in steady state – and thus the energetic separation of the average electron and hole, are modulated by generation and recombination within the absorber.

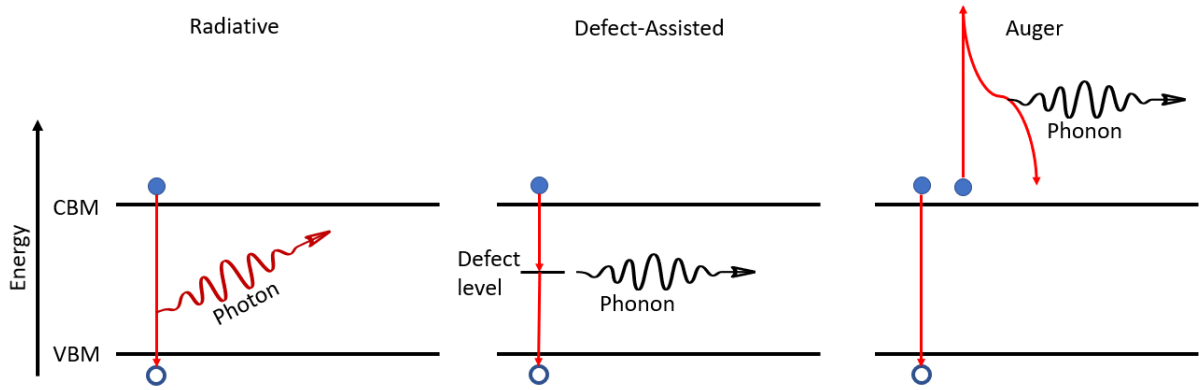

Figure 9: The various pathways of recombination

In order to describe the energy within the system available for extraction, useful tools have been developed. Specifically, one needs to determine the mean separation of energy between the excited electrons and holes – or at what energy 50% of the population "exists." The Fermi-Dirac distribution for a band of carriers allows for determination of precisely this, although computationally, the Boltzmann approximation is used assuming that $E-E_F >> k_BT$ (typically 3x or more) as shown in eq 4 where f(E) is the Fermi Distribution probability at a given energy, E_F is the energy of the Fermi level, k_B is the Boltzmann Constant, and T is the Temperature in K [41, 42, 43]. Multiplying this distribution by the available density of states in the band produces a density of carriers, providing a relation between the density of carriers and the density of states within a band to the energy at which you are 50% probable to find an electron (the Fermi-Level), even though this energy typically sits within the forbidden region (found in eq 5 where the new

term n is the density of carriers in the band and N_{band} is the available states for the carriers to occupy); this energy corresponds to the potential of the carriers [41, 42, 31].

$$f(E) = \frac{1}{\exp\left(\frac{E - E_F}{k_B T}\right) + 1} \approx \exp\left(-\frac{E - E_F}{k_B T}\right) \qquad (4)$$

$$n = N_{band} \exp\left(-\frac{E - E_F}{k_B T}\right) \qquad (5)$$

Interestingly, when in equilibrium, only one fermi-level is allowed within the material, the populations of carriers in each band must be at the same potential in this condition. As such we achieve the state where there is an equilibrium density of carriers in both bands governed by the relation $np=n_i^2$. However, under other conditions this is no longer the case, and excitation of electrons from the valence band into the conduction band as well as injection of carriers from an external circuit violate this equilibrium. Recall here that we have a large number of electrons and holes generated by the sunlight. As such, using the number of carriers in a band, both from excitation and the equilibrium concentration, to calculate a Fermi-level, we find each band now has it's own separate quasi-Fermi-level (qFL) representing the mean of electrons in the conduction band and in the valence band separately [31]. Both the equilibrium case and the non-equilibrium cases are found represented in figure 10. A demonstration of this self-consistency with the equilibrium condition is that the $np=ni^2$ relationship will force each band's carrier density to produce a quasi-Fermi-level at the same place in the bands. Additionally, it is worth noting here that the electro-chemical potential of electrons is simply the opposite sign of that of holes for each band, as the filling of higher energy states by electrons in higher energy states and thus an increase in their potential is equivalent to the reduction of holes in the same energy states and thus an reduction of their potential due to the opposite charge. The result of this is that it is

common to discuss the qFL of the conduction band in terms of the increase in electro-chemical potential of electrons, and simultaneously, the qFL of the valence band in terms of the increase in electro-chemical potential for holes, rather than the difference in electro-chemical potentials for one or the other.

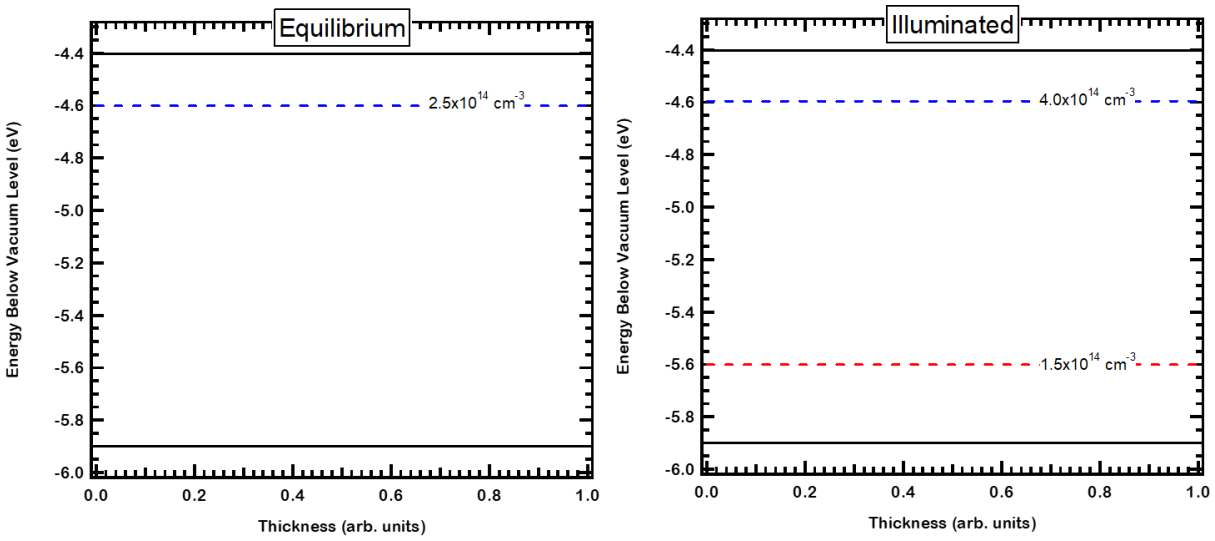

Figure 10: a) Fermi Level of an n-type CdTe Material b) The same Material with excess carriers showing a fermi level for each band

2.2.2) Charge Carrier Separation

Following generation, we need to have carriers traverse some imbalance in electro-chemical potential to flow [29, 30]. In order for this flow to be useful, the electrons and holes must exit at opposing membranes to create a unidirectional net flow for like changes across some external difference in potential. It is well known that as charged particles, electrons and holes will flow in response to two potential differences: chemical and electrical in nature. Typically, this results in the calculation of flow in terms of both “drift” due to the electrical driving force and “diffusion” related to differences in concentration within a band. The mathematical description of each can

be found in equation 6 and 7 respectively where μ is the mobility of the carrier, q is the charge, n is the concentration of the carriers, E is the electric field, and D is the diffusion constant.

$$J_{electric} = q\mu nE \qquad (6)$$

$$J_{chemical} = qD\nabla n \qquad (7)$$

The total current is then the sum of these two components, it is often discussed in terms of the separate contributions from each. It is, however, not true that there are separate currents from each contribution physically, and carriers instead only move as a function of the sum of these two currents, resulting from the net force due to the two potential differences [44]. A combined picture, and that which is less likely to lead to confusion about the physicality of the currents, is adequately described by combining the driving forces, which results in the driving force of the potential difference within a band for a given carrier. This is described mathematically as gradients in the quasi-Fermi levels, with the single current for any region in a band being found in equation 8 where all symbols are the same as equation 6 and 7 and E_F is the fermi-Level for the band/carrier of interest.

$$J = q\mu n\nabla E_F \qquad (8)$$

It is easily demonstrated that under illumination in steady state, there exists a gradient in the quasi Fermi-level for each band toward each terminal for operational points where power is produced [44]. This is obviously not ideal when a current is desired to flow in one direction, however, the magnitude of that charge flow along the gradient can be controlled. Conductivity/resistivity as defined by equation 9 is the pre-factor to the gradient in Fermi levels, and thus the magnitude of the flow of charge carriers down any gradient in their qFL is determined by this value. This allows for two main variables – with one being more controllable

than the other – mobility and carrier concentration for alteration of the magnitude of current along the gradient of a Fermi level. Mobility is often constant or close to constant and as such is often discussed as a set material property, which leaves control of this property to the carrier concentration [26, 27, 45]. So far we have discussed that light alters the concentrations of the carriers – but this modification produces equal increases in carrier concentration for both electrons and holes and thus a minimal imbalance of conductivity, determined by the different mobilities of electrons and holes [26, 27]. However, what is clear is that there has to be a dramatic asymmetry in the conductivity for a carrier from one electrode to the other, forcing the net current in the band to be effectively unidirectional.

$$\sigma = q\mu n \qquad (9)$$

For this asymmetry, we often need to artificially alter the conductivity, a process typically done by adding impurities to a semiconductor which donate electrons to the conduction band or holes to the valence band in the absence of light or other alteration from equilibrium, thus increasing the conductivity to a specific carrier by an increase in the concentration of that carrier.

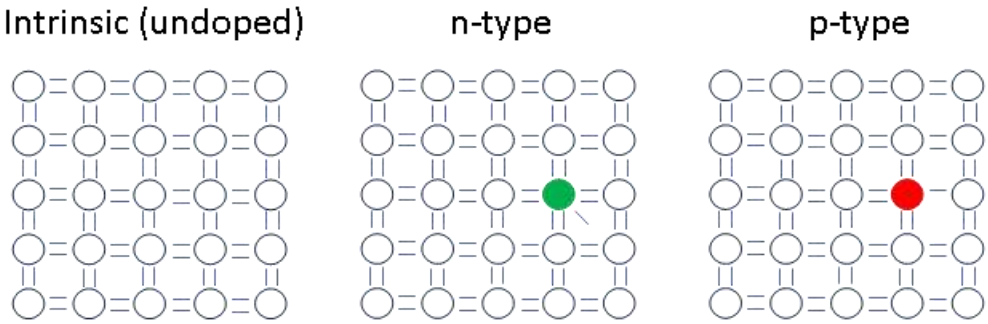

Figure 11: Demonstration of doping mechanism where the circles are atoms and the lines are electrons in the valence shells

This is called doping and is most easily demonstrated by examining silicon. Silicon is a group IV element, and as such, it bonds with 4 other Si atoms, sharing two electrons with each of them to fill the valence orbitals of each to 8 electrons as demonstrated in figure 11 where circles are crude depictions of nuclei and lines are crude depictions of electrons. It is then easy to see how one might dope a semiconductor – simply remove one of those Si atoms from the crystal and replace it with an atom that has a different number of valence electrons (red and green atoms in figure 11). The selection of an element with one extra electron (green), a group V element such as the common phosphorus in this case, or a group III element like Boron with one less electron (red), then allows for additional electrons or fewer electrons than the intrinsic – or undoped – state. In the simplest view, excess electrons must exist in the conduction band – as they cannot occupy states within the full valence orbitals. Similarly, the reduction of electrons causes a hole in the valence band as now not all available states within the valence orbitals are occupied. This is of course the ideal case. It is complicated by the energy level of the state this electron or hole resides naturally relative to the bands. Generally, the electron or hole will only contribute to the density of states within the band if it is within one thermal voltage of the band's maximum or minimum as the energetic barrier for that carrier to enter the band is easily overcome with only thermal energy. Deeper states contribute their intended carrier to the bands in a statistical manner depending on the difference in energy of the state and the band, as well as the temperature [27]. In this way artificial control of conductivity to electrons and holes can be achieved through doping, with the greatest success for dopant atoms which introduce states very close to the band to which they are donating an electron or a hole.

There are limits to doping. The most obvious is that only a small number of atoms in the crystal can be replaced before the bulk properties, other than carrier concentration, start to shift from

those of the original semiconductor. A fine line can exist between these conditions, but often limits are reached well before the density of dopant atoms affects the material in this way – creation of an alloy, second phase, or precipitate. These other limits have to do with how readily the dopant atoms sit in the proper site in the lattice of the semiconductor's crystal, as only dopants that are properly coordinated with the rest of the crystal tend to produce the desired increase or reduction of electrons in the material, typically placing the defect energetically as close as possible to the band [26, 27]. Other coordination within the crystal tends to place available levels from these defects that can produce the opposite effect of that desired, or introduce allowed states in the middle of the bandgap which encourage non-radiative recombination, often due to straining the lattice and thus locally changing the interatomic spacing [26, 27]. As such – dopant densities are on the order of <1% of the atomic composition in the material, with carrier concentrations often significantly lagging the number of dopants incorporated [26, 27].

Knowing how to add electrons or holes to our materials without illumination, we can incorporate this into our solar cell. If we asymmetrically dope the material n-type (added electrons, increased conductivity to electrons) and p-type (added holes, increased conductivity to holes) spatially, we would expect that we now have the required asymmetry in conductivity needed to produce unidirectional current of excess carriers. In addition to the conductivity, the electro-chemical potential of the equilibrium electrons/holes relative to the band is altered as the concentration in either band is altered, as demonstrated in figure 12.

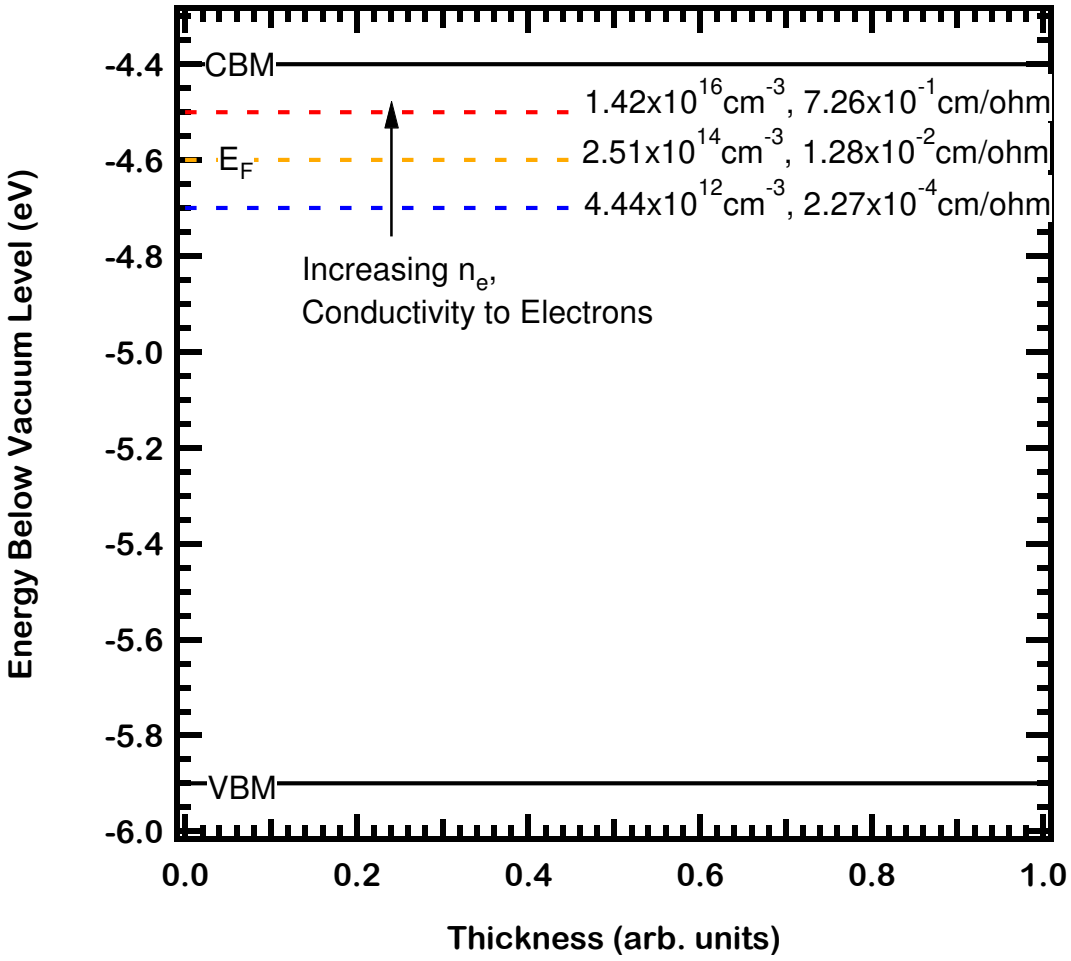

Figure 12: n-type doping in CdTe and the effect on electron conductivity

Traditionally, it is believed that the p/n junction is necessary for solar cells, based on a fairly simple notion – when an n and p type material come in intimate electrical contact, the electrons and holes due to doping are at different potentials, resulting in diffusion and annihilation of electrons and holes in the diffused region as the carriers in each band trend toward the equilibrium state of a single Fermi-level [26, 27]. The result of this is an electric field developing in this region due to the charge imbalance resulting from the induced mismatch of charge between the dopant nuclei and electrons in the orbitals [26, 27]. This electric field grows as more

diffuse and annihilate, until the point where the diffusion stops because the diffusional driving force is matched by the force exerted by the electric field, at which point carriers cease to diffuse and annihilate [26, 27].

The typical description is that electrons and holes generated within this region are separated by that electric field force, and will continue to do so until the electric field goes to 0 (or close to it), at which point V_{oc} is reached, which is dictated by the doping (the "built in voltage") [26, 27]. This idea is graphically shown by the bending of the bands in the equilibrium band diagram, as found in figure 13.

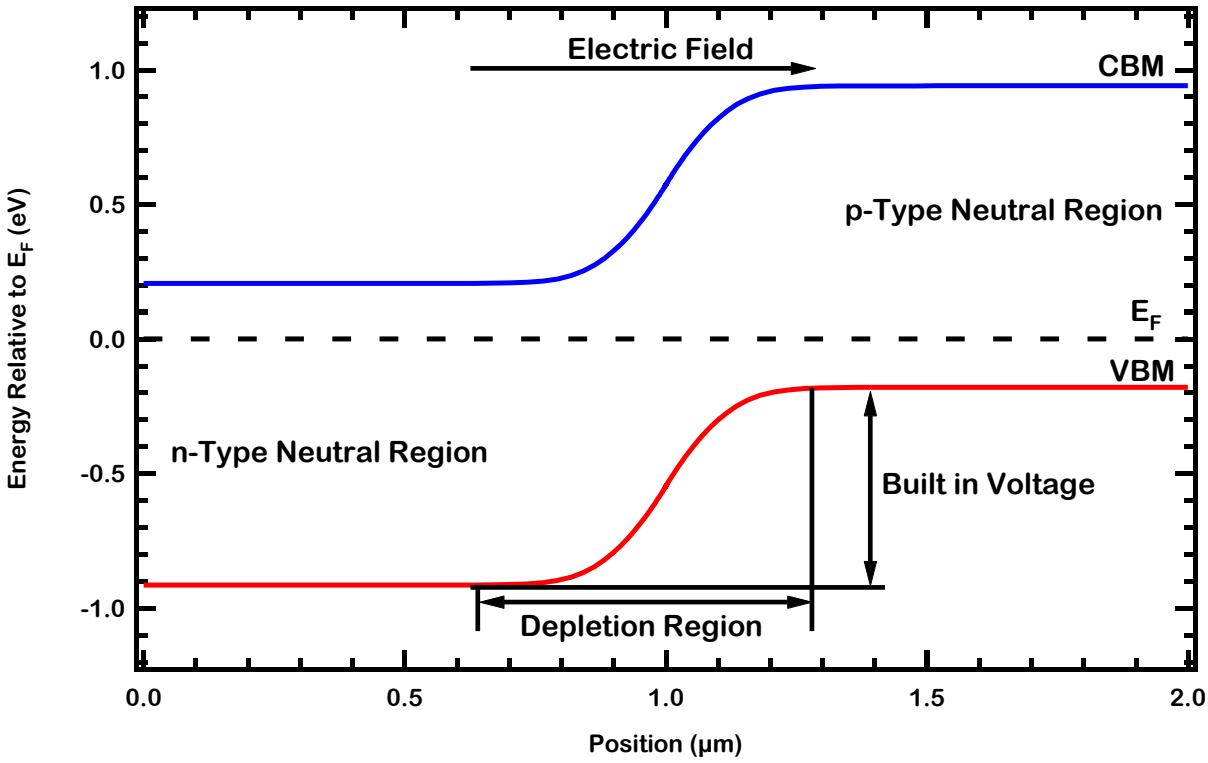

Figure 13: Si p/n junction in equilibrium

While this works as a first approximation of cells there is one glaringly large flaw – you can't pick and choose which forces a carrier feels. The same diffusional forces that pushed the carriers to diffuse in the material still exist when the electric field is present, and any individual carrier would see no net force as the above band diagram depicts the equilibrium condition. As already discussed, carriers will only flow under a sufficient net force!

This brings us back to our qFLs. These are present when the equilibrium condition is violated and the density of carriers in both bands is altered, either by generation from light absorption or injection from an applied bias. This shows us where the extra force to drive carriers comes from in the case of a p-n junction solar cell, generation of carriers reduces the diffusional force for the carriers because the gradient in carrier density through a band is reduced by the generated carriers, and the net force becomes non-zero in favor of the electric field. The result is movement of carriers, but they are not accelerated by the full strength of the electric potential dictated by the field strength. Instead, the interplay between diffusional and electrical forces plays out to create a gradient in the electro-chemical potential, along which carriers then flow. This potential difference along the gradient follows the electric field direction, but the magnitude is determined by the concentration of generated carriers, or perhaps appropriately for a power-generating device, how large the energetic deviation from the equilibrium condition is.

Additionally, the V_{oc} condition is not then reached when the electric field goes to 0 and the electrical force no longer exists. Rather, an applied bias or a resistance in the external circuit increases the electrochemical potential of carriers at the electrodes by reducing the rate of their extraction. Because this buildup of carriers reduces the imbalance of charge across the depletion region, the electric field is somewhat reduced, in line with the previous view. However, this again would seek to ignore diffusional forces. The increase in electro-chemical potential (which

again accounts for the electric field and the diffusional forces) at the terminals serves to reduce the gradient which forms the electro-chemical potential difference within each band. Because this potential difference is reduced, the net force driving carriers to flow in the desired direction goes to 0 at sufficient resistance and at some point the flow of carriers through both electrodes from the same band match yielding a net flow of 0, producing the V_{oc} condition. It is noted that this often occurs at differences in the electro-chemical potential that are well below the condition which produced an electric field strength of 0.

This is demonstrated in figures 14 and 15 – which shows a silicon p/n junction under AM1.5G illumination. At only 2 μm of Si, the excess carrier concentration is reduced from ideal due to incomplete absorption of the allowed spectrum due to the indirect bandgap and thus low absorption coefficient [46]. Thus, the concentration of carriers occurring from generation when there is no net extraction is quite a bit smaller than the 10^{16} cm^{-3} used in both n and p regions at V_{oc}. Because this is a homojunction, if the excess carrier concentration at Voc was equivalent to the doping, the electric field would go to 0 at as the buildup in charge from excess carriers would be sufficient to counter the imbalance of charge in the space charge/depletion region. However, since this is not the case, the V_{oc} condition occurs at ~400 mV when the gradients in each band's electro-chemical potentials toward the desired contact (qFL) is 0. This is well below the ~700 mV expected if just the strength of the electric field (electrical potential difference) was what dictated the open circuit voltage. This is visualized clearly in the band bending still present at the V_{oc} condition in figure 15.

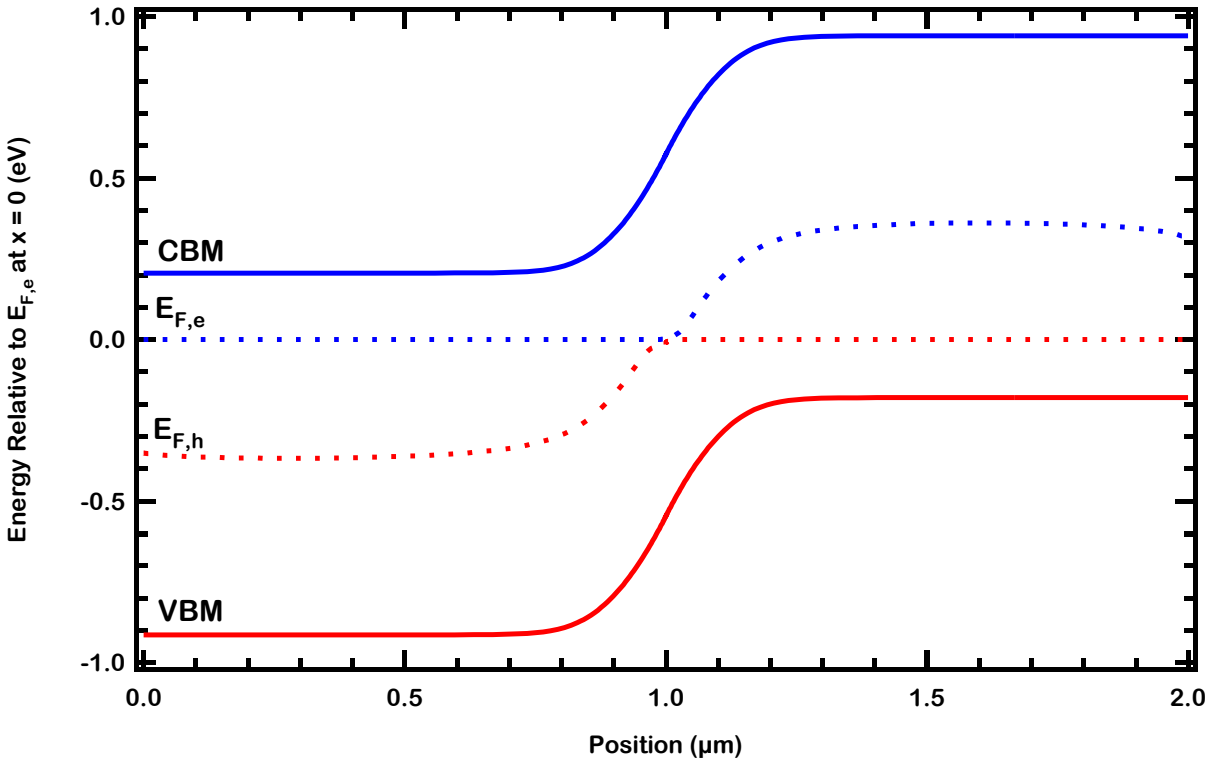

Figure 14: Si p/n junction under illumination at short circuit

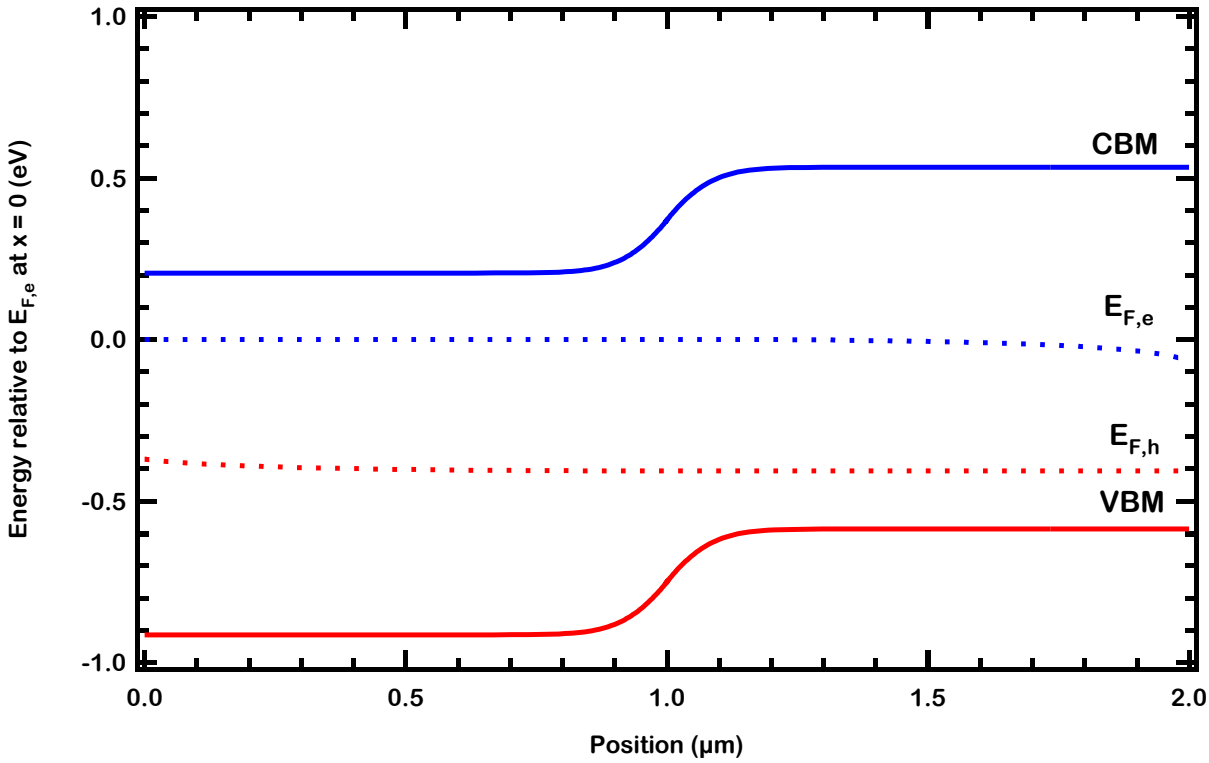

Figure 15: Si p/n junction under illumination at Voc

However – we know that a p/n junction works, it shows gradients in the qFLs at Jsc and separation of the flat qFLs at Voc! So why is this the case? Indeed, the p/n junction is just a way to achieve an imbalance in conductivity to carriers. A sufficiently doped semiconductor, either n or p, leads to the condition that the concentration of minority carriers is orders of magnitude less than the majority carrier, especially in equilibrium – leading to a large discrepancy between different conductivities for the different carriers through the same material. As such, a highly n-type and a highly p-type semiconductor would appear to be excellent selective materials with a large imbalance in conductivity between the two carriers. This is demonstrated in the equilibrium band diagram and calculation of conductivities for a baseline CdTe Solar cell as modelled in SCAPS 1-D found in figure 16.

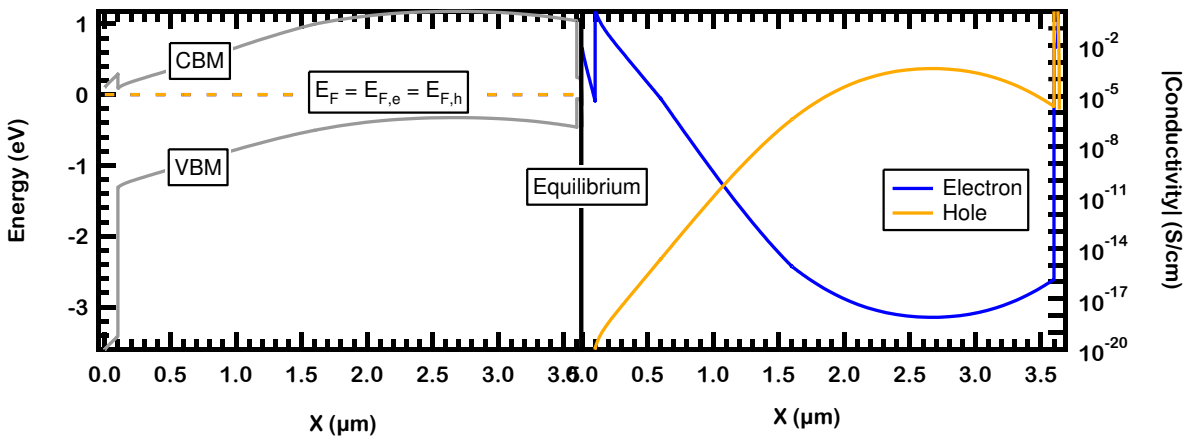

Figure 16: CdSeTe/CdTe Solar Cell under equilibrium and partial conductivities throughout

Unfortunately, the diffusion of minority carriers forces this selectivity to typically be non-ideal. This process, necessary to current production, increases the density of the minority carriers within the semiconductor, severely reducing that difference in conductivities to electrons and holes through the semiconductor. This is demonstrated in figure 17 for a CdTe solar cell both at the Jsc condition, and demonstrates that the imbalance in conductivity is further decreased at Voc due to the buildup of these excess carriers. The idealized selectivity that a p/n junction can produce exists only in the dark since the condition $n*p = n_i^2$ holds under equilibrium. This can be found in an illuminated cell if and only if the generation region is greater than a number of diffusion lengths from the surface of the semiconductor – otherwise minority carriers can reach the metal and recombine through the continuum of states the metal provides within the bandgap of the semiconductor, the result being reduction of qFLS by increasing the recombination current [26, 27]. A long diffusion length is desirable in an absorber material, as a long lifetime is desired to increase the excess carrier concentration as high as possible and a high mobility is desired so excess carriers of both types see little resistance in extraction. As such, the material usage requirements for a doped region of the same semiconductor as the absorber to achieve its full

selectivity tend to be excessive if the cell is to approach its radiative limit. Ultimately, a real p/n homojunction is non-ideal with very few exceptions due to this effect. The first issue is that there is generation starting at the surface of the semiconductor, which prevents the full selectivity at that contact from ever being realized since excess carriers are unavoidably present at the metal interface. The second is that even if an interdigitated back contact style structure is used where the n and p regions are on the back surface and there is no generation, the diffusion lengths through the n and p regions of minority carriers is often too long for diffusion of dopants to effectively produce n and p regions of adequate thickness to achieve the ideal selectivity [47]. The result is that a heterojunction solar cell is practically a better solution, and will be discussed in the following sections.

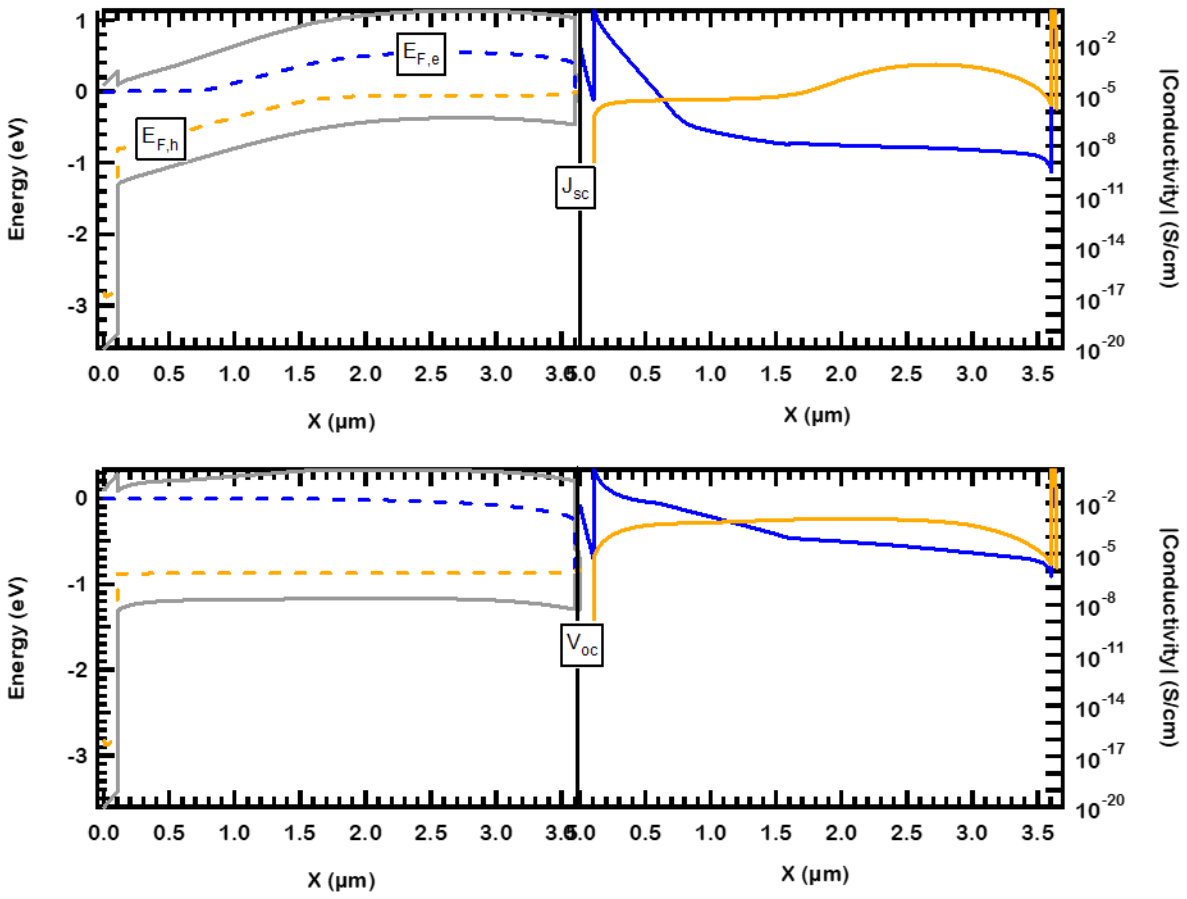

Figure 17: Energy band and partial conductivities for a) the Jsc condition, and b) the Voc condition

2.3) An Ideal Solar Cell

Understanding now how concentrations of electrons and holes in our absorber, necessarily finely tuned to the solar spectrum, create the potential across which the carriers must traverse, and the asymmetry of conductivity is required for production of a unidirectional current, let's now examine an ideal solar cell. This first requires selection of the absorber material.

For this we turn to what is now called detailed balance analysis, originally developed by Shockley and Queisser in 1961 [26, 27, 48]. This technique essentially is a thermodynamic

analysis, finding the efficiency of a heat engine operating between the temperature of the sun and the temperature of the cell and accounting for the specific loss mechanisms inherent to how semiconductors interact with light. The result essentially is a calculation of generation as a function of the bandgap energy and relating that to the qFL separation given the ideal case where the recombination current in the cell occurs by emission of a photon, a reversible process [26, 27, 48].

The maximum current density due to light generated carriers is simply derived first. The idea is that each absorbed photon produces one electron-hole pair. The maximum short circuit current occurs, logically, if every one of these is extracted, producing a current equal to the fundamental charge multiplied by the number of particles excited. This leads to the relation found in equation 10 where J_{sc} is the short circuit current, q is the fundamental charge, a is the absorptance, and Φ is the incident photon flux. In the original Shockley and Queisser calculations, the absorptance was assumed to be a step function, as they were considering a semi-infinite slab of semiconductor, but this analysis can be applied to real absorbers given knowledge of their absorptance [26, 27, 49-51].

$$J_{SC} = q \int a(\lambda)\Phi(\lambda)d\lambda \qquad (10)$$

The open circuit voltage is then found by calculating the maximum qFL separation produced by this generation current, corresponding to the condition when none of the carriers are extracted and all recombine within the absorber or at the "incorrect" contact. This calculation accounts for the lower limit to the recombination current, the case of only radiative recombination within the absorber which is given by equation 11 where $J_{0,rad}$ is the radiative limited generation and recombination current in equilibrium, q is the fundamental charge, a is the absorptance, and

$\Phi_{BB,Tcell}$ is the black body spectrum emitted at the temperature of the cell and its surroundings [26, 48-51]. This condition only occurs if the contact perfectly rejects the "incorrect" carriers and the material of the absorber is flawless. Again, this can be used for a real cell with knowledge of the actual absorptance.

$$J_{0,rad} = q \int a(\lambda)\Phi_{BB,T_{cell}}(\lambda)d(\lambda) \qquad (11)$$

It is worth noting here that $J_{0,rad}$ is simultaneously the generation rate due to light in the "dark" and the recombination current at equilibrium in the radiatively limited case. This is easily obtained from understanding the equilibrium condition where energetic exchange is only allowed by exchange of photons, as it is the only formulation that obeys the fundamental conservation laws by exchanging equal amounts of energy in and out of the cell. As a result, the total generation is the sum of J_0 and J_{SC}, but the minimum recombination current is just J_0. The result is qFL separation governed by the equation 13 which is simply a rearrangement of equation 12 at the radiative limit. This results from the understanding that the rate of recombination is exponential with the separation of the quasi-fermi levels due to their exponential relationship with carrier concentrations [26, 27, 31], and that the maximum qFL separation due to sunlight occurs when the recombination current is equal to the generation current as demonstrated in equations 12 and 13 where J represents a current density noted by the subscript, QFLS is the separation of the quasi Fermi Levels, k_B is the Boltzmann constant, and T is the temperature in K [26, 27].

$$J_{recombination} = J_0 e^{\frac{QFLS}{k_B T}} = J_{Generation} = J_{SC} + J_0 \; at \; V_{OC} \qquad (12)$$

$$QFLS_{max} = k_B T \ln\left(\frac{J_{SC} + J_{0,rad}}{J_{0,rad}}\right) = k_B T \ln\left(\frac{J_{SC}}{J_{0,rad}} + 1\right) \qquad (13)$$

It is notable here that under illumination from the sun, $J_{sc}>>J_0$ and as such a very reasonable approximation is found by dropping the +1 in the logarithm, which can also be thought of as the generation due to the black body radiation at the temperature of the cell and surroundings being negligibly small relative to the generation due to the sunlight. However, the cell's maximum power output is needed for the efficiency limits and so we now need to find some point where there is simultaneously current and voltage.

This relationship is easily modified to show that the net current must simply be the difference between the light generated current and the recombination current, assuming that the qFL separation through the absorber is equal to the terminal voltage. This results in the current-voltage relationship in equation 14, from which the power at some operating point of the cell can be calculated, with the maximum occurring somewhere between J_{sc} and V_{oc} and the efficiency of the cell being the ratio between the maximum power and the impinging power from the sun. This is demonstrated for a 1.4 eV cell in Figure 18. Here it is worth noting that the direction of current flow (positive or negative) is arbitrary so long as the recombination current and the generation current are opposite, and many JV curves are displayed with a negative light current due to the sign convention in the microelectronics industry for the recombination current being positive.

$$J = J_{SC} + J_0\left[1 - \exp\left(\frac{V}{k_B T}\right)\right] \qquad (14)$$

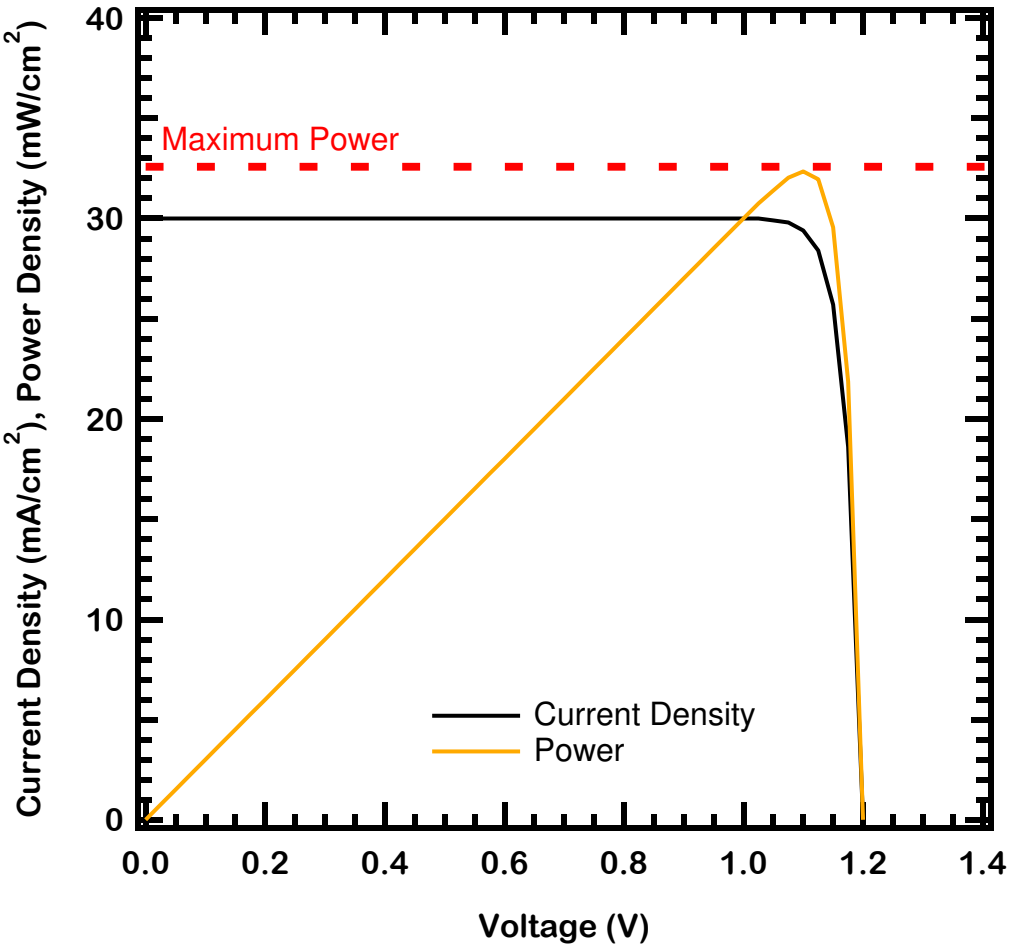

Figure 18: The ideal Current- and power- voltage curves for a cell with a bandgap of 1.48 eV.

From this derivation it is clear that both the maximum of voltage and current are dependent on the absorptance, which then is set by the bandgap (or more accurately the combined density of states separated by a certain energy) of the semiconductor. Using the assumption of idealized (step) absorptance the maximal efficiency has been calculated as a function of bandgap, and for the standard AM1.5G spectrum used to test cells the spectral effects produce a broad peak with two bandgaps which are just about matched at ~33% as the upper bound – ~1.1 and ~1.4 eV as calculated in [85] and seen in figure 19, balancing the increased current that accompanies a

narrower bandgap with the increased voltage that is enabled by a wider bandgap. While real cells will never have the ideal absorptance qualities, the sharper the absorption edge around those photon energies, the closer the cell can be to this calculation of the limit.

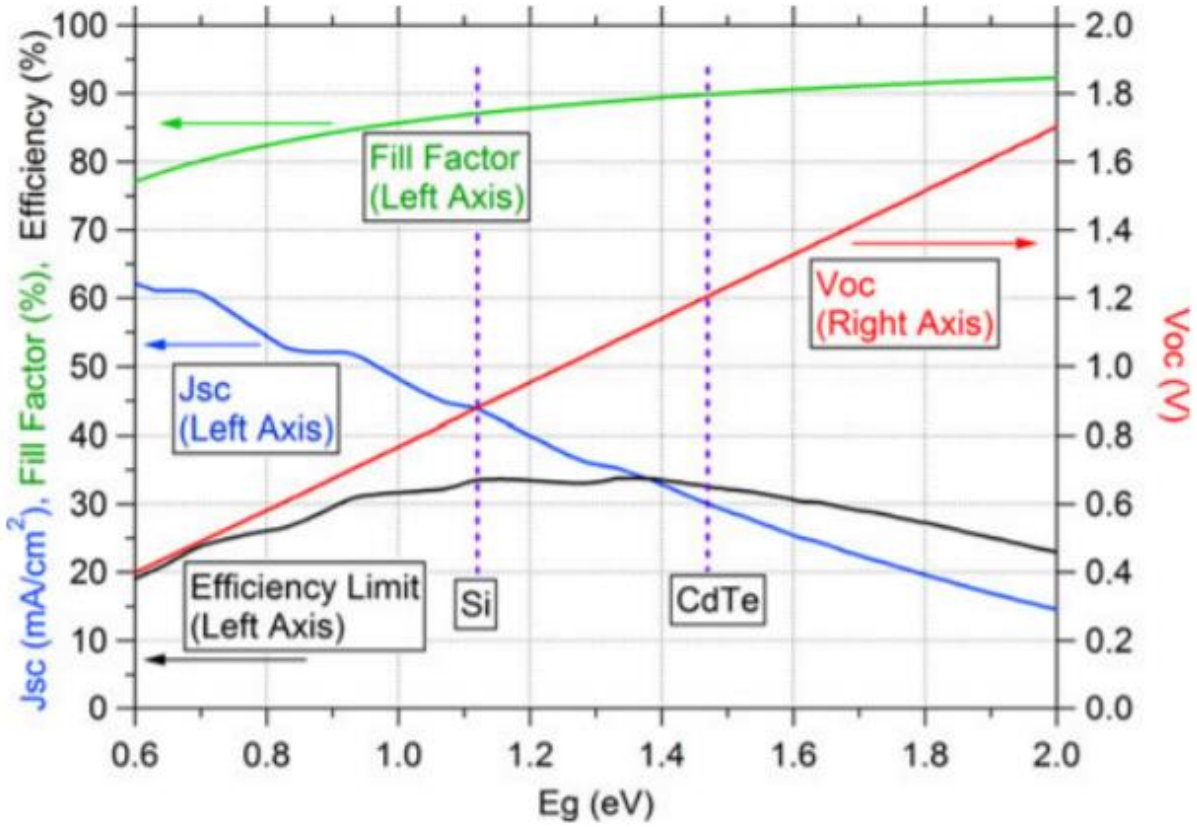

Figure 19: Detailed Balance limits to solar cell parameters based on bandgap. Retrieved from [85]

From this we can see that the absorber should have an absorption edge of about 1.1 or 1.4 eV, and ideally quite sharp, which would suggest the need for a direct bandgap semiconductor, as the momentum component needed for absorption in indirect semiconductors reduces the probability of any one photon of sufficient energy yielding generation of an electron hole pair, necessarily

broadening the absorption edge for any real thickness [26, 27]. This then requires either increased thickness/smart photon management, which can cause losses and increase costs, or a loss of generation and therefore both current and voltage.

Now that we have an idea of what is needed for our absorber, we need to tackle the asymmetry of conduction. The traditional solar cell uses the n/p homo-junction as discussed earlier. While certainly the simplest manner to produce this difference in conductivity, it is not the ideal way to achieve this effect. There are two reasons this may be the case – the first being that defects due to doping can severely increase the rate of non-radiative recombination when done improperly and the second being the lack of most effective prevention of "forward current" or more simply, a lack of sufficient ability to reduce the conductivity to the unintended carrier as discussed in that section.

This leaves hetero-junctions – which would be highly unexpected from the standpoint of a traditional solar view. This is because heterojunction contacts allow for material selection suitable for extraction of one and only one carrier. The ideal material will have a very high conductivity to the preferred carrier, with no states within the bandgap of the absorber to assist recombination, and more than that, a wide bandgap with the alignment of the bands such that there exists a large energetic barrier to conduction of the incorrect carrier. This energetic barrier leads to a dramatic reduction in the carrier concentration of the minority carrier and thus conductivity approaching the electrode, better forcing a minimized current along the gradient in the qFL in that direction. A hypothetical example of such a structure is found in figure 20 at the Open circuit voltage, demonstrating the far more favorable reduction in conductivity to electrons through this region remaining under illumination, which allows for a greater voltage. The greater electron Fermi-level in the hole contact than the absorber is believed to be an artifact of the small

concentrations of carriers being exchanged with the absorber coupled with the imperfect convergence criteria in the simulation. It is worth noting here that this effect can also be in part achieved by a smaller difference in bandgap, and an abrupt energetic offset is not necessary. There is literature suggesting that both CdTe and CIGS solar cells which feature grading of bandgaps achieve this effect to some extent [52, 53, 54].

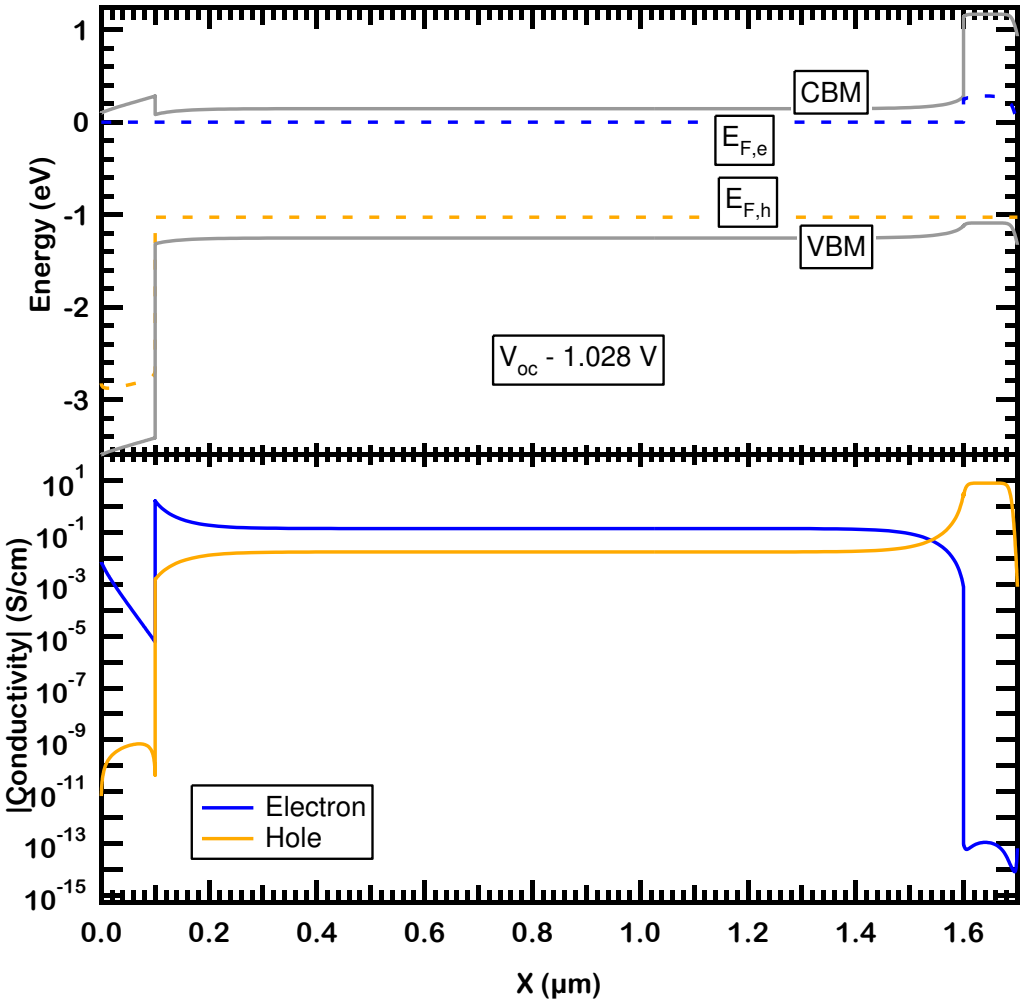

Figure 20: V_{oc} band diagram and partial conductivities for a relatively ideal structure

2.4) The Open Circuit Condition

As V_{oc} is the focus of this community, it is worthwhile to take a closer look at the condition within the cell. At V_{oc} and under normal operation (steady state) the continuity equation for the cell from terminal to terminal is quite simple. Since there is no change in the carrier concentration over time, and no net extraction of carriers through the terminals with time, we can set these two values to 0. This leaves only generation and recombination, and to keep the steady state condition the total rates of each must be equal.

From this, we have the first indication that recombination is exceptionally important to minimize, as the rate of generation is relatively fixed, but recombination rate is a factor of the defects within the cell – something the engineers and scientists can work to minimize. The lower limit for rate (upper limit for lifetime) is given by the rate of radiative recombination, as discussed when finding the upper limit for V_{oc} in the ideal absorber section, and thus the closer to this rate/lifetime the better. The effective lifetime is generally much shorter as no real material is entirely defect free. Since the rate of recombination and generation are equal, and the development of the potential difference between the bands depends on the density of carriers in each band, we can use the relationship to approximate the density of excess carriers. This is done by setting the rate of generation and equating that to the rate of recombination, as given by $\Delta n/\tau_{eff}$ – leaving Δn on average to be equal to the product of the photocarrier effective lifetime and the generation rate.

Generation and recombination, however, can be localized within the cell. In direct bandgap materials generation is quite close to the surface upon which the sunlight is incident due to the large absorption coefficients, while the recombination will occur throughout any region of the cell which sees excess carriers from that sunlight. Typically, this is dominated by defect assisted

recombination, and thus is localized to the surfaces or defects within that region. The result is some distribution of photogenerated carriers which produces no net current through the absorber from terminal to terminal, irrespective of bending in the bands. A visual representation of this spatial non-uniformity of carrier density from local generation, recombination and band structure is demonstrated in figure 21 for a CdSeTe/CdTe cell at V_{oc} where the spacing of electrons (blue circles) and holes (open red circles) is a crude representation of the local density.

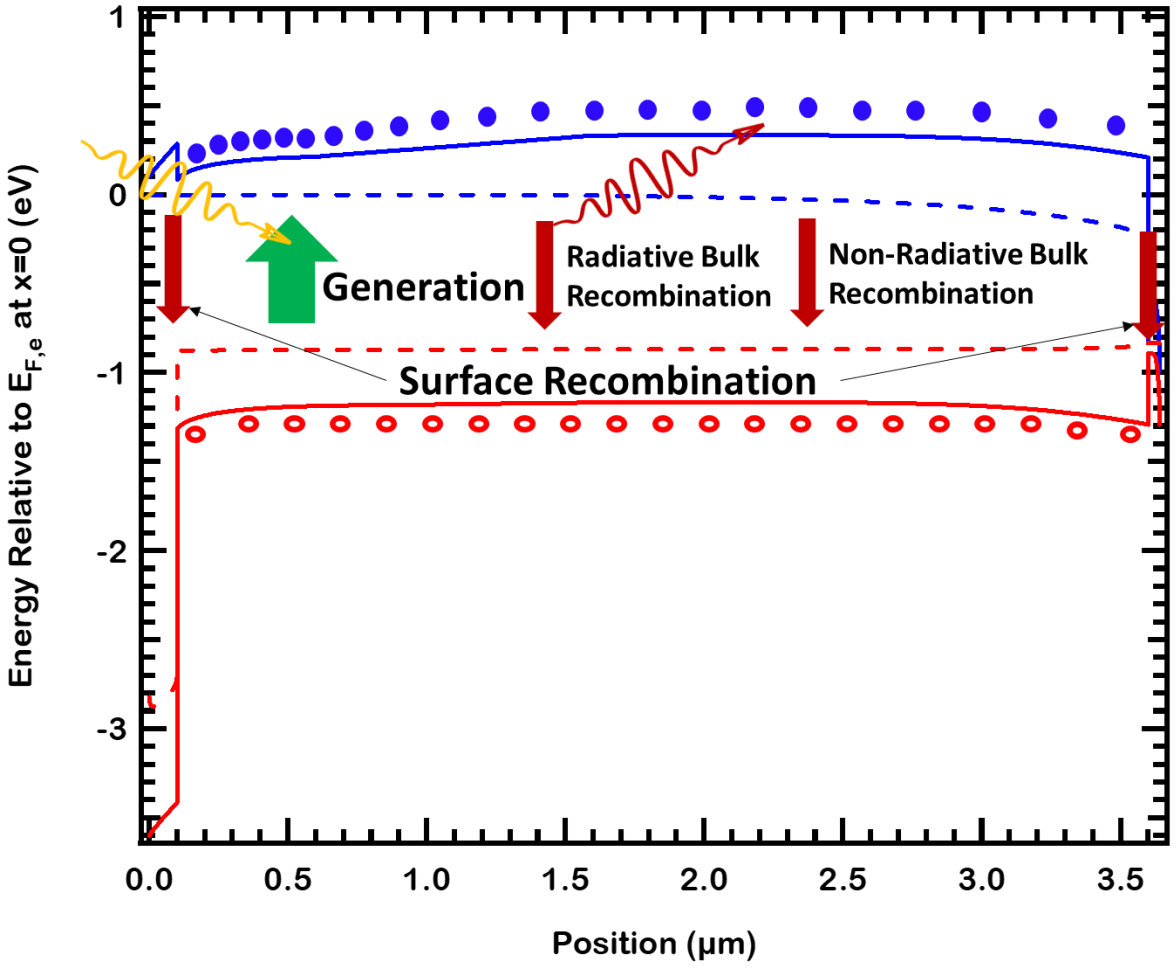

Figure 21: A CdSeTe/CdTe cell modelled at V_{oc} demonstrating QFLS and the various generation and recombination pathways and locals.

At one terminal, flow of one carrier is ideally stopped by an increase in the terminal's electro-chemical potential for the desired carrier, forcing the electrochemical potential difference carriers in the band see to go to near 0 across the contact. Because flow of the carrier is desired at this terminal in other conditions the resistance to this carrier must be quite low, and further this low resistance to the carrier allows the electro-chemical potential to nearly match that produced by the excess carriers in the cell, thus allowing the electrochemical potential at the terminal to match that in the absorber. This condition should be met at one contact for one carrier and the other contact for the other carrier, thus producing the potential difference between the terminals equal to that in the absorber.

Since at one contact this 0 flow is achieved for a carrier by a matched electrochemical potential, the other contact (which has the matched electrochemical potential for the other carrier) is more problematic. Here we find that there must be convergence of the qFLs, at the metal where only one Fermi level is allowed, if not before. Since the electro-chemical potential of the opposite carrier is flat through this contact, the difference of the electro-chemical potential between the absorber and the converged level must be equal to the difference of in the electro-chemical potentials created in the absorber, the same driving force that produces current, yet little to no current must flow. Here we examine Ohm's law for a simple yet telling relation for this. Since $R = V/I$, and there is a large V divided by a very small I to produce this effect. This means that the resistance to that carrier as it approaches the terminal must be quite large indeed if it is going to prevent flow of that carrier, and it must be infinite if there is to be no flow of that carrier at all.

No real contact has infinitely small resistance to one carrier and infinitely large resistance to the other carrier, so in reality V_{oc} is achieved when the partial currents through each contact for a given carrier sum to zero. Since the resistance to one carrier is infinite and the resistance to the

other carrier is negligible in the ideal case the contact is said to "select" for the carrier with negligible resistance. Thus the term carrier selectivity is used to describe contacts. However, this term has been defined in numerous ways, some of which focus on a single carrier's ability to flow through both contacts (i.e. electron selectivity defined as the ratio of the equilibrium exchange current through each of the two contacts) and other that focus on a single contact's resistances to each carrier [45, 54]. While both are appropriate descriptions in their own right, it is appropriate to distinguish between the definitions: the prior defines a cell's overall selectivity to a carrier and is appropriate for examining the effects of selectivity at all operating points of the cell, while the latter is most appropriate for examining the effects of individual contacts at the V_{oc} condition (as the partial resistance to carriers will change as with the concentration thereof) and thus will be used for the remainder of the discussion.

This selectivity is intrinsically linked to the splitting of the qFLs for the simple reason that a non-selective contact will produce a sink for the unwanted carrier by allowing flow of that carrier to the opposite terminal, thereby reducing its concentration in the absorber. It is through this effect that lack of resistance to the contact's "minority carrier" reduces Voc. To again discuss the non-ideal nature of homojunction, the resistivity/conductivity is related to the density of carriers, and as such a large qFL separation, requiring large numbers of carriers, simultaneously increases the potential driving that current to the wrong terminal and reduces the resistance to that carrier – increasing the current and therefore allowing more of those carriers to recombine at the contact and reducing the concentration in the cell. This can be mitigated in part by ultra-high doping in the contact region of the cell – inducing band bending and thus some reduction of the concentration of these carriers at the cell's contact interface, but again, a heterojunction with a

band offset that necessarily reduces the number of carriers present for a given qFLS is a more ideal solution.

Just as the lack of resistance for the contact minority carrier reducing the potential the cell is capable of producing, an increased resistance to the majority carrier is also detrimental. However, in this case, the effect is in a reduction of the external voltage relative to that produced by light inside the cell. This resistance increases the required potential difference for the majority carrier between the cell and terminal to produce the equal and opposite current to that at the other contact. This reduces the electro-chemical potential at that terminal from that within the cell and its difference from the other terminal, and therefore the potential difference across the external circuit below that produced by the sunlight within the cell.

2.5) Characterization

2.5.1) Current-Voltage

The most classic and common characterization is the current voltage measurement. This is because this relatively simple measurement is how one extracts the power conversion efficiency, while additionally providing insight into a number of other solar cell parameters with further analysis of increasing complexity. In the CSU lab, the current is measured as an external bias is applied to the solar cell, a common technique. If you know how large of an area is illuminated during this time, normalization of the current to the area allows for easier calculation of efficiency, as the power of the light from the solar spectrum is also dependent on area. As such, all I-V plots will be converted to current density – voltage plots (JV).

From the JV plot (example in figure 22), the first two common points of interest are the current density at short circuit (J_{sc}) and the Voltage at open circuit (V_{oc}). As P = IV from a basic circuits

class, the product of the J_{sc} and the V_{oc} are the upper limit on that solar cell for power production, representing when all possible photocarriers are extracted and the greatest external potential from photocarriers is measured respectively. This JV curve would look like a rectangle. However, this power will never be realized, as energy/mass balances reject the idea that both the rate of recombination and extraction can simultaneously be equal to the rate of generation. As such, the maximum power occurs at some other point on the curve, which appears as an exponential function, and the FF describes how close that maximum real power is to the upper limits. Thus the equations 15 and 16 are how one calculates the conversion efficiency where FF is the fill factor, P is the power density specified by the subscript, J is the current density specified by the subscript, V is the voltage specified by the subscript, and η is the power conversion efficiency.

$$Fill\ Factor = \frac{P_{max}}{J_{sc}V_{oc}} = \frac{J_{mp}V_{mp}}{J_{sc}V_{oc}} \qquad (15)$$

And

$$\eta = \frac{P_{max}}{P_{incident\ light}} = \frac{FFJ_{sc}V_{oc}}{P_{incident\ light}} = (at\ STC)\frac{FFJ_{sc}V_{oc}}{P_{AM1.5G}} \qquad (16)$$

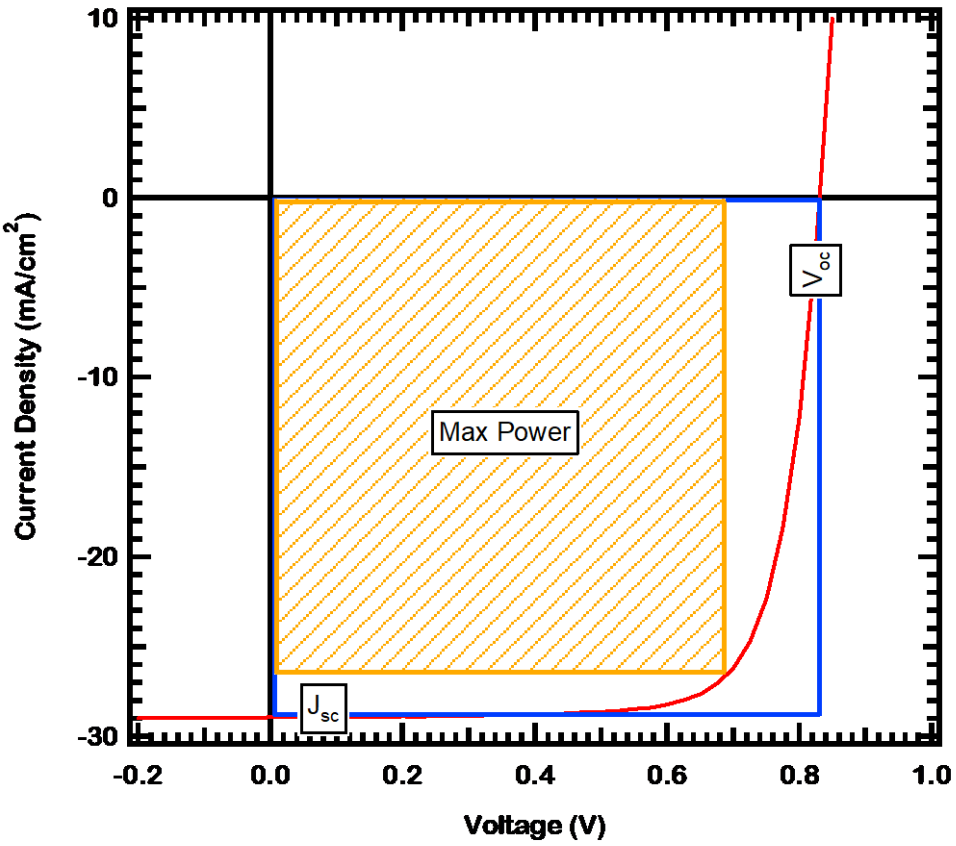

Figure 22: JV curve of a MZO/CdSeTe/CdTe/Te cell. The maximum power is represented by the area of the orange box and the FF is visualized by the ratio of that area to the area of the blue box. J_{sc}: 28.9 mA/cm^2, V_{oc}: 830 mV, FF: 76.3%, η: 18.2%.

2.5.2) Measurement of Implied Voltage via External Radiative Efficiency

Measurement of implied voltage in CdSeTe needs to be done by photoluminescence rather than the photoconductance technique typically used in Si due to the low lateral mobility of CdTe and high conductivity of the TCOs on which the films are deposited. However, it has been shown by Wurfel that the spontaneous emission of radiation from a semiconductor to remain equilibrium with it's environment is related to the chemical potential of the valence and conduction bands, and thus separation of the quasi-fermi levels in our vernacular. This is demonstrated by generalization of the radiation laws first derived by Planck and Kirchoff for thermal exchange of

photons [27, 45]. This is presented in eq 17 where $\Phi$is the photon flux specified by the subscript, abs is the absorptance, c is the speed of light in a vacuum, λ is the wavelength, k_B is the Boltzmann constant, h is the Planck constant, QFLS is the separation of the quasi-Fermi levels, and T is the temperature in K, showing the relation to both QFLS and absorptivity for the current of spontaneous emission. From this, it is clear that one can find the QFLS if they know the absorptivity and the spectrally resolved emission currents. From a measurement perspective, however, it is simpler to measure the total emission current and absorptivity separately, and use some thermodynamic or optoelectronic analysis to extract the QFLS. This analysis starts from the same equation simplified by the Boltzmann approximation that $hc/\lambda - QFLS >> k_BT$ when the absorptivity is greater than 0, resulting in equation 18. It is clear that the emission flux at a given wavelength is proportional to the absorptivity, the black body emission flux, and an exponential of the QFLS normalized to the thermal voltage.

$$\Phi_{emission}(\lambda) = abs(\lambda)\frac{2\pi c}{\lambda^4}\left[\exp\left(\frac{\frac{hc}{\lambda} - QFLS}{k_BT}\right) - 1\right]^{-1} \qquad (17)$$

$$\Phi_{emission}(\lambda) = abs(\lambda)\Phi_{BB}(\lambda)\exp\left(\frac{QFLS}{k_BT}\right) \qquad (18)$$

The absorptance spectrum dictates the thermodynamic limiting voltage through the ratio of the excess generation of electron hole pairs due to solar illumination to the generation of electron hole pairs from the thermal black body radiation within the absorber, or more aptly, the recombination current due to illumination, assuming all excited carriers recombine radiatively, and the equilibrium recombination current, again assuming all carriers recombine radiatively.

This can be shown by manipulation of the above equation and simplifies to the equation 19 where the new variables are current density represented by J and specified by the subscript.

$$QFLS_{limit} = k_B T \ln\left[\frac{\int abs(\lambda)\Phi_{excitation}(\lambda)d\lambda}{\int abs(\lambda)\Phi_{BB}(\lambda)d\lambda}\right] = k_B T \ln\left[\frac{J_L}{J_{0,rad}}\right] \qquad (19)$$

Thus, if all recombination in the absorber is radiative and leaves the front of the absorber (ERE=100%), the implied voltage will equal the thermodynamic limiting voltage. The ERE is used then to determine the deficit from this limiting voltage, and can be seen as an entropy generation measurement or alternatively, the deviation from this radiative limit due to non-radiative recombination. In real solar cells, this is always less than 1, and as such it produces a negative value in its natural logarithmic dependence and thus mathematically produces the deficit. This whole relationship can be found in equation 22 below starting with equation 20, and results in calculation of the QFLS.

$$\int \Phi_{emission}(\lambda)d\lambda = \int abs(\lambda)\Phi_{BB}(\lambda)d\lambda \exp\left(\frac{QFLS}{k_B T}\right) \qquad (20)$$

and

$$\int \Phi_{emission}(\lambda)d\lambda = ERE * \int abs(\lambda)\Phi_{excitaion}(\lambda)d\lambda \qquad (21)$$

Thus

$$QFLS = q * iV_{oc} = k_B T \ln\left[ERE\frac{\int abs(\lambda)\Phi_{excitaion}(\lambda)d\lambda}{\int abs(\lambda)\Phi_{BB}(\lambda)d\lambda}\right]$$

$$= k_B T \ln\left(\frac{\int \Phi_{excitation}(\lambda)abs(\lambda)d\lambda}{\int \Phi_{298.15K\ BB}(\lambda)abs(\lambda)d\lambda}\right) + k_B T \ln\left(\frac{\int \Phi_{emission}(\lambda)d\lambda}{\int \Phi_{excitaion}(\lambda)d\lambda}\right) \qquad (22)$$

$$= k_B T \ln\left(\frac{J_L}{J_{0,rad}}\right) + k_B T \ln(ERE) = V_{oc,ideal} + V_{deficit,recombination}$$

It is important to use the actual absorption of the solar cell to calculate the ideal voltage. In the often used Shockley-Quisser limit, the assumption is that the bandgap acts as a step function for absorption and thus the recombination currents that define J_0 and J_L are step functions with wavelength. This would be the above $V_{oc,ideal}$ term if the absorptivity was 1 from wavelengths of 0nm to the wavelength corresponding to the bandgap energy and 0 after this. As discussed previously, real materials with defects and finite thickness do not behave in this manner, and thus J_L and J_0 will not reflect the idealized case, as discussed in literature [50, 51].

2.5.3) Quantum Efficiency

The quantum efficiency is a measure of how well photo-excited carriers are extracted into an external circuit, and is usually measured at J_{sc}. Each absorbed photon can produce exactly one electron-hole pair within the absorber. As such the QE is defined as the ratio of extracted electron hole pairs to incident photons of a given wavelength, and is always less than or equal to unity. Most commonly, this is presented as the external quantum efficiency (EQE) because weighted integration of this will allow for verification of the short circuit current density, as seen in equation 23 [87]. However, if an interested party is looking to examine losses to the short circuit current from recombination, the internal QE (IQE) can be calculated [87]. This is because the internal quantum efficiency is the ratio of extracted carriers to that which reached the absorber and thus interacted in a way that had a probability of producing an electron-hole pair. Typically, this is approximated as EQE/(1-R), however a more complete picture of carrier extraction from the carriers produced in the absorber would also consider parasitic absorption from free carriers or other contact layers with E_g small enough to absorb significant portions of the solar spectrum but unable to contribute to the current density. Free carrier absorption in the TCO is often what the difference between 1-R and EQE is attributed to across the region where

EQE is >85% in the cells shown in figure 23. In figure 23, a CdS/CdTe cell EQE is shown, demonstrating parasitic losses from the CdS for wavelengths less than 520 nm.

$$J_{SC} = q \int \Phi_{AM1.5G}(\lambda) EQE(\lambda) d\lambda \qquad (23)$$

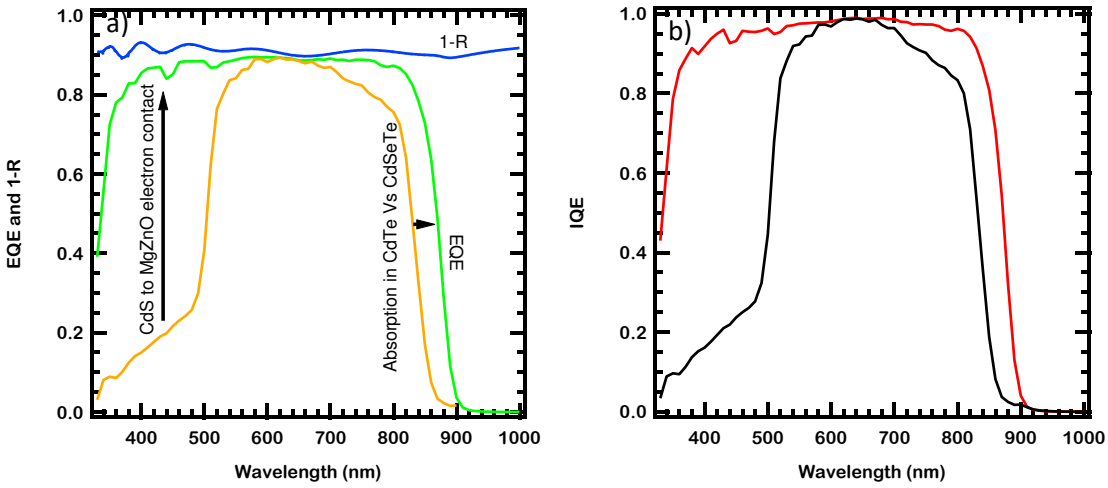

Figure 23: a) 1-R and EQE of a MZO/CdSeTe/CdTe/Te cell b) approximated IQE from the same data

2.5.4) Time Resolved Photoluminescence

As discussed when examining the concept of QFLS, the duration photo-excited carriers survive before recombining is one of the major factors. While a number of methods to determine this exist, the most common in thin film PV, and therefore CdTe, is time resolved photoluminescence (TRPL). In this method, using time-correlated single photon counting, a pulsed excitation is repeated and a single luminescent photon is counted as the signal. Sophisticated timing electronics determine the time difference between the excitation pulse and the emitted photon being sensed [89-90]. This is repeated many thousand times until a histogram of when the

photons are sensed after the pulse is developed, representing the distribution of how long carriers survive in the material.

Interpretation of this would seem straight forward, however it is plagued with difficulty. The continuity and Poisson equation must be used to model the behavior to get the most meaningful information from these results [93,94]. This is because the measurement is transient and so there is no simplifying assumption about carrier density distribution. In fact, generation is typically confined to the first micron of a many micron thick film, meaning that the locality of carriers and the time it takes to reach a quasi-equilibrium distribution are impactful on the measured results, and often forces a distinct “short lifetime” region and “long lifetime” region within the decay. The short lifetime is often assumed to be relating to the dynamics during this period prior to quasi-equilibrium, and the long lifetime relating to the decay of the excess carrier concentration while the absorber is in the quasi-equilibrium state [91]. This simplified view is OK in some cases such as double-heterostructures and films with minimal electric fields such as a low doped-bulk, but is complicated by strong electric fields. Additionally, the rate of recombination is different between different recombination pathways, each with it’s own dependance on the excess carrier concentration, and so different pathways for recombination will be dominant at different points as the excess carrier concentration decays. One method of keeping the complexity of a varying decay is presented in figure 24 by using local fits to produce a time-dependent fit (alternatively using the derivative works with less noisy data).

In spite of this, the measurement can be incredibly full of information with the appropriate combination of fitting and modelling, detailing specific rates for and locality for recombination processes. However, if one simply wants to be able to model the QFLS based on the time carriers survive and the doping density, they need a measure of the effective lifetime. While imperfect,

this is often approximated to be the decay constant at later times in the TRPL histogram, as this is when the distribution of carriers is assumed to be at quasi-equilibrium, and thus impacted by all pathways [91]. In this state, the effective lifetime, τ_{eff} is defined by the parallel sum of all recombination lifetimes, as found in equation 24 where τ_n represents that each SRH or surface lifetime is specific to a defect.

$$\frac{1}{\tau_{eff}} = \frac{1}{\tau_{SRH,1}} + \frac{1}{\tau_{Auger}} + \frac{1}{\tau_{Radiative}} + \frac{1}{\tau_{surf,1}} + \cdots + \frac{1}{\tau_n} \qquad (24)$$

Some terms can be lumped into single simplifying terms, by assuming that the set of contributing, although different, factors is uniform through the example. For example, τ_{SRH} is often cited as one term even though many defects contribute to so-called Shockley-Reed-Hall recombination, and similarly, surface recombination is usually included as a single term inclusive of the surface, or surfaces as the case may be without distinguishing between the different defects.

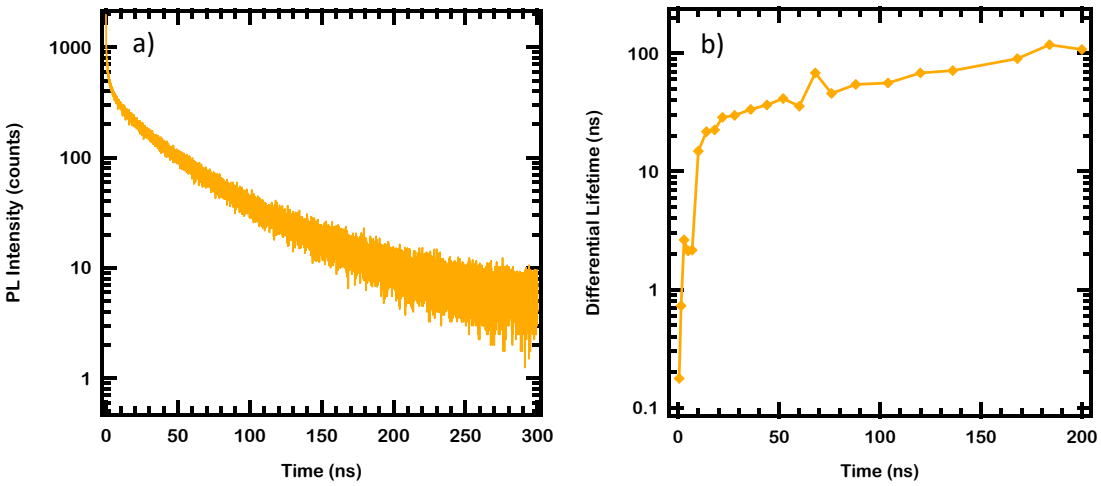

Figure 24: a) TRPL Decay of a MZO/CdSeTe/CdTe/Te cell b) Differential (using variable fit areas) lifetimeof the same cell demonstrating difficulty of listing a single number by TRPL fitting

After crystalline silicon, CdTe solar cells are second in both power production and manufacturing output [56]. CdTe, the binary compound, has a bandgap of ~1.5 eV, but it can be tuned to 1.4 eV through the addition of Se, which is quite close to that ideal found in the previous section [57, 58]. Additionally, it is a direct bandgap semiconductor, so it has a high absorption coefficient and as such cells are typically 2-8 μm thick [59]. This seems to be an ideal absorber, however the market dominant technology is polycrystalline as a result of this being the path to low cost manufacturing [56]. This inherently introduces many surfaces at which carriers can recombine unless appropriate measures are taken to mitigate this.

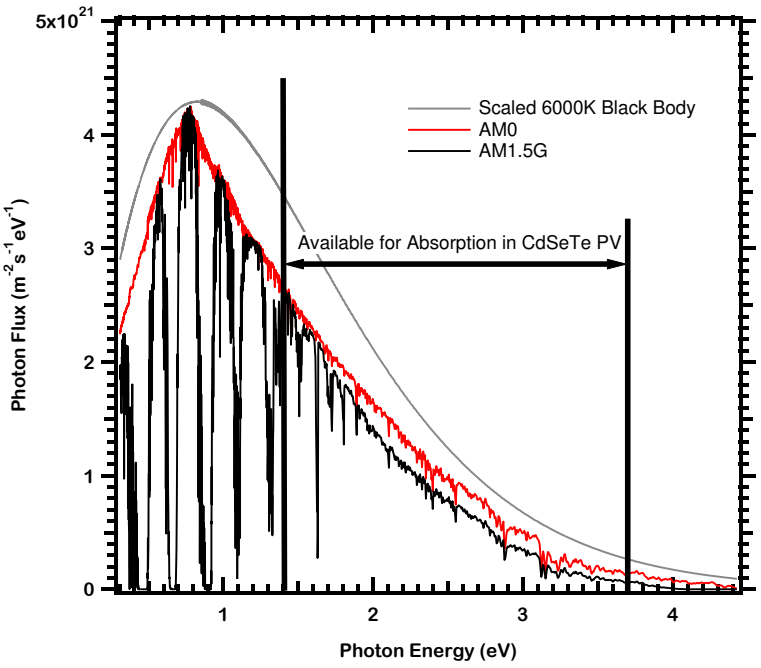

Figure 25: Available energy from the solar spectra for CdSeTe solar cells with a bandgap near 1.4 eV and a 3.7 eV window layer that does not contribute to extracted energy. AM spectra from [30].

For CdTe, this “bulk passivation” of the grain boundaries was one of the first major breakthroughs which allowed for a large increase in efficiency [60-63]. The binary CdTe system can be annealed in an environment with $CdCl_2$, either vapor or a deposited film, and the effects can be seen in figure 26. The results are two-fold: alterations to the grain structure and passivation of the grain boundaries [60-63]. First, during the anneal, Cl acts as a flux and the Cd-Te-Cl phase diagram shows a eutectic point dramatically reducing the melting temperature of CdTe [64]. This allows for fast self diffusion leading to recrystallization and grain growth, dramatically increasing the size and quality of the grains themselves, resulting in a reduction of grain boundary density and density of recombination active stacking faults within the grains [60-64]. Second, it places Cl at the remaining grain boundaries – typically there are still many as the grain growth typically brings grain size from <1 μm to 1+ μm or larger, still ~4 orders of magnitude smaller than the cell size – which has been shown to reduce the density of states within the bandgap, and thus reduce non-radiative recombination [62, 63 65]. There is also hypothesized “field effect” passivation where the grain boundaries become charged and form a depletion region, but there is no consensus as to the polarity of this charging, perhaps as it could be varied for different types of grain boundaries [66, 67]. There is however significant evidence that the grain boundaries act as conduits for conduction after the $CdCl_2$ anneal process [68].

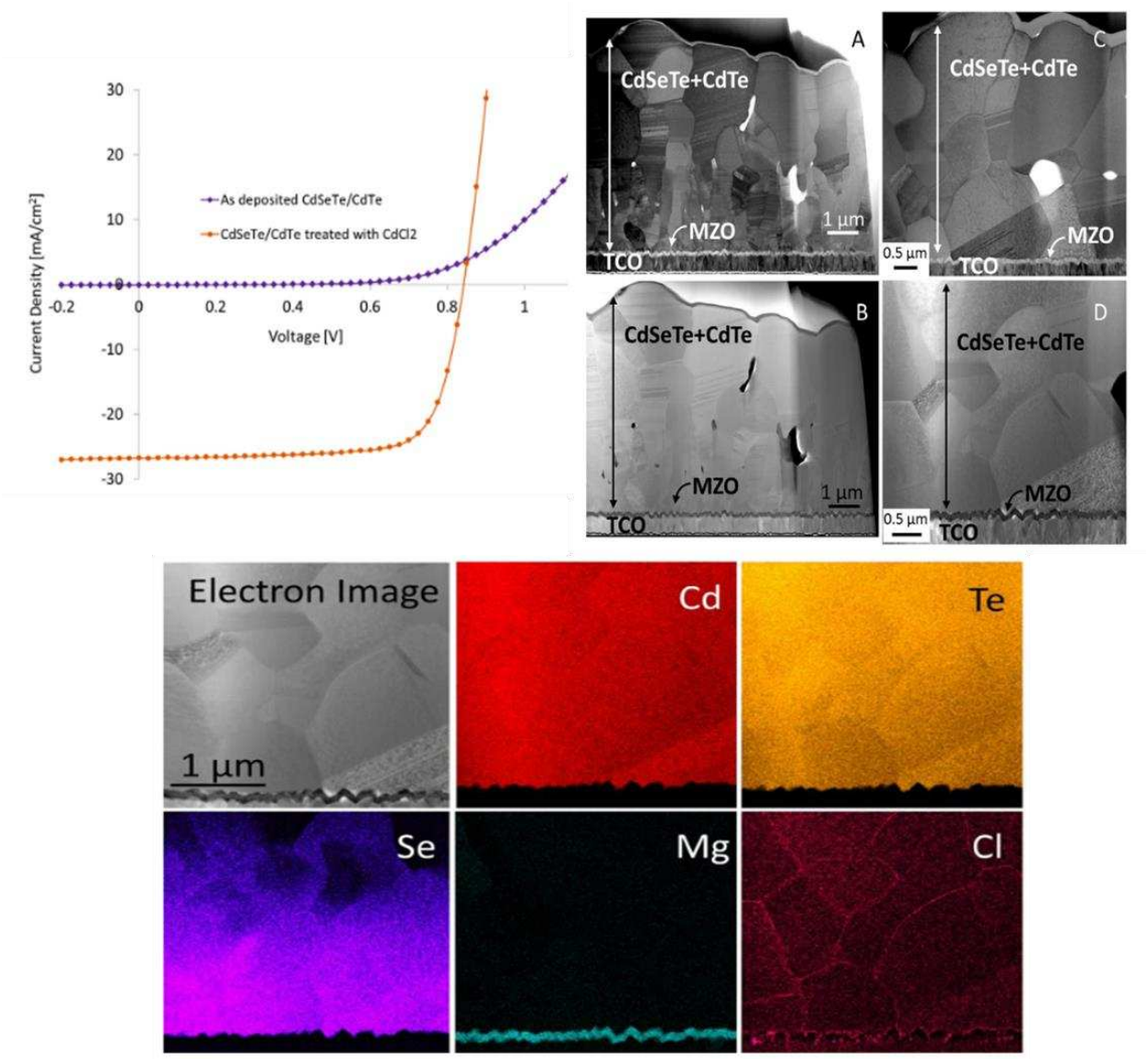

Figure 26: Effects of $CdCl_2$ passivation of CdSeTe/CdTe solar cell bi-layers from [63] showing improvement in device performance, reduced line defects and increased grain size and both Se diffusion and Cl at the grain boundaries.

In addition to the $CdCl_2$ treatment, the absorber quality has been dramatically increased by the addition of Se. The initial efforts to include Se into the absorber were to reduce the bandgap to ~1.4 eV, closer to that ideal from the detailed balance limit [57, 58]. This was accompanied by an exciting surprise; the addition of Se was accompanied by measurements of dramatically

increased carrier lifetimes [69-71]. While this effect is still under investigation it is clear that increasing Se content, up to replacing about 40% of Te sites in the lattice, increases the lifetime [71]. This may be due in part to bulk effects, but there is a growing body of evidence that the Se-Cl combination at grain boundaries acts more effectively than Cl alone to reduce the density of states within the bandgap at the grain boundaries as seen by the CL intensity in figure 27 below [72].

To gain a better understanding of what these effects have been, it is important to understand the defects in CdTe. There exist a number of grain boundary defects, and each is specific to the type of grain boundary, the relative orientations of the crystals, and the species that terminate the crystals at the grain boundaries. To simplify the picture, a number of studies by have examined various types of grain boundaries using DFT and electron microscopy to study the effect of Cl and other species on the electronic structure at the grain boundaries [151-155]. Due to the lattice mismatch the DFT efforts showed numerous states to fill the bandgap, meanwhile the effects of Cl and the combination of Se and Cl are shown to dramatically reduce the density of these states within the bandgap providing some evidence for how Se and Cl are effective at increasing the lifetime in CdTe based materials through grain boundary passivation [151, 152, 154, 155]. These types of defects are unavoidable in polycrystalline materials, and the understanding of how addition of species like Se and Cl can reduce the density of states within the bandgap at these interfaces is crucial to development of further passivation.

Although grain boundaries have been and continue to be the believed source of the majority of non-radiative recombination in CdTe cells, it is also important to understand the bulk defects. These are typically studied through DFT as well, and in particular, point defects with the potential to become shallow donors and acceptors (dopants) and native defects (vacancies,

defects related to the (mis)placement of Cd and Te within the lattice) are well studied [157, 160]. While many can produce shallow defects, it is clear that all dopant species can also produce deep defect when not coordinated properly in the lattice[123, 124, 157-160]. For example, in the case of Cu, the current most common dopant in CdTe technology, the dopant species, $Cu_{Cd,}$ sits relatively deep for a dopant at slightly more than 0.2 eV above the valence band, but Cu_i places states reported both deeper into the bandgap and shallower to the conduction band and in all can produce very short lifetimes with high concentrations of Cu [123, 124, 157-160]. Additionally, native defects if formed, all produce defects within the bandgap, although at varying energies. In particular, Te anti-site, Te vacancies, and both Te and Cd interstitials produce numerous deep defects, and although chlorine acts to passivate the grain boundaries, the presence of chlorine in the bulk crystals, especially when not coordinated in the Te cite, can form complexes that are more than 0.3 eV into the bands [157, 160]. Although some of these defects are not expected to form readily due to high formation energies, the formation energy is dependent on the stoichiometry, and even small stoichiometric changes toward the group II or group VI can encourage the formation of otherwise unfavorable defects [123, 124, 159, 160].

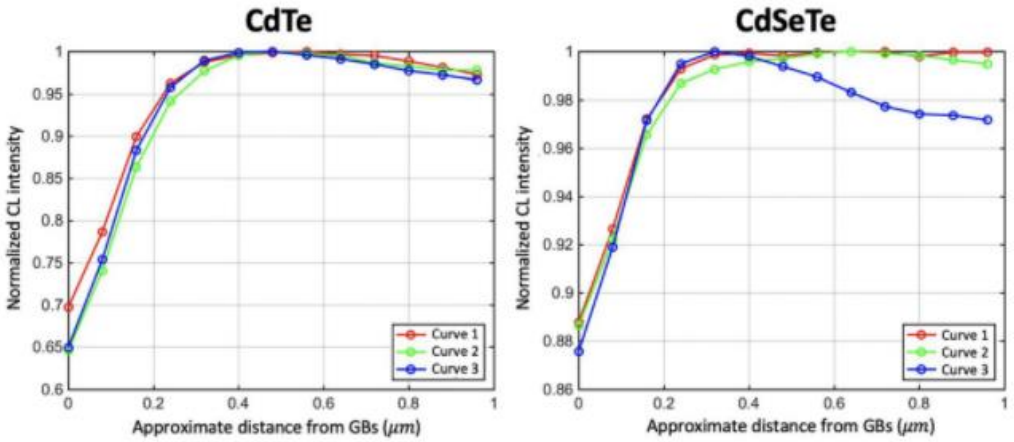

Figure 27: CL intensity scanned across grain boundaries in CdTe and CdSeTe from [144]

Despite the defects, with Se alloying and Cl passivation the absorber has reached excellent quality despite it's polycrystalline nature. In typical cells the structure is more complex – this Se incorporated absorber at the "sunny side" of the cell with the Se content grading down to near 0 at the "dark side" of the cell, which leaves nearly binary CdTe. Despite CdTe's measured smaller lifetimes, the cells without CdTe in the bulk semiconductor material underperform their graded counterparts [73]. This is believed to be in effect because of the bandgap grading forces minority electrons toward the front of the device [73].

Now examining the asymmetry of conductivity, the electron contact has been a source of device improvement in recent years. First, the development of more transparent electron contacts has been beneficial to device performance by allowing for a greater generation current in the absorber since the illumination occurs through the electron contact in the standard structure. This was achieved by switching from the historical CdS – which shows great electron conduction but with a bandgap of ~2.42 eV parasitic absorption of high energy photons is unavoidable – to

"oxygenated" CdS, the oxygenation of which increased the bandgap considerably shifting the absorption edge further toward the high energy portion of the spectrum [74, 75]. Additionally, $Zn_{1-x}Mg_xO$ (MZO) has become popular in recent years within the research community. MZO has a tunable bandgap and band-alignment with the absorber [76-78]. MZO's much wider bandgap (>3 eV) mitigates parasitic absorption across that portion of the spectrum with a large photon flux, and the band alignment is believed to be crucial to achieving somewhat increased voltages [76-78]. Specifically, the large valence band offset reduces the number of holes that can reach the TCO and recombine there, while the tunable offset in the conduction band allows for reduction of the rate of recombination at the absorber interface even with a large surface recombination velocity through local band bending [76-78]. MZO, however, has its drawbacks – it is believed to require photoconductivity from excitation by UV photons to gain the full necessary electron conductivity to operate at its best [79]. The improvements from a more transparent electron contact and Se alloying can be seen in the IV and EQE curves of figure 28, which is from [85]. Additionally, in figure 29 the record cell using such advancements produced by CSU is found.

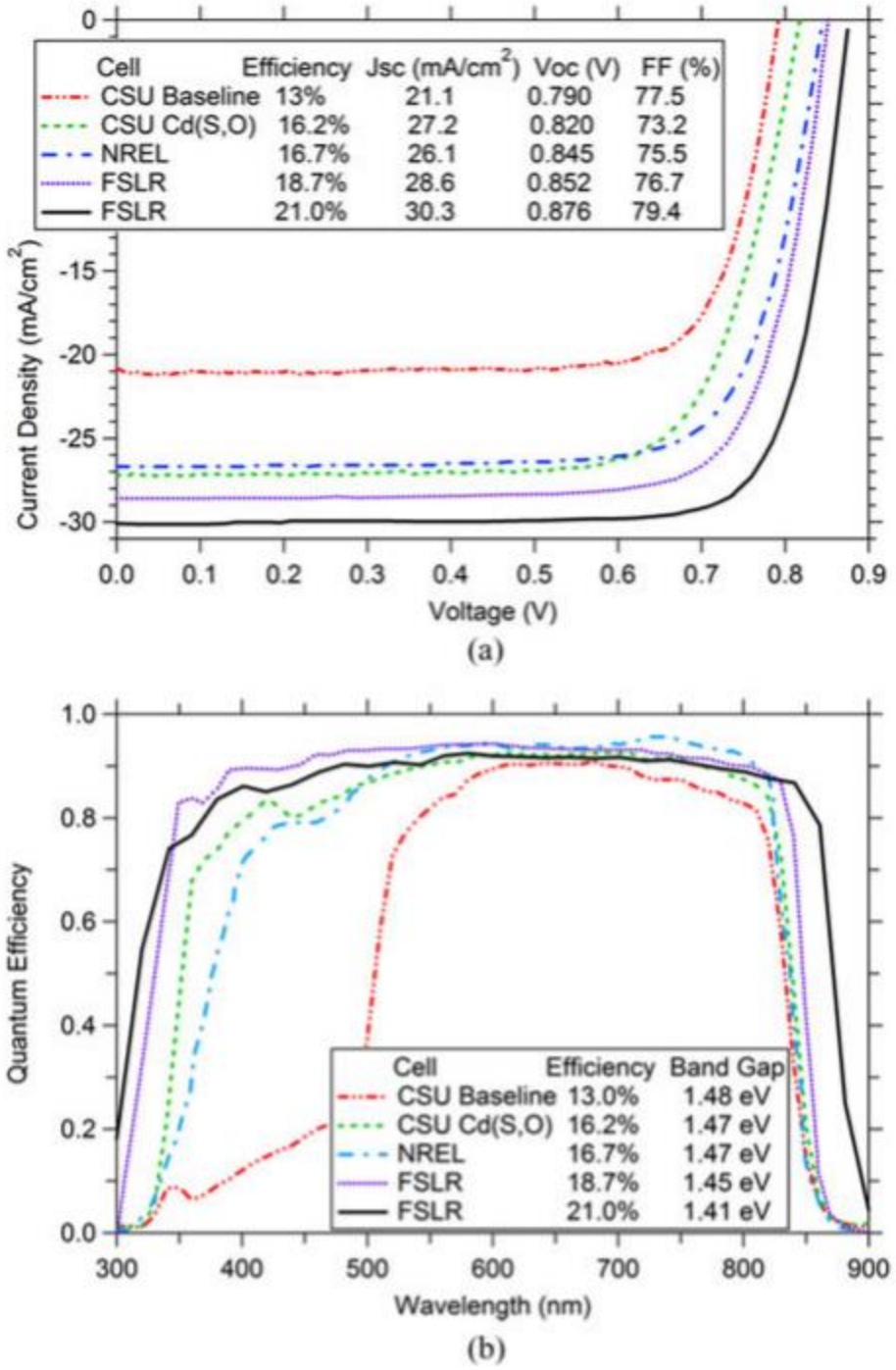

Figure 28: Some notable CdTe-based solar cell's IV (a) and EQE curves (b) as of 2016. [85]

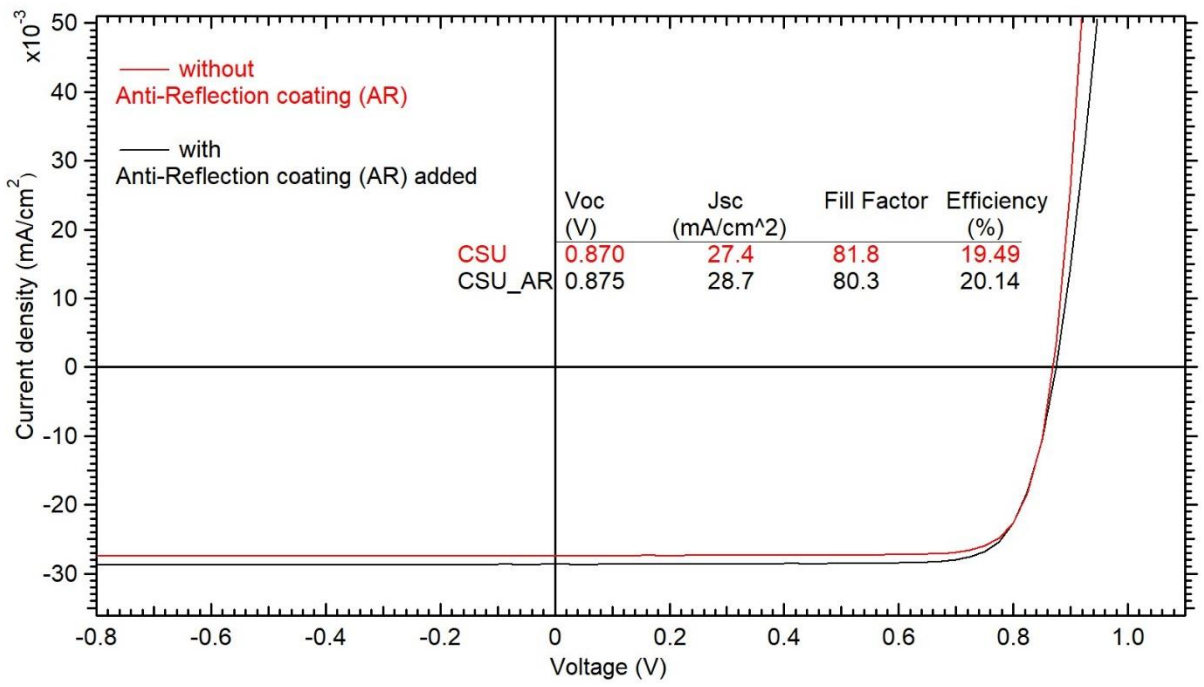

Figure 29: Champion Cell at CSU using the CdSeTe/CdTe absorber and a MgZnO transparent electron contact, both with and without an anti-reflective coating. Fabricated by Tushar Shimpi.

In CdTe the hole contact has always been a major issue. Typically – based on the p/n junction model – efforts were squarely focused squarely at reducing the "back barrier [80, 81]." This "barrier" is essentially the formation of an opposing depletion region to the one formed at the front between the TCO/MZO and the absorber by the formation of a Schottky diode with the metal, and is "blocking" to hole extraction as well as encourages electron current into the hole contact [80, 81]. A more updated view of this would be reduced conductivity to holes and increase in electron conductivity due to depletion from the metal. This is a difficult issue to overcome in CdTe-based PV because few metals have a fermi-level aligned with the hole fermi-level in CdTe, a condition required to maintain the hole conductivity at the back. This can be seen in the depth of the two fermi-levels below the vacuum level. This, in a metal, is typically defined by the work function, or energy requirement to excite an electron from the surface of the

metal to the vacuum level [26, 27]. Due to the large number of free electrons forcing the average electron at the surface to reside very close to that in the bulk, it is rarely significantly different than that of the bulk fermi-level, and it most metals it is less than 5 eV. In the case of semiconductors, it is more appropriate to talk about the fermi-level relative to the electron affinity – or the energy difference between the minimum in the conduction band and the vacuum level, as surface effects are more likely to change the average energy of electrons relative to vacuum due to the typically lower carrier concentrations. However, no matter how it is examined the hole fermi-level in CdTe is typically thought to be 5.7-5.9 eV below the vacuum level, while most metals are less than or close to 5 eV below vacuum level [82]. This mismatch is the source of the Schottky diode "back barrier."

Attempts to mitigate the effect of this back barrier have ranged from highly doping the back surface of CdTe to finding alternative inter-layers between the metal and the CdTe [81, 83, 84]. The first method was the one initially developed – a Cu doping process was incorporated, and the effect of the back barrier was mitigated significantly, preventing in most cases the characteristic s-shape in the current-voltage behavior of the devices by allowing transport from the CdTe to the metal with minimal resistance [79, 51]. In addition to this, the current state of the art devices either use a Te or a ZnTe:Cu interlayer between the semiconductor and the metal [81, 83, 84]. Both of these are believed to have a very large carrier concentration to allow tunnelling from that material to the metal and exists at the proper energy to mitigate the "barrier" in the CdTe itself, as seen in figure 30 [81, 83, 84]. ZnTe is believed to have the additional benefit of its wide bandgap and band alignment producing somewhat of a mirror image of the MZO on the other side – a barrier to electron conduction to the metal [81, 83, 84].

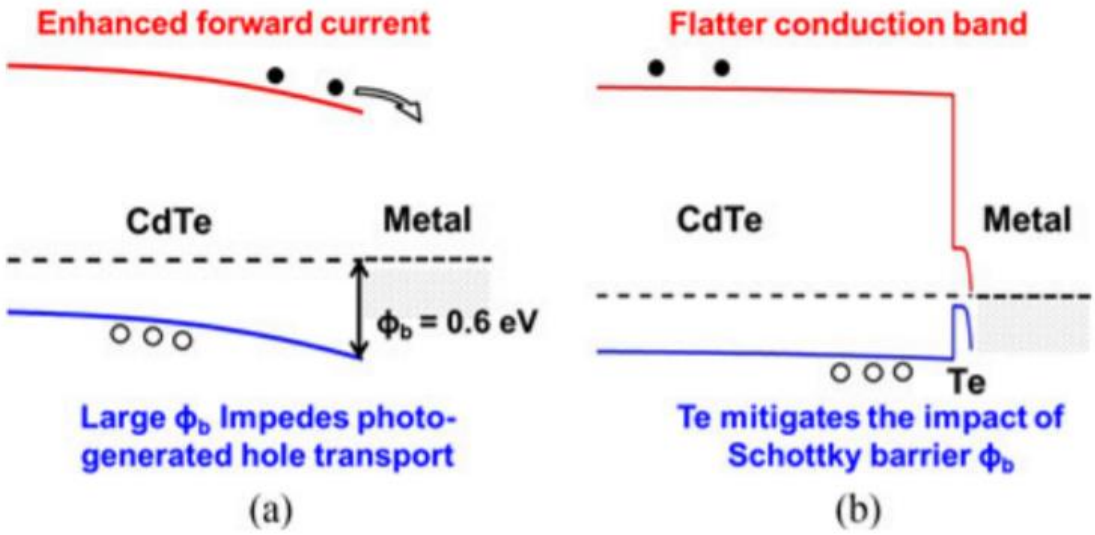

Figure 30: Demonstration of the back barrier at the CdTe hole electrode and how a Te layer reduces it. [83]

The result of all of this work has been highly efficient cells – the record being 22.1% power conversion efficiency – but cells that remain well below the theoretical limit for the bandgap [85, 86]. Thorough analysis of the technology has discovered that the current production in the best cells is >90% of the theoretical limit [85]. This leaves the V_{oc}, and with it, although to a lesser extent the fill factor (maximum power normalized to the theoretical power if the current from J_{sc} and voltage from V_{oc} were achieved simultaneously – a measure of how square the current-voltage dynamic is) as the major deficits and in fact V_{oc} is only 75.8% of the limiting value in the record cell [85].

CHAPTER 4: INVESTIGATION OF PASSIVATION IN CADMIUM TELLURIDE BASED SOLAR CELLS

The internal voltage of a CdTe-based cell had not been measured to the knowledge of the authors, and use of understanding the difference between the internal and external voltage was not to be found. It is possible that this is because the radiative efficiencies of these materials has only recently been high enough for reliable measurement on relatively low cost systems, but it is more likely the reliance on the use of the diode equation to characterize effect of the cell's recombination behavior on voltage. In publications where the ERE was measured, the corresponding internal voltage was not determined [95, 96]

This is all in spite of the use of this to great benefit in other PV technologies [97-100]. In c-Si, they acknowledged early on that reaching the SQ limit for their material was impossible because the indirect bandgap leads to Auger recombination [101, 102]. Inherently, this eliminates the possibility of reaching the SQ limit since in this case, not all recombination will be radiative no matter how good the crystalline quality is or how well passivated the interfaces are. While that is a discussion of *internal* radiative efficiency (IRE), it is well known that an ERE of 100% requires an IRE of 100%, and thus the IRE below 100% limits the ERE, and thus iVoc. In Si, they rarely measure the actual radiative efficiencies because the implied voltage can be accessed through simpler measurement of photo-conductivity [97].

In III-V materials, the ERE is of utmost importance, since these materials are approaching the SQ limit in efficiency. A wealth of literature discusses the possibility of producing ERE of near 100%, requiring proper optical design [103-105]. Since the thermodynamic analysis which the

SQ limit was based on requires exchange of photons through only one surface and radiative recombination has an equal probability of emission in any spherical direction, reabsorption and re-emission processes of photons directed outside a narrow escape cone are required to reach ERE approaching 100% for a solar cell, and thus the internal voltage can only approach the upper limit with appropriate optics.

4.1) Implied Voltage in CdTe Solar Cells

The first order of business was to understand these effects in our current vernacular, namely, lifetime and doping for cases with and without photon recycling, and for bandgaps that are relevant to CdTe. A model of QFLS for a semiconductor in a quasi-equilibrium state when under steady state illumination was created to demonstrate trends in QFLS as a function of carrier lifetime and equilibrium carrier density. Although in most solar cells there is a space charge region (or multiple) in the cell, rendering the equilibrium concentration variable, this is a good approximation. For a low doped cell where the depletion region extends through more of the bulk, the excess carrier concentration will be the major factor in the QFLS. In a highly doped cell, depletion regions are quite narrow and the bulk of the cell is in the quasi-neutral state in equilibrium, so the assumption is valid for the vast majority of the absorber. The implied voltage or QFLS is calculated assuming all excess carriers are homogenously distributed in the bulk, a condition similar to the diffusion length greatly exceeding the thickness of the semiconductor. In this scenario, the excess carrier concentration can be calculated from the theoretical current density based on the semiconductor bandgap divided by the thickness of the semiconductor. Because this condition assumes there is no extraction of excess carriers, the excess concentration of both electrons and holes should be homogenous as well under steady state illumination, which implies that the excess carrier concentration of both is equal. Finally, the steady requirement for

steady state implies that the rate of recombination is equal to the generation and thus the excess carrier concentration can be calculated knowing the effective lifetime of photo-electron-hole pairs as in equation 25 where Δn and Δp are the excess carrier concentrations, G is the generation rate, and τ_{eff} is the effective lifetime.

$$\Delta n = \Delta p = G\tau_{eff} \qquad (25)$$

The QFLS is then calculated by equation 26, with n and p being the concentrations of electrons and holes (in one case equal to the excess carrier concentration and the other being the sum of the excess and equilibrium concentrations), n_i^2 being the square of the intrinsic density of states, k_b being the Boltzmann constant, and T being the absolute temperature of the semiconductor.

$$qxiVoc = QFLS = k_B T \ln(\frac{np}{n_i^2}) \qquad (26)$$

Figure 31 shows a contour plot of QFLS as a function of carrier concentration and effective lifetime for various approximate bandgap energies commonly found in CdTe based cells. There are a number of general phenomena that are apparent from this plot which are worth including in discussion of how to increase QFLS. First of all, at sufficiently long lifetimes, photon recycling dramatically increases the effective limit of lifetime (how long the energy survives in the cell, rather than just a single carrier's lifetime) and thus QFLS, indicating that a reflective back surface or interface would be ideal to implement. Notably, the theoretical limit of QFLS calculated by the detailed balance method is only attainable when the lifetime is appropriately adjusted for when the photons from recombination are only emitted through the front of the cell.

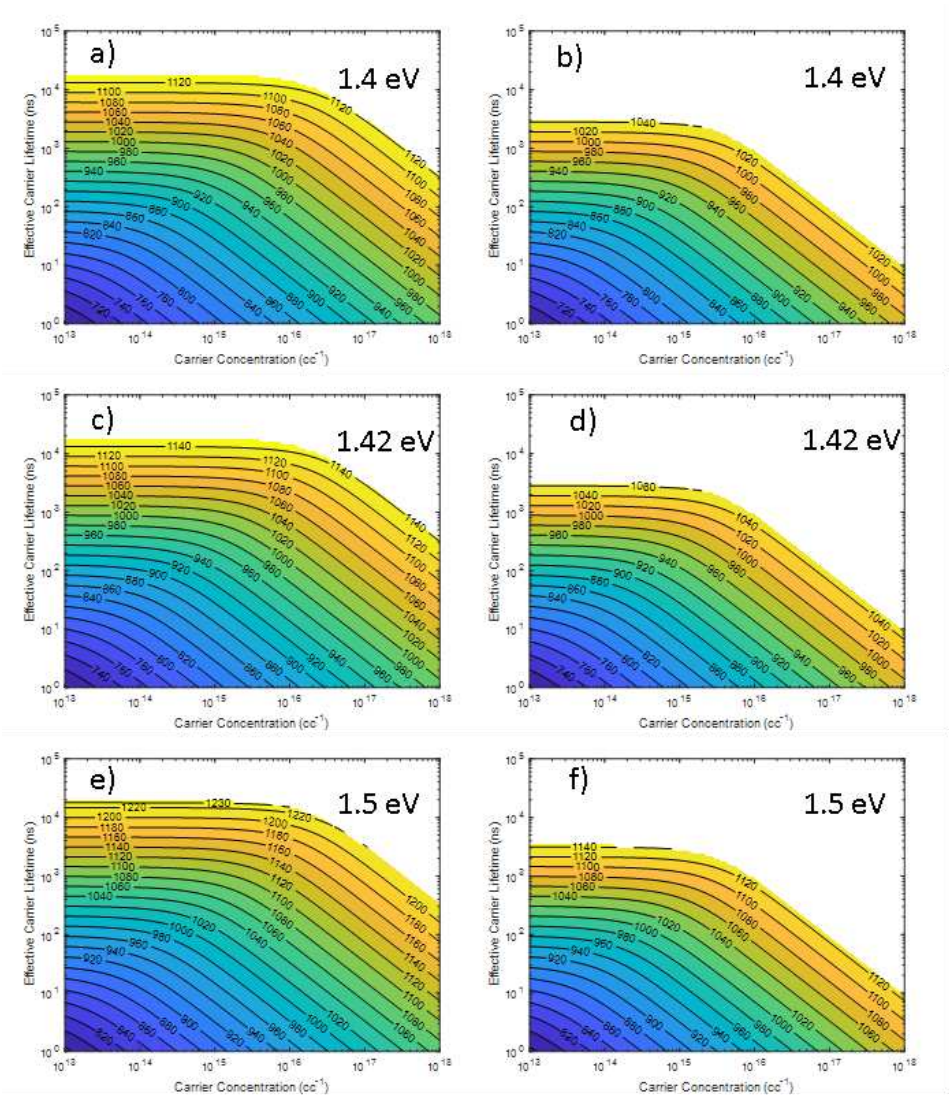

Figure 31: CdSeTe at 1.4 eV with and without photon recycling (a) and (b) respecively. Subsequently (c) and (d) represent the same conditions for a 1.42 eV CdSeTe, and (e) and (f) for a 1.5 eV CdTe. Generation currents used are 29 mA/cm^2, 28 mA/cm^2, and 26 mA/cm^2 for the different absorbers in ascending energy gap order, with carriers assumed to be uniformly distributed in a 2 micron thickness. The edge of the colored regions indicates the material limit (accounting for both radiative and auger recombination), with an apparent increase in the effective limiting lifetime due to photon recycling as the energy of the initial photon from the sun remains useful through a number of excitations.

Next, there are two obvious regions of the plot, one where the cell operates in low injections (excess carrier concentration << equilibrium carrier concentration) and one where the cell operates in high injection (excess carrier concentration >> equilibrium carrier concentration)

with a transitional regime between the two. In the case of low injection, the contours are diagonal because one of the quasi fermi-levels is effectively set by doping and the other is set by the injection. However, when operating in high injection, the quasi-fermi-levels are both primarily set by the injection and thus the contours are flat as doping has minimal impact. Consequentially, the transition regime is rounded on the plot because effects of both doping and injection are significant for the quasi-fermi level of the carrier which is present in greater numbers at equilibrium.

It is also apparent that the limit for effective lifetime depends on the state of injection, high or low, as the limiting lifetime follows an identical trend to the contours of iVoc. This makes sense because the rate of radiative lifetime is governed by the equation 27 where R_{rad} is the rate of radiative recombination, β is the radiative coefficient, n_0 and p_0 are the equilibrium carrier concentrations and Δn and Δp are the excess carrier concentrations. To simulate perfect photon recycling, this rate of radiative recombination can be multiplied by the escape cone for emitted photons, which is about $1/4n^2$ where n is the absorber's index of refraction, although this should not be interpreted as a single electron hole pair's lifetime, but the lifetime of useful energy from a single photon due to multiple reabsorption events [103]. From this relationship and knowing that the rate of recombination is equal to the excess carrier concentration divided by the lifetime, you can derive the relationship in equation 29 for the lifetime assuming that only one carrier has an equilibrium concentration and the np product under illumination is much greater than $n_0 * p_0 = n_i^2$, and the excess concentration of holes and electrons are the same (in this case solved for a p type material). When in low injection, the radiative lifetime is then effectively determined by doping ($\tau_{rad} = 1/\beta p_0$), in high injection by the excess carrier concentration ($\tau_{rad} = 1/\beta \Delta p$), and in the transition the full relation must be used. The important consequence of this is that in the

regime of low injection, the "same lifetime" for a cell with greater doping is a misleading statement, as it then has to operate closer to the radiative limit, and thus cannot have increased rates of non-radiative recombination due to bulk deep defects or non-passive surfaces. This renders the modest increases in lifetimes from historical cells with dramatically increased doping, as the modelling guidance for increasing voltage suggests, non-trivial despite appearing more attainable than dramatically increased lifetimes at first glance.

$$R_{rad} = \beta[(n_0 + \Delta n)(p_0 + \Delta p) - n_0 p_0] \qquad (27)$$

$$\Delta n = \Delta p \qquad (28)$$

$$R_{rad} = \frac{\Delta n}{\tau_{rad}} \rightarrow \tau_{rad} = \frac{1}{\beta(p_0 + \Delta p)} \qquad (29)$$

Examining state of the art CdSeTe and CdTe cells, Capacitance-Voltage measurements suggest that CdTe and CST/CdTe absorbers have carrier concentrations in the high 10^{13} to low 10^{14} cm^{-3} in nearly all historical devices, with lifetimes in the range of 2-10 ns for binary CdTe and up to a few hundred ns for the best cases of CdSeTe/CdTe absorbers[106-110]. Although there are simplifying assumptions that went into producing those plots, it is clear that these numbers allow for QFLS numbers between 800 and 900 mV, which matches or slightly exceeds the range of typical external V_{oc}, suggesting that these cells are currently limited primarily by the QFLS and not selectivity. It is also worth noting that this is in agreement with the common notion that the longer lifetimes in CdSeTe is what has enabled the voltage to remain in the same range despite the reduction of the energy gap. In any case, the useful nature of calculation of the implied/internal voltage is yet to be fully explored in CdTe photovoltaics, and as such, these measurements and insights are applied here and the learning will be leveraged to move the technology toward.

4.2) Fabrication of and Potential Material Issues in Colorado State University's Baseline Cells

Although the general structure and typically identified problems in CdTe-based solar cells was presented in the introduction, it is worth re-examining this structure in the light of implied voltage as determined by ERE. At CSU, the baseline structure of a cell starts with commercially available TEC10 (soda-lime glass with a ~400 nm SnO_2:F transparent conducting oxide (TCO) pre-deposited on a 80 nm barrier to Na diffusion composed of two 40 nm layers of intrinsic SnO_2 and SiO_2. On this TCO, a 100 nm film of $Zn_{1-x}Mg_xO$ (MZO) is deposited by planar magnetron sputtering at 140 W from a 4 in. diameter target containing 11% MgO by weight in an ambient of 5 mTorr maintained with a flow of Ar and O_2 maintained to be 97% and 3% of the flowrate respectively [76]. After this step, the substrate is moved to a separate chamber in which the absorber is deposited and the post-deposition $CdCl_2$ step is carried out. The absorber deposition is done by an automated set of close-space sublimation (CSS) processes occurring in an environment of 40 mTorr N_2, where the substrate is transferred between various sources and heaters by a computer controlled arm with linear movement between the stations and rotational movement into the stations [111]. All heaters and sources are graphite, and heat transfer to the substrate is primarily radiative in nature. The TEC10/MZO stack are first pre-heated for 140s between two heaters at 620°C, then moved into the source containing $CdSe_{0.4}Te_{0.6}$ at 575°C with a top heater at 420°C to set the substrate temperature during deposition. Following a deposition of 500 nm of this material, with the thickness determined by the dwell time and deposition rate, the stack is moved into a CdTe source at 555°C with a top heater at 500°C for a 3 μm deposition. Immediately following this, the stack is transferred into a $CdCl_2$ source at 450°C with a top heater at 420°C for 600 seconds, followed by an anneal for 1200 seconds between two heaters at

400°C. After the substrate is allowed to cool 180s in the same ambient conditions, the sample is removed from this tool and transferred to a separate vacuum chamber with 3 linearly aligned sources for a Cu doping process, with the sources and ambient being near identical in design to those in the absorber deposition and $CdCl_2$ processing chamber. The stack is re-heated between two 330°C heaters for 120 seconds, then transferred into a source containing CuCl at 190°C with a top heater at 170°C for 280 seconds. Prior to removal from the chamber the sample is annealed between two heaters at 200°C for 560 seconds. To assist hole extraction and reduce the "back-barrier," the cells have 30-40 nm of Te evaporated on the now room-temperature substrate in a separate chamber, deposited between 3 and 10 Å/s, prior to application of the electrode. The electrode used for baseline cells at CSU is a spray-coated set of two films [111]. The first is a relatively thin layer of polymer containing carbon, and the second is a thicker (to encourage current spreading) layer of a polymer containing nickel. This structure typically produces 16-18% cells, although it has produced cells in excess of 19% (20% with an anti-reflective coating on the glass surface).

In spite of this, the structure is not ideal. Prior to analysis of the internal voltage with ERE, it had been noted that the cells often show voids under advanced characterization (TEM) in the CdSeTe region of the devices, including a publication in Nature Energy [112]. Images clearly show a large density of voids in the CdSeTe portion of the absorber, indicative of less than ideal material properties despite the increased lifetimes [112]. Voids leave free surfaces, which generally have high recombination rates due to the abrupt disruption of the crystal lattice creating deep defects.

Voids are often caused by two mechanisms: 1) non-ideal deposition and 2) significant material changes during post-deposition processing. The first option is well known in the thin film deposition industry, and in fact is a prominent feature of "structure zone" theory of thin film

depositions by physical vapor deposition [113]. In this theory, the surface mobility of ad-atoms is modulated by the substrate temperature, with reduced temperatures causing the depositing atoms to stick where they land. This often ends up causing “shadowing” effects where places that see more atoms at first due to normal spatial fluctuations grow marginally faster. The faster initial growth causes atoms to land on that growth and stick, further reducing deposition behind the feature by blocking the line of sight for the impinging adatoms.

Significant material changes from post-processing are known for CdTe-based systems, especially during the $CdCl_2$ activation step [60-64]. However, these large changes are often beneficial for the material properties with Cl acting as a flux for recrystallization, removing stacking faults and growing grains [64]. However, in special cases such as CdMgTe and CdZnTe, this process is detrimental and effectively removes the ternary element from the grains. Especially in the case of CdMgTe this ends with the formation of voids through the material to accommodate the reduction of material within the bulk [114-118]. However, this appears to be the result of a high favorability for formation of $MgCl_2$ over MgTe, as demonstrated by the calculation of the gibbs free energy of reaction [119]. Additionally, in the CdSeTe cells this process induces diffusion of Se, but it is observed through the bulk of the grains, even when assisted by grain boundary diffusion, rather than leaching the Se from the grains and allowing it to leave by resublimation off the back surface [69-71]. This ends with a diffused region of CdSeTe between the CdSeTe of composition it is deposited with and the binary CdTe at the back of the devices, but no net depletion of Se from the full structure.

Another material consideration is in the change of phase present in CdSeTe from hexagonal at high Se concentrations to cubic at lower concentrations [57, 58]. However, this is highly unlikely as the cause of voids graded region of CdSeTe/CdTe structures post-$CdCl_2$ would act as a strain

relief in the lattice between the higher Se concentration CdSeTe to the CdTe. Additionally, CdSe and CdSeTe with a higher Se concentration is more densely packed than CdTe, and void formation is related to increased densification rather than decreased as would be expected from the transition caused by an increase in Te over Se due to the smaller lattice constants [57, 58]. Reduced densification typically leads to highly strained films or adhesion issues. However, it has been shown that the hexagonal phase in the absorber is detrimental to device performance [120]. In fact, the $CdCl_2$ process, rather than promote voids from the phase change, is thought to eliminate this detrimental structure by way of the previously listed benefits of the $CdCl_2$ induced re-crystallization in CdSeTe/CdTe films.

This leaves the most likely option the as deposited film forming with voids. In line with the theory and the structure zone model, a simple experiment to examine the as deposited properties would be to vary the temperatures of the source and the substrate during deposition. Increased temperature of the source increases the flux of ad-atoms impinging upon the deposition surface, locking previous ad-atoms in place more quickly. Alternatively, increased temperature of the substrate increases the surface diffusivity of ad-atoms, allowing them to migrate across the depositing surface and find more ideal locations to sit in the forming lattice, and reducing the possibility of shadowing effects.

4.3) Investigation of Absorber Deposition[1]

The first look was at the change in deposition rate of the CdSeTe with variations in both substrate temperature and source temperature. This data can be found in figure 32. The reduction in deposition rate follows the exponential nature of the vapor pressure of materials with increased temperature. The decrease in deposition rate with increasing substrate temperature

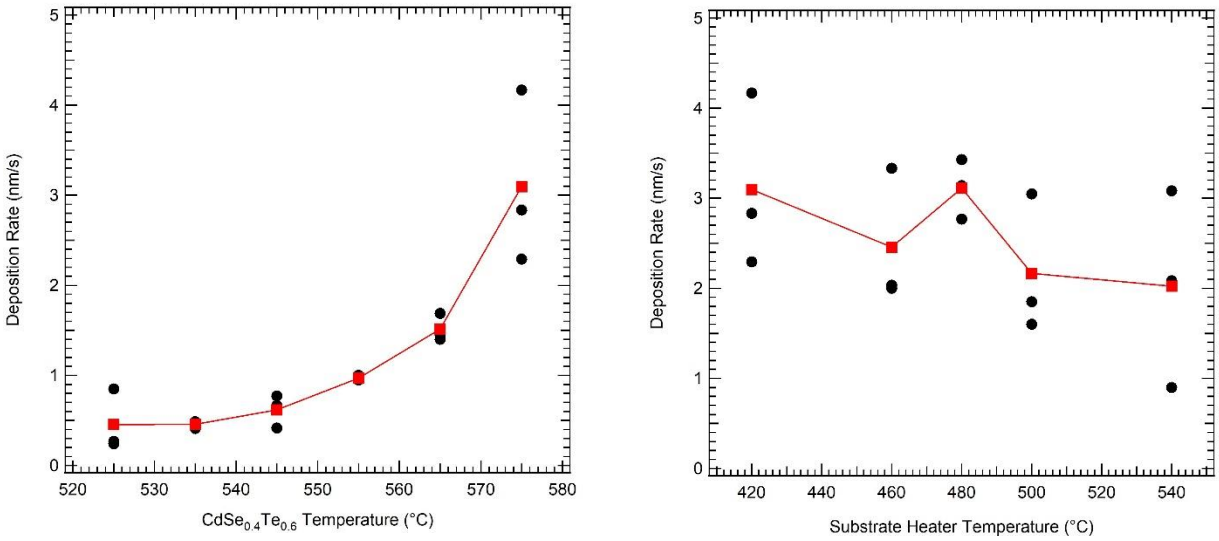

Figure 32: CdSeTe from a source containting 40% CdSe deposition rate vs a) Source temperature, b) substrate heater temperature.

(here controlled by the temperature of the substrate heater, actual temperature will be slightly less) is less clear. It could be either due to the increase in surface mobility smoothing the apparent vertical growth into the horizontal plane, but it similarly could be caused by an increased rate of re-sublimation due to the increased temperature of the substrate.

From here, we decided to focus on a variation of the top temperature, and therefore the substrate temperature. There was a clear indication that this temperature would affect the film, both by

[1] Work in this section anticipated to be published in Danielson, A., **Reich, C.**, Bothwell, A., Drayton, J., Shimpi, T., Sites, J., & Sampath. W.S. A Comprehensive Material Study of CdSeTe Films Deposited with Differing Selenium Compositions. *Thin Solid Films*, (Under Review)

theory and by the change in deposition rate, and furthermore, the less pronounced drop in deposition rate from top temperature changes meant that it was more viable for the fast manufacturing of CdSeTe films, a necessary attribute for cost effective solar cells based on this material.

We then used X-Ray Diffraction (XRD) to examine any material changes that may have accompanied the changes in substrate temperature. The diffraction patterns can be found in figure 33 with a focus on the region of the pattern that corresponds to either the (111) plane in cubic zinc-blende CdSeTe, or the (0001) plane of hexagonal CdSeTe. It has been shown that CdSeTe's peak shifts with increased Se until the formation of the hexagonal phase (and thus peak in an XRD spectrum) forms and continues to shift [57, 58]. It is apparent that previous standard top temperature, and even increased top temperatures to a certain point, produce a film with both phases present, but increased top temperature forms a film which produces only the ideal cubic structure, within the ability of XRD to detect. While this suggests that the material quality of the hotter deposited CdSeTe is greater, it is worth remembering the recrystallization that occurs during $CdCl_2$, and thus it was not conclusive that a hotter deposition of CdSeTe would result in a different amount of cubic vs hexagonal CdSeTe in the final cells. It did, however, indicate that there was likely a reduction in necessary post-processing. Additionally, with the standard post-processing, it produced greater PL intensity indicating that there is indeed greater film quality in the final films resulting from higher quality initial deposition as seen in figure 34.

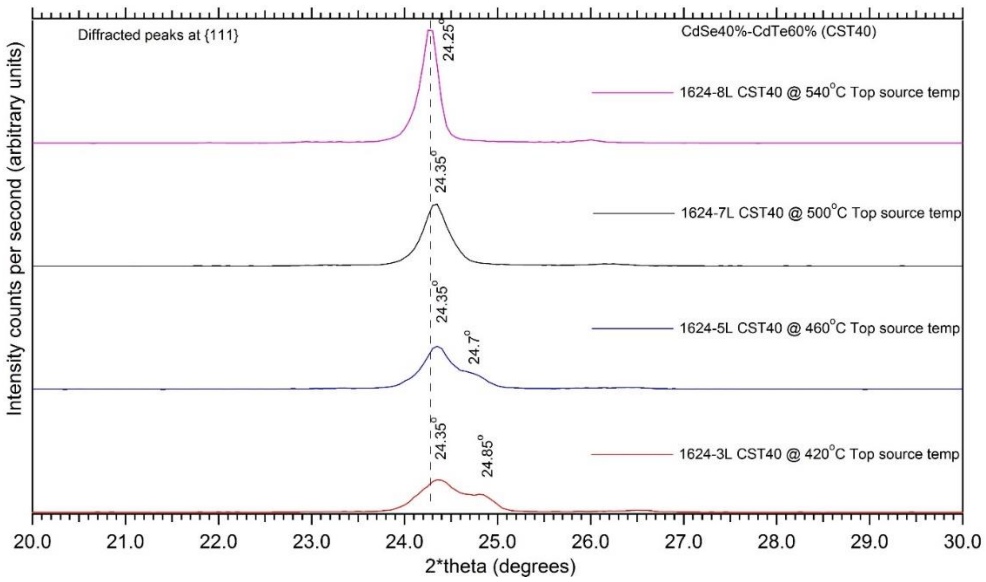

Figure 33: XRD of CdSeTe films from a CdSeTe source containing 40% CdSe with varied substrate heater temperature. Measured by Tushar Shimpi

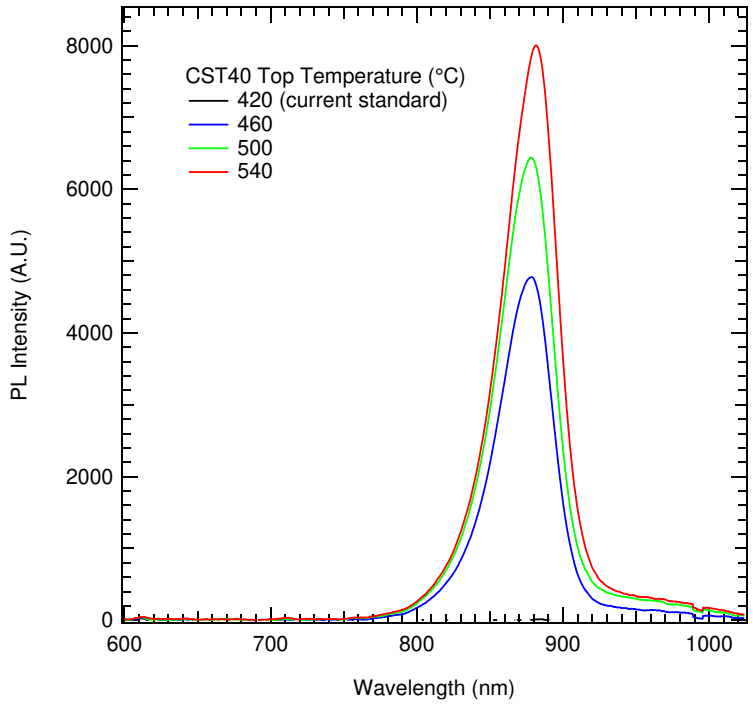

Figure 34: Photoluminescence Spectra of CdSeTe films deposited with Different Substrate Temperatures

Next, we examined the morphology of the films with varied top temperature through SEM imagining as the initial indication that prompted the investigation was the presence of voids in the cells measured by TEM. The images are found in figure 35 with the corresponding substrate heater temperature labelled. It shows quite clearly that the standard conditions produced a set of pillar-like structures with spaces between them. While these spaces likely do not completely remain after the deposition and diffusion with CdTe, they are strong evidence for the origin of voids in the CdSeTe region with standard processing since shadowing effects are expected. However, we did not only want to identify the origin of the voids, but also see if any alternative processing was adequate to eliminate their presence in the resulting cells. As such, it was a welcome observation in line with PVD theory that the hotter substrate temperatures (hotter top temperatures in the figures) first transitioned to coalesced grains then to large grains greater than

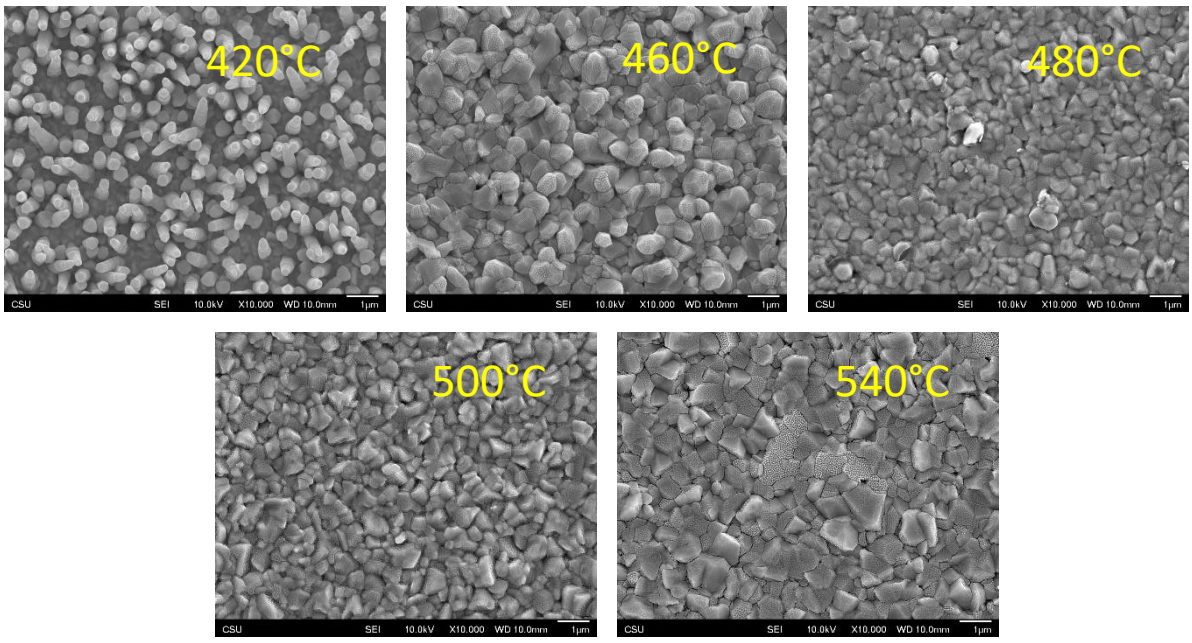

Figure 35: SEM Images of CdSeTe deposited from a CdSeTe source containing 40% CdSe with varying substrate heater temperatures. Images taken by Adam Danielson.

a micron in size. This indicated that the voids could be eliminated by increasing the top temperature, while keeping the deposition rate of the film relatively high.

Although ERE was not measured on devices which use differing top temperatures, the material quality of the higher-temperature deposited CST was assessed with a series of cells fabricated with varying intensity of $CdCl_2$ treatment. Since the $CdCl_2$ process allows re-crystallization and grain growth, it is expected that a poor as deposited film can be to some extent rendered passive in the device through a longer $CdCl_2$ process to provide additional time for recrystallization and grain growth. It is then logical that a reduced $CdCl_2$ process should be needed in a film that has a higher as-deposited quality. In figure 36 boxplots of 25 cells each from cells with the CdSeTe deposited with a 540°C top temperature and the $CdCl_2$ process varied show asymptotic behaviors at $CdCl_2$ processes using a 540s dose and anneal. This asymptotic behavior at a process 60% of the duration of the standard suggests the material quality as deposited is better at higher top

temperatures. Although these cells used 540°C, a top temperature of 480°C was used for the remainder of the work to maintain fast deposition, but take advantage of the apparently dense films seen in the SEM of figure 35.

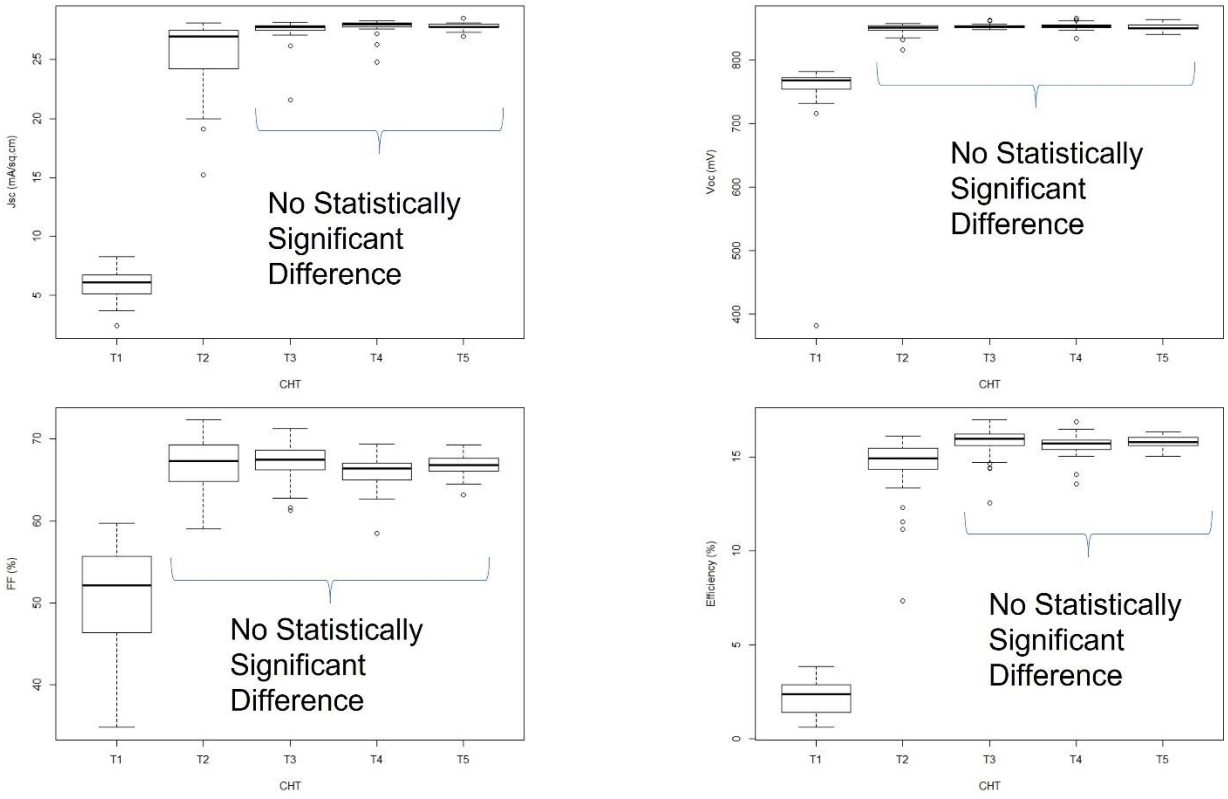

Figure 36: JV parameter boxplots of CdSeTe cells with the only deviation from baseline being a 540°C top temperature during CdSeTe deposition. CHT = $CdCl_2$ Heat Treatment, ($CdCl_2$ dose time (s), anneal time(s)) T1 – (180, 180), T2 – (360, 360), T3 – (540, 540) T4 – (600, 720), T5 – (600, 900).

4.4) Investigation of Recombination Losses in the Baseline Structure[2]

4.4.1) Electron Contact Interface

In binary CdTe cells using MgZnO as the electron contact, it is believed that the energetic offset of the conduction band at the interface is what determines the recombination behavior at the interface leading to the improvement in V_{oc} that was observed [76-79]. As such, it has remained a constant in discussion of the front interface, this CBO must be maintained since it reduces the rate of recombination. However, the V_{oc} has not been reduced since the change to CdSeTe, which has a different bandgap and electron affinity to CdTe, and thus the "ideal" MZO for CdTe has been used to great effect with CdSeTe despite it's non-ideal band alignment as the thinking goes [78, 79].

In collaboration with Dr. Wolden at Colorado School of Mines, we systematically varied the Mg content of MZO in baseline devices. The Mg content is known to control the electron affinity of MZO, simultaneous with bandgap, and as such acts as the knob to turn when varying the CBO at the interface in accordance with the Anderson Rule [76, 78, 79]. The hypothesis was to see an increase in V_{oc} with increasing CBO, followed by a reduction in fill factor as the CBO became too large and the conductivity to electrons through the material is reduced. Indeed, this is what is seen with CdTe cells, and it was primarily expected to see the exact same behavior with a different optimum of Mg content for efficiency due to the difference in electron affinity between CdSeTe and CdTe.

[2] Work in this section published in [78] or anticipated for publication in part in Reich, C., A. Onno, A. Danielson, A. Bothwell, C. Wu, D. Kuciauskas, Z. Holman, W. Sampath, High Efficiency Un-doped CdSeTe Solar Cells Enabled by Long Lifetimes. Under Preparation. And Reich, C., Onno, A., Danielson, A., Mahaffey, M., Holman, Z., Sampath, W. S., Optical Considerations to Maximize Photovoltage in CdSeTe Solar Cells with Long Lifetimes. Under Preparation

The bandgaps were chosen to produce somewhere between a match of the CBM between the two layers and a large CBO where MZO's CBM sits much higher relative to vacuum level. Baseline devices were made with this variation in MZO from 3.68 eV to 3.92 eV, co-sputtering from Mg and Zn targets in the presence of argon and oxygen and varying the relative power applied to each target [78]. Absorbers and the hole contact were prepared exactly as in section 4.2. Boxplots of JV parameters of the devices can be found in figure 37, showing little deviation in performance. In fact, the only statistically significant differences between parameters was found in the J_{sc} and FF, with the widest bandgap (and largest CBO) producing a very minor reduction in each. Such an effect was not unexpected for the reasons that we expected to see an optimum previously discussed. However, not in line with the hypothesis was that the V_{oc} and efficiencies were identical between the various conditions, suggesting that the size of the CBO was not impacting recombination at the interface as it appears to with binary CdTe at the interface.

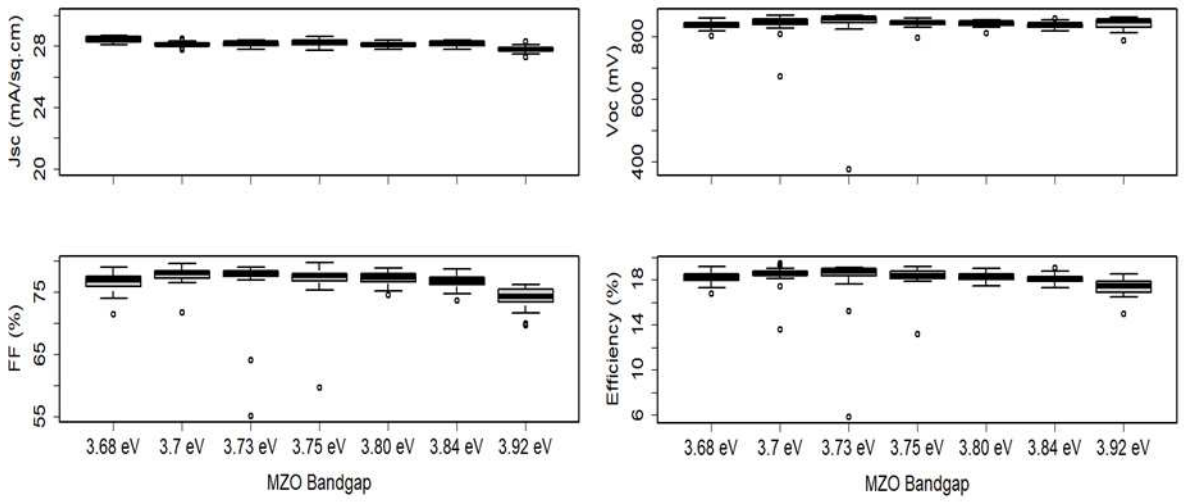

Figure 37: Boxplots of JV parameters for baseline cells with varied Mg content (Eg, CBO).

In light of this, the ERE and TRPL was measured on 5 cells in each condition. The ERE was converted into implied voltages after calculation of the $V_{oc,limit}$ using the EQE as a proxy for absorptance, and can be found along side the TRPL decays in figure 38. It is obvious that the recombination losses are approximately the same between all cells (3 of which had degraded during storage for 3 months and produced slightly lower ERE values – 3.75 eV, 3.80 eV and 3.84 eV) producing implied voltages between 880 mV and 900 mV. Additionally, the tail lifetime of the TRPL measurements was quite similar between all samples, between 30 and 80 ns for all measurements for which the variation between measurements on the same condition dwarfed the condition to condition variation. The ERE and TRPL showing insignificant variation between conditions demonstrated that the recombination behavior in these cells is 1) not affected by the CBO or more likely 2) the limiting recombination in the cells is elsewhere in the devices such that different recombination behaviors at this interface did not noticeably impact the overall recombination behavior in the devices.

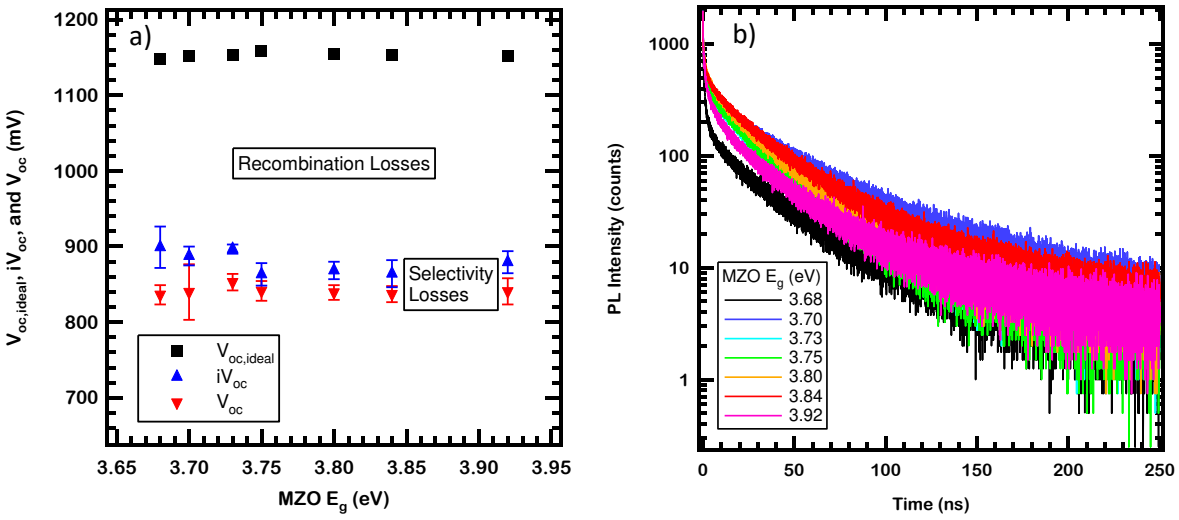

Figure 38: a) V_{oc} loss analysis showing lack of sensitivity to MZO E_g. ERE measured by Arthur Onno. b) TRPL decays showing approximately the same decay constant at later times between samples with differing MgZnO compositions.

This lack of difference in apparent recombination behavior suggests in any case that the rate of recombination at the interface of MZO/CdSeTe is less than the MZO/CdTe interface. It is important to note that this effect is possible through two mechanisms: increased band bending at the interface reducing the hole (minority carrier) concentration available to recombine with the majority electrons, or a reduction in the surface recombination velocity, likely due to differences in the density or nature of defects found at the interface. There is some evidence that the carrier concentration at the interface is increased in the MZO due to oxygen vacancies, but with no changes in the absorber doping, increased band bending should be minor. This leaves a reduction in the SRV, and there is literature which suggests this to be the case, and to be encouraged by the inclusion of Se. Out of NREL, literature has recently been published linking the increase in effective lifetime to the increase in the density of TeO_x formed at the MZO/Cd(Se)Te absorber interface, formation of which is encouraged by increased Se alloy content [121]. This suggests that oxygen is passivating the interface by bonding to Te, which would effectively account for a reduction in SRV rather than hole density.

In additional support to this, the absorbers with exceptionally long lifetimes produced in the next section (investigation of absorber structure and quality) analysis of TRPL decays produced estimates of 10 cm/s for the SRV of a MZO/CdSeTe interface by matching the variation of injection dependence in a TRPL decays to models in COMSOL as seen in figure 39 [93]. The simulation properties which provided the best match to the measured data (shown here) are: 0.2 eV spike at MZO interface, low doping ($10^{12}/cm^3$), 20 cm^2/Vs and 12 cm^2/Vs mobility for electrons and holes respectively, 3.5 micron thickness, graded bandgap, S_{front} = 10 cm/s, S_{back} = 100 cm/s, and τ_{bulk} = 900 ns. Deviation is likely due to the single τ_{bulk} and high MZO carrier

concentration, when in real cells bulk lifetime varies with Se content and the MZO is low doped. Such an estimate suggests that the SRV of that interface is reduced by 3-4 orders of magnitude (MZO/CdTe believed to be $10^4 – 10^5$ cm/s). It is apparent from the modelling that with such a low SRV, increased band bending or a CBO is no longer necessary to reduce the interfacial recombination.

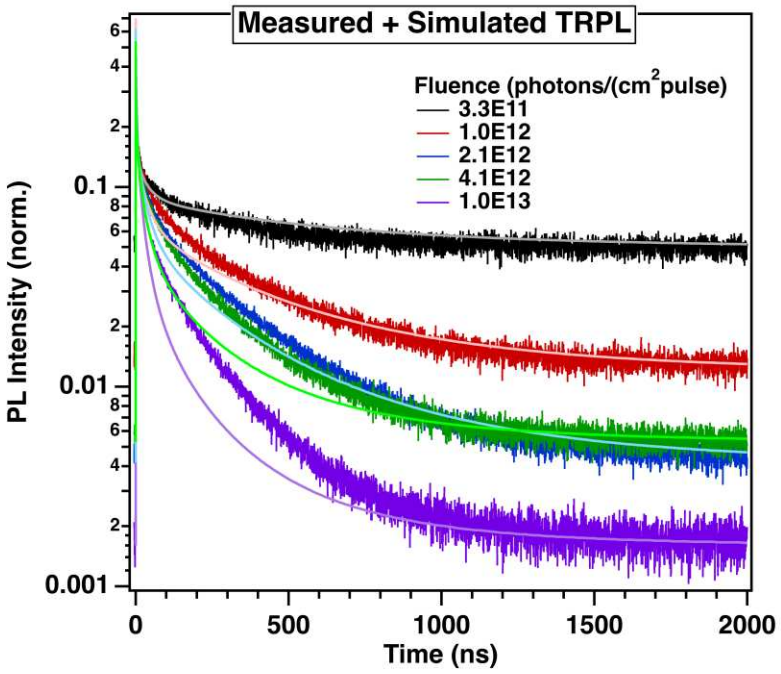

Figure 39: TRPL with Fits from COMSOL suggesting low front SRV. Measured, fit, and plotted by Alex Bothwell.

4.4.2) Investigation of the Bulk Semiconductor

Since it is apparent that recombination at the front interface is not currently limiting the devices, the bulk semiconductor was investigated as a potential source of the large non-radiative recombination losses to V_{oc}. It is worth noting here that the bulk semiconductor in these cells is not all an "absorber" layer, as there is typically 3.5 microns, and >90% of the light is absorbed by the first micron with ~99% of the light absorbed by the second micron [122]. Thus, the

absorber portion of the cell can be thought of as effectively that first micron, perhaps two. Nonetheless, the recombination behavior through the entire bulk will affect the density of excess carriers through the entire cell, as any source of increased recombination accessible to excess carriers acts to reduce the carrier density everywhere at open circuit. Thus, since the recombination mechanisms are all related through the bulk, the absorber and non-absorber regions of the bulk should be simultaneously considered.

In the bulk of a CdTe-based cell since around 2016 there is typically a region of graded CdSeTe alloy, followed by a thicker region of binary CdTe. It is well known in the community that the use of CdSeTe has enabled increases in TRPL measured carrier lifetimes in the devices, and further that the lifetime of carriers in CdSeTe double hetero-structures far exceeds those found in comparable structures made without the Se alloy [69-71]. However, the use of CdTe is, as previously mentioned, believed to be essential to the efficiencies of cells due to the superior efficiencies and hypothesized “electron reflector” effect [52]. Exactly how detrimental the increased recombination through the CdTe bulk is has never been identified, since the community believed it essential to electrical performance.

In addition to the recombination behavior in binary CdTe, the traditional dopant of Cu has been identified as a source of reduced lifetimes as well [123, 124]. However, much like the binary CdTe, the use of Cu has allowed for efficiencies to exceed that of cells without the dopant, and thus has remained incorporated in much of the community’s best performing cells, without much regard for the full extent of the losses due to recombination that are enabled by the use of this dopant. However, it is possible that the implied voltage remains the same or increases, since it is a dopant and a higher carrier concentration does not require as high of lifetimes to achieve the same implied voltage.

To test this hypothesis, we utilize ERE measurement of iVoc extensively to quantify the losses due to recombination that occur through the bulk material. To do this, the baseline structure is compared to the same structure without undergoing the Cu doping treatment, and then again to a structure made entirely of Se-alloyed material. Bulk materials were deposited as described in section 4.2, without the Cu doping process for undoped cells and the modification of a 480°C substrate heater during the deposition of CdSeTe for most absorbers. In fact all absorbers were prepared with this heater temperature except some of those of the baseline structure, but there was no significant difference between the two top temperatures in the Cu-doped Bi-layer structure. This comparison of ERE can be found in figure 40. It is clear that not only does Cu doping reduce the ERE significantly from the bi-layer structure without doping, but that undoped CdSeTe produces an ERE an order of magnitude higher than the undoped bi-layer structure. These structures are limited to 257 mV, 220 mV, and 146 mV below their radiative limits respectively by recombination following the equation derived in previous sections. This presents a clear case for CdSeTe to be utilized since it's limit is a full 74 mV greater than the best of these contacted bi-layer structures. A 74 mV difference in V_{oc}, all else the same, produces a 1.7% absolute increase in efficiency, while a greater increase in efficiency could be expected since the same mechanism should improve FF.

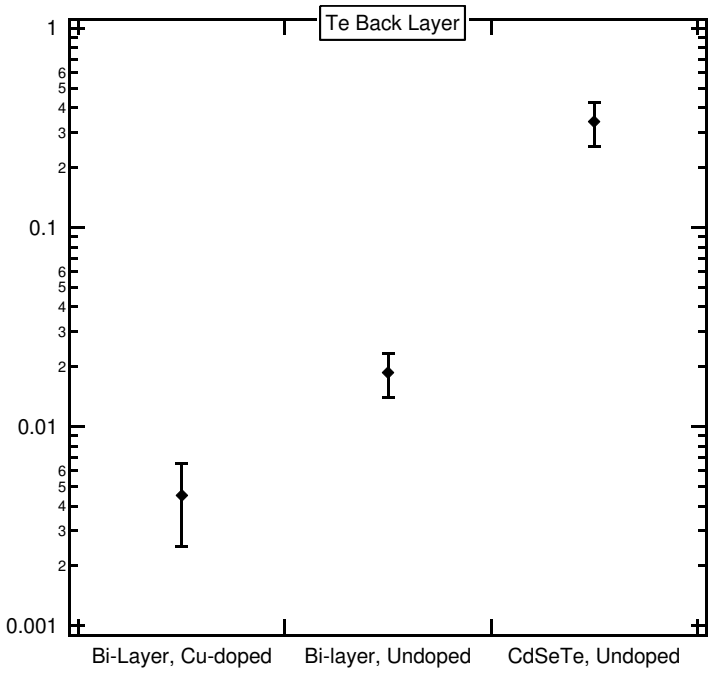

Figure 40: ERE of different stacks of bulk films (Cu-doped bi-layer, undoped bi-layer, and undoped CdSeTe) deposited on TEC10/MZO with Te deposited at the back surface. Mean ERE values correspond to deficits of 257 mV, 220 mV, and 146 mV respectively, demonstrating the superior recombination behavior of CdSeTe. ERE measured by Arthur Onno.

These increases in ERE are also in agreement with TRPL measurements. A simple fit of the tail of the structures demonstrates (figure 41) that the ERE correlates quite well with the TRPL-determined lifetime. This is consistent with a greater fraction of the recombination occurring through the radiative mechanism, as the radiative lifetime sets the lower limit for the rate of recombination. In perhaps simpler terms, the longer the carriers survive the more excess carriers there are in a steady state balance at V_{oc} thus the two quasi-Fermi levels are closer to their respective bands.

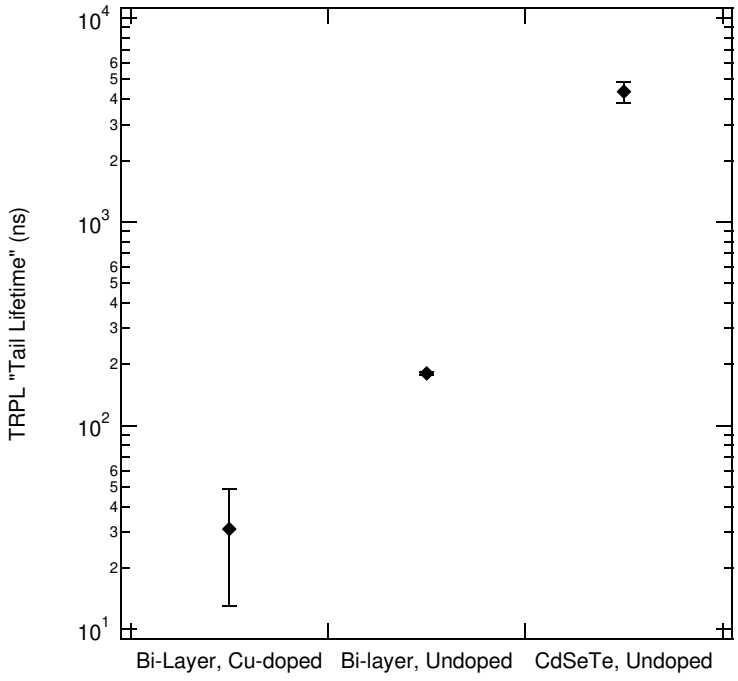

Figure 41: TRPL - determined lifetimes for the 3 structures, showing much the same trend as the ERE. The listed lifetime is the decay constant of a fit for a TRPL histogram at times later in the decay. ERE measured by Arthur Onno.

4.4.3) Investigation of the Hole Contact Interface

It is occasionally assumed that the back surface recombination is not a major parameter in the advancement of CdTe solar cells. Indeed, it is a major conclusion of some modelling that has guided the community that the back surface doesn't really matter if certain conditions are achieved, such as exceptionally high doping with a moderate lifetime in the absorber [106, 107]. This assumption is only valid when the rate of recombination is negligible relative to the rates elsewhere in the device. The typical thinking is that the devices with large doping densities are sufficiently thick that the rate of recombination at the back surface will be negligible since minority carriers do not diffuse through the thickness. While it is somewhat more complex in reality, especially in the case that there is effective carrier spreading through reabsorption of

emitted photons from radiative recombination, the rule of thumb is that the thickness of the bulk must be many times the diffusion length of carriers past the region responsible for absorption of photons. This is because the diffusion length is the length at which 50% of carriers have recombined, so a single diffusion length only reduces the carrier concentration by 50%. While a corresponding reduction in the rate of recombination 50% at that interface is desirable, it is unlikely to dramatically change the internal voltage, since the rate of recombination linearly affects the excess carrier concentration, and the voltage is dependent on the natural logarithm of the carrier concentration. It is therefore needed to reduce the rate of recombination by orders of magnitude to have a significant effect on the voltage of the cell, which requires numerous times the diffusion length of the carriers to achieve.

Of course, the diffusion length depends on the lifetime of the excess carriers through the bulk material as well as the mobility thereof. While the assumption that TRPL is a good measure of bulk lifetime is inherently flawed, not for the least reason that lifetimes in CdSeTe/CdTe cells are expected to be dependent on the local Se content, it is the best starting point we have for approximating diffusion length. Using the SCAPS standard mobility for electrons of 320 cm^2/Vs, we see that the diffusion length rounded to the nearest micron is: 5 μm, 12 μm, and 60 μm for the lifetimes above for CdSeTe/CdTe:Cu, CdSeTe/CdTe, and CdSeTe respectively, and the smallest changes to about 3 μm if a smaller mobility of 100 cm^2/Vs is used. Since these structures are 3-3.5 microns thick, and generation of 90% of the carriers occurs within a micron, the remaining thickness is less than a diffusion length for electrons, thus a significant concentration of electrons is expected to be available at the back surface to recombine. In the graded structures, again, it is complicated by band structure and variable lifetimes through the bulk material, but as a starting

estimate, carriers are likely at the back surface, which enables recombination there to limit the voltage.

Since carriers are expected to be at the back surface in significant quantities, it then is apparent that to reduce the recombination at the surface appropriate measures must be taken to locally reduce the carrier density or reduce the quantity of states in at the interface which would contribute to non-radiative recombination. In this section, we compare the Te contact typically used at CSU to a known passivation layer of Al_2O_3 and further an air-exposed bare surface in both CdSeTe and CdSeTe/CdTe (undoped) structures. CdSeTe absorbers are 3 microns thick and thickness of the bi-layer structure are the same as the baseline, and absorbers are deposited as described in section 4.2, but with the 480°C substrate heater temperature during CdSeTe deposition. The Al_2O_3 layer was 10 nm deposited by RF planar magnetron sputtering in 5 mTorr of 8% O_2/balance Ar with 240 W across the 4 in diameter target. For these samples, $CdCl_2$ was done after the deposition of Al_2O_3, where the other samples received $CdCl_2$ just after the absorber deposition.

In figure 42, it is first apparent that there is a difference in the ERE between various back surfaces. This suggests that the initial estimate that carriers are at the back surface in significant quantities is correct, as the recombination behavior is modified by the back surface. This provides good evidence that engineering of back surface recombination is necessary in current state of the art CdTe-based solar cells.

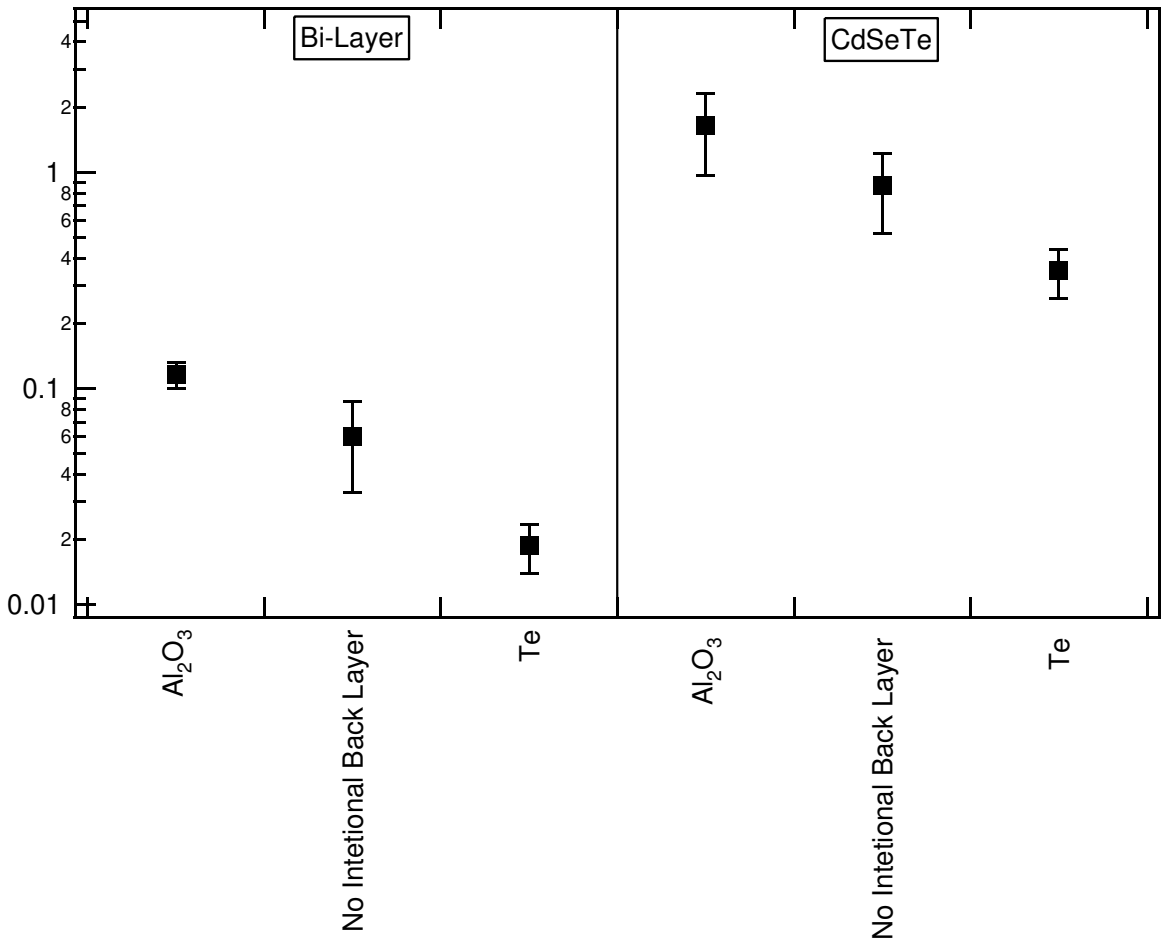

Figure 42: ERE of Bi-Layer (CdSeTe/CdTe) and CdSeTe only structures with differing rear surfaces. Samples with no intentional back layer had been stored in dry air for 16 days prior to measurement. ERE measured by Arthur Onno.

More specifically, the Te contact showed a significant amount of reduction of ERE in both structures. This is only possible if the rate of non-radiative recombination at the back surface of otherwise nominally identical structures is significantly increased relative to the other cases. It is expected that Te would produce such an effect, the far narrower bandgap allows for a continuum of states through ~1.1 eV of the bandgap of CdSeTe, and further, has been shown to produce numerous interface states depending on the relative orientations of the Te and CdTe-based

crystals. All of this would provide (minority) electrons at the contact an easy pathway to thermalize during recombination at this surface rather than emitting a photon. With its much wider bandgap, Al_2O_3 does not provide a density of states within the bandgap of CdSeTe unless these are defects within the bandgap, possibly due to the non-ideal nature of interfacial bonding between unlike materials. However, without excessive interfacial defects, this eliminates a pathway for thermalization that Te provides readily. Additionally, passivation using Al_2O_3 with CdTe has been shown to stem at least in part from the formation of TeO_x at the interface after $CdCl_2$, and passivation of c-Si with Al_2O_3 has been shown to be the result of a fixed negative charge keeping electrons from approaching the defective interface [125]. Following all of this, this passivation layer has shown itself to be extremely effective as a back surface passivation layer, increasing the ERE by an order of magnitude.

Unexpectedly, the sample with no intentional layer at the back surface showed nearly as bright of ERE as the Al_2O_3 passivated sample. Based on the literature from NREL that both MZO and Al_2O_3 interfaces with CdTe form TeO_x as at least a portion of the passivation observed there, it was hypothesized that air exposure produced such an oxide at the surface providing passivation that is comparable [121, 126]. To investigate, ERE and XPS were measured on CdSeTe films that were stored for 2 weeks in dry air, mimicking the conditions these samples had been stored in prior to measurement. In XPS, a peak corresponding to Te^{4+} is indicative of native oxide formation, so the fraction of this relative to the usual Te^{2-} peak was used to correlate to ERE. It is clear in figure 43 that both the Te^{4+} fraction at the surface and the ERE both increased, providing strong evidence in support of the hypothesized effect.

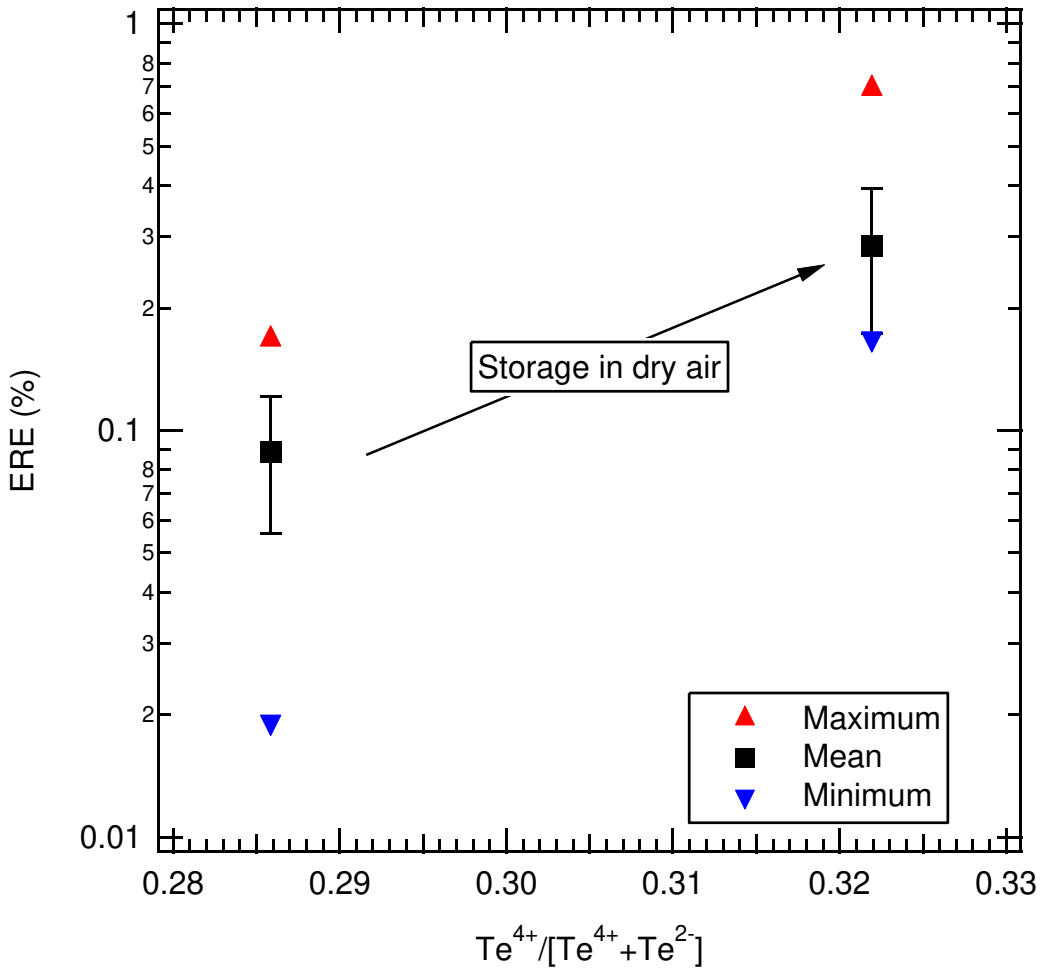

Figure 43: ERE measured vs fraction of surface Te signal from Te^{4+} oxidation state. Measurement was on the same sample stored in dry air for 2 weeks between measurements, showing both an increase in Te^{4+} fraction and ERE. ERE measured by Arthur Onno.

In addition to the increased ERE correlated to the presence of the 4+ oxidation state, the ERE was measured from both the front and the back for both bilayer and CdSeTe only structures and can be found in figure 44. The ERE is found to be slightly diminished in the back. In the bilayer structure, this is a more significant effect, likely due to the excitation for the ERE being localized to the lower lifetime binary region at the back. In the CdSeTe only cells, the ERE from the back is hardly diminished, less than a 50% reduction in both the TeO_x and Al_2O_3 cases, indicating excellent passivation. It is also noted that the change in ERE front to back with the Al_2O_3 layer

vs the TeO_x is greater in the bilayer cells. This could either be from a reduction in the formation of TeO_x on the CdTe surface or the TeO_x passivation being less effective on the surface of the binary.

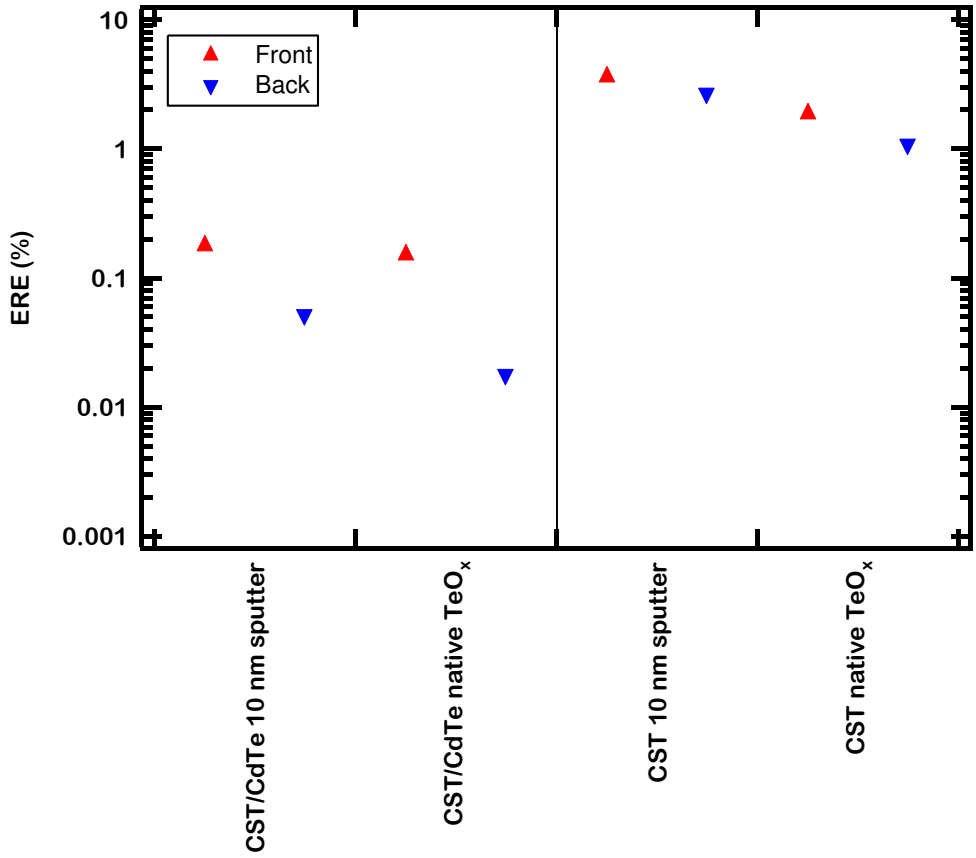

Figure 44: ERE measured from the front and back of the films with Al_2O_3 and TeO_x passivation layers. Measured by Arthur Onno.

To test if the formation of the TeO_x was hindered by the lack of Se as might be suggested in the work at NREL, a CdTe and a CdSeTe film were deposited and stored under identical conditions for two weeks. XPS was measured and again the fraction of Te^{4+} to total Te was calculated, with results that suggest very similar amounts of Te had oxidized as seen in figure 45. The non-zero oxide presence for the fresh sample is likely due to overnight storage in air prior to XPS

measurement. Based on this, it was more likely that there is an effect due to Se in the bulk semiconductor that is responsible for the increased passivation rather than an increased fraction of oxidized Te, perhaps relating to the smaller atomic spacing or simply the smaller fraction of Te present at the surface.

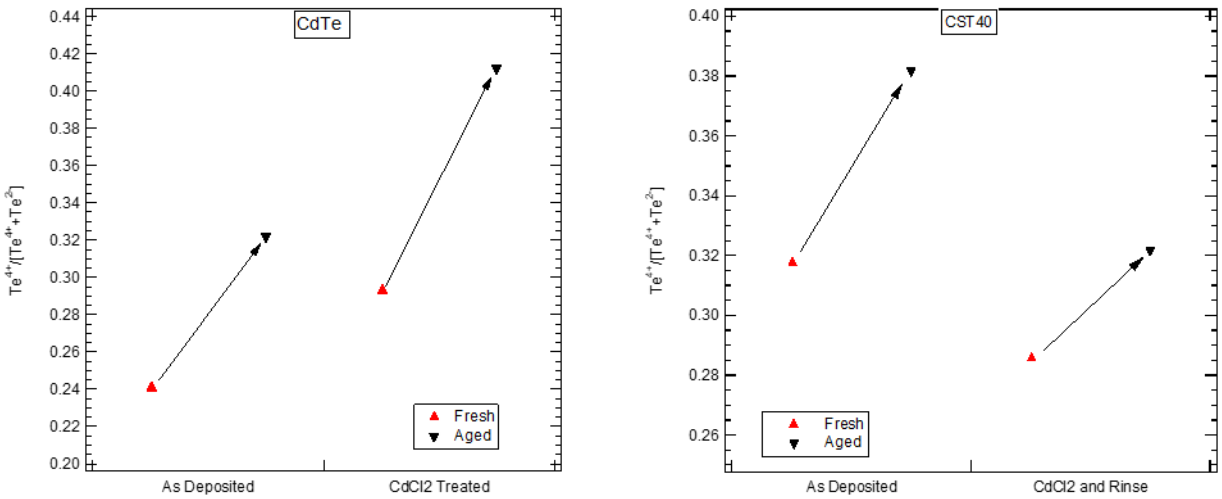

Figure 45: Te Oxide fraction on the surface of CdTe and CdSeTe over a two week storage period in dry air, both as deposited and $CdCl_2$ treated.

Preliminary efforts to understand the passivation mechanism have been carried out using Density Functional Theory by Anthony Nicholson [126]. This work, focused on CdTe, shows an increase in upward band bending due to the presence of TeO_2:H and TeO_2:H:Cl, and sufficient chlorination of this layer reduces the density of states within the bandgap at the surface, although a larger density of states is present at the energies they remain, extending deep from the CB to the middle of the energy gap. In the case of CdTe, it is then possible that the passivation observed is primarily field effect, allowing for excellent passivation when excitation occurs at the front of the device and the electron at the population at the interface is already diminished by the CBO offered by CdTe and shorter diffusion length therein. The effectiveness of this

passivation would then be diminished when the back is illuminated since the excitation of excess carriers is occurring directly adjacent to the interface and therefore the population of excess carriers available at the interface is proportionally greater. This does not seem to match the mechanism in CdSeTe alone, however, since the passivation is not diminished, which would suggest a smaller DOS in the interface through which carriers can recombine non-radiatively. It is additionally worth noting that this initial work requires further investigation to be more confident in the observed effects, including additional crystal orientations, larger simulations with more atoms, TeO_x thicknesses, and extending the analysis to CdSeTe.

4.4.4) Effect of Cell Optics on Implied Voltage

Interestingly, photons emitted by radiative recombination are not guaranteed emission through the front surface, a necessary condition to contribute to the ERE, and further, approach the thermo-dynamic limit to voltage [48]. In fact, since the emission probability is isotropic from any single event, only a small fraction of the photons emitted by radiative recombination will be within the narrow escape cone through which they will be transmitted through the front surface, with the remaining being internally reflected [103-105]. There is a non-zero probability that the emitted photons are reabsorbed, producing a second (temporally differentiated) electron-hole pair with the useful energy of a single photon. This electron hole pair will again recombine with some probability that this occurs through the radiative mechanism which then has the same isotropic spatial emission probability.

In materials where non-radiative recombination composes a large percentage of the overall recombination, there is little repetition of this process and the ERE and IRE are nearly the same. However, in very good materials where radiative recombination is a significant fraction of the overall recombination, this process can repeat itself until the emitted photon is within the escape

cone and contributes to the ERE. This necessitates excellent optical design of the cell when IRE is high. If an emitted photon outside the front escape cone is absorbed without contributing another electron hole pair to the absorber, that energy is lost to the system and there are no further opportunities for that energy to be used. In such a cell, a back reflector is necessary at the minimum, since photons will "see" that back surface due to emission toward the back surface, including in some cases those reflected from the forward emission direction due to total internal reflection. This is even true in the event of an optically thick absorber with a short radiatively limited diffusion length (highly doped) material since the bulk semiconductor is luminescent coupled with itself, and so reabsorption of emission toward the back will inevitably spread excess carriers through the thickness where some of the emitted photons from their recombination interact with the back surface.

A significant effort in the III-V community has been paid to approaching the thermodynamic limit of their cells since the materials are nearly radiatively limited in their recombination dynamics. Such efforts use probabilistic models to approximate the effect of a back surface that is perfectly reflective or perfectly absorbing (and some in between, although this adds complexity to the calculations) [104, 105]. From this work it is apparent that, just as conceptually described above, a perfect back reflector is needed to reach an ERE of 100%. Equation 30 was derived by Steiner et al. as the relationship between ERE, IRE, Average Escape Probability (P_{esc}), and Average Probability of reabsorption (P_{reabs}) [104, 105]. It is worth noting that the ERE output can only be less than or equal to 1 because the average probability of escape and average probability of reabsorption cannot sum to greater than 1, although smaller than 1 is allowed since photons can be parasitically absorbed in materials that do not contribute electron hole pairs to the absorber such as a light-absorptive back contact.

$$ERE = \frac{IRE * P_{esc}}{1 - (IRE * P_{reabs})} \qquad (30)$$

In figure 46 this relationship is plotted as a function of IRE for two different escape probabilities ($1/4n^2$ and $1/2n^2$ corresponding to the approximate fraction of the emission sphere that is directed into the escape cone and double this which assumes optically thin bulk to the emission and a perfect planar rear reflector. It is important that implementation of a rear reflector or otherwise altering the optics of the cell will affect both the escape probability and the reabsorption probability. For example, the implementation of a perfect back mirror will double the escape probability in optically thin absorbers, which impacts the ERE and thus iV_{oc} at all values of IRE. Simultaneously, the implementation of a back mirror, no matter how thick the cell is, will increase the probability of reabsorption since photons that interact with that surface will be more likely to traverse the semiconductor for additional distance thus improving the chances it is absorbed. This effect, while universal, only begins to be significant in the ERE when the IRE is not negligible, with the most pronounced effects occurring when the IRE is in the 10s of percentage.

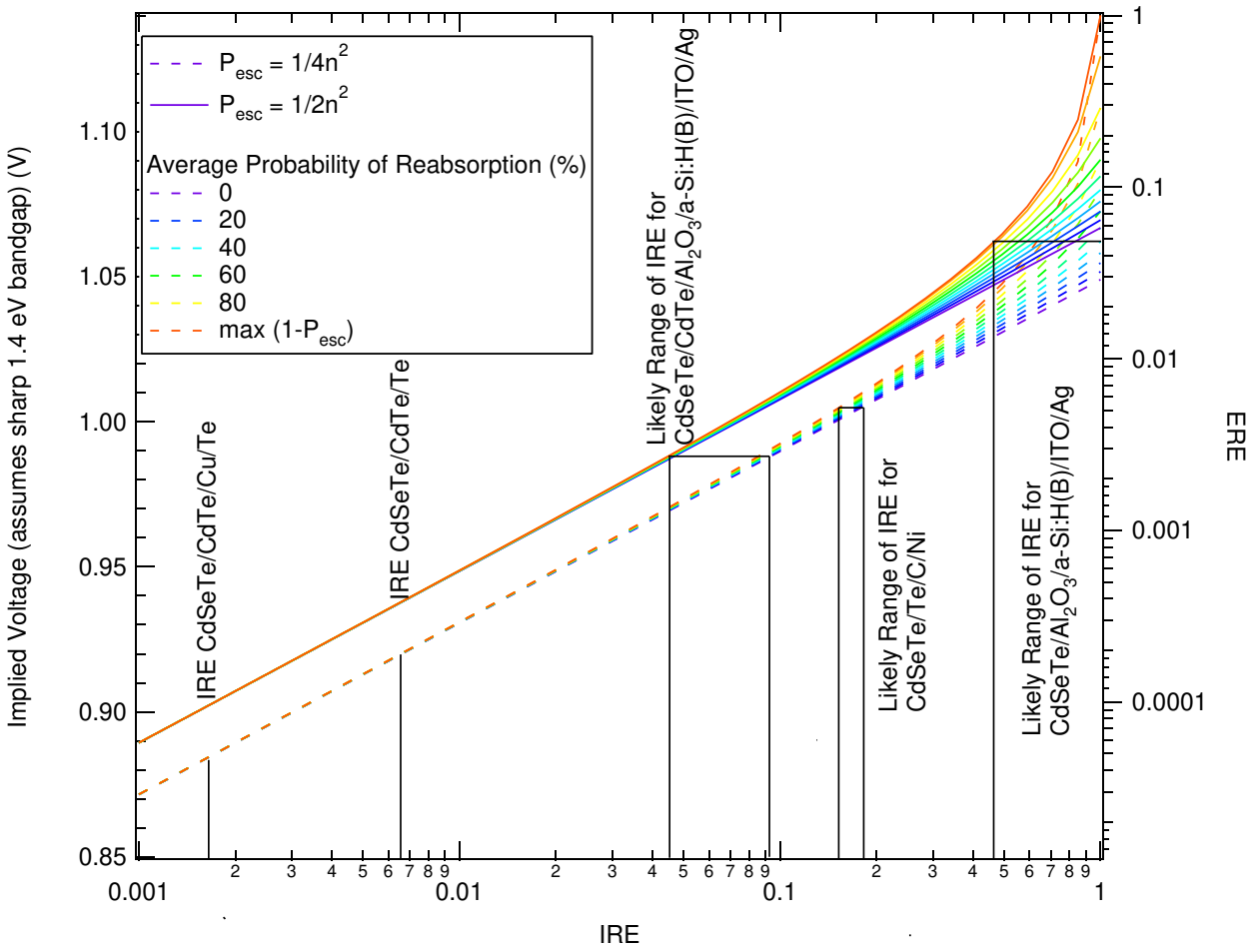

Figure 46: Relationship between Internal and External Radiative Efficiencies as impacted by average escape probability and average probability of reabsorption for emitted photons. Values and estimate ranges for common structures produced at CSU are identified.

CdSeTe/CdTe cells at CSU show ERE values typically in the $1x10^{-5}$ to $1x10^{-4}$ orders of magnitude, placing the IRE in the range where the escape probability could have an impact on ERE, but the probability of reabsorption shows little effect. The ERE of CdSeTe only films is above 0.001, above which point the IRE is sufficiently high that the divergence due to not only escape probability but also the probability of reabsorption becomes apparent. As such, implementation of a rear reflector should be capable of ~2x increase in ERE but not more with CdSeTe/CdTe cells, depending on the optical thickness of the cell. However, if the ERE being

near 1% with an absorbing back surface (Te and painted electrode) places the IRE high enough, the effects of the increased back reflectance can boost the ERE by more than 2x. In figure 47 we find the ERE measured on both a bilayer cell and a CdSeTe only film for various back reflection conditions, both with excellent passivation from Al_2O_3. These are the same cells as the bi-layer and CdSeTe absorbers with Al_2O_3 passivation from the previous section. Notably, the bandgap of Al_2O_3 is quite wide and thus photons in the escape cone toward the back surface will escape without parasitic absorption, allowing reflection from the material behind the Al_2O_3 to re-direct photons into the absorber where they can be re-absorbed.

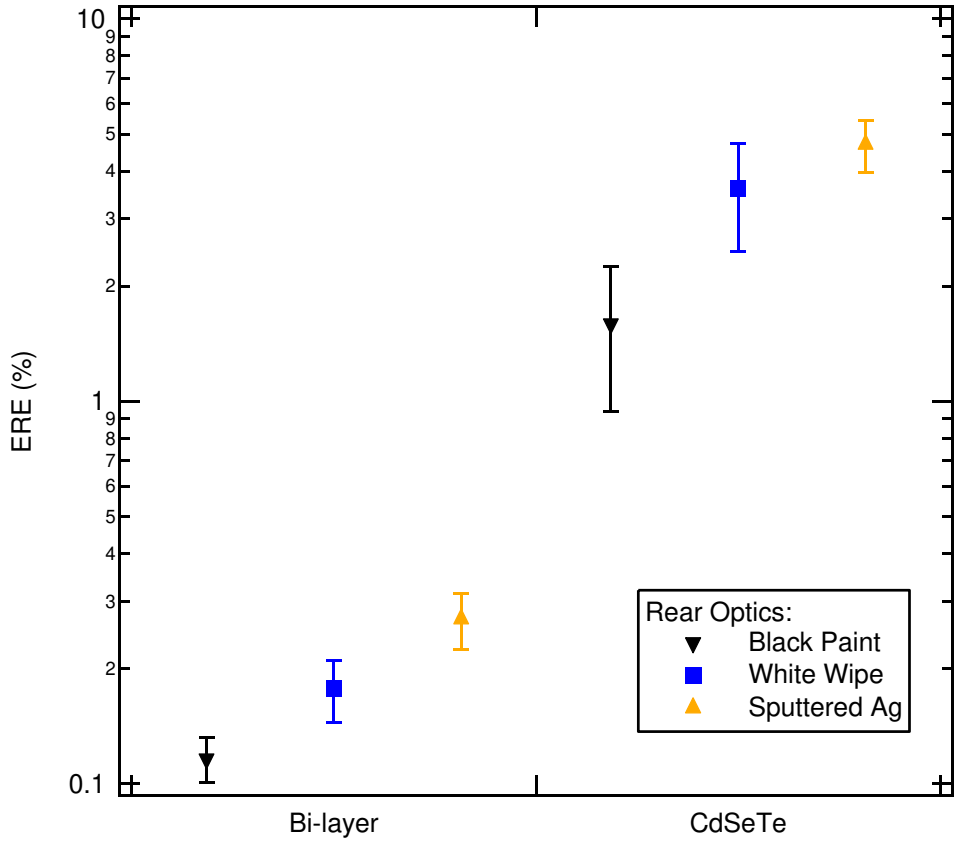

Figure 47: ERE with various back "reflectors" for bi-layer and CdSeTe only cells passivated with 10 nm Al_2O_3

It is apparent that the ERE approximately doubles between the case with a black back surface and with a Silver surface behind the Al_2O_3. The laboratory wipe is a less effective reflector, and as such the increase in ERE is present but somewhat less than the silver reflector for both cases. Although it was possible and not guaranteed with the ERE of a little more than 1% with an absorbing back surface, the ERE does indeed more than double with the use of a silver back reflector for the CdSeTe film, implying that emitted photons are being reabsorbed and emitting again.

If we assume that a cell that is optically thin to its own luminescence with a perfect reflector is the upper bound of escape probability, we can estimate the lower bound of possible internal radiative efficiency for the average value of ERE from the CdSeTe films with excellent passivation and the Ag reflector by numerically solving the above equation for IRE with the maximum probability of reabsorption. This gives an IRE greater than 0.446, with any smaller escape probability, or smaller probability of reabsorption requiring a greater IRE to produce the same ERE. When the same calculation is done for the comparable back structure on a CdSeTe/CdTe film stack, this time accounting for the maximum which occurs when the escape probability is at a minimum and since the ERE is low enough that the variation with reabsorption is minimal, we see that the range of IRE is between 0.045 and 0.093. It should be noted that the average probability of reabsorption is never completely 0, as modelled in some cases above, since a large amount of luminescent emission is directed with significant horizontal components, allowing for a large possible path length through the absorber before interacting with a potentially absorptive back surface. Thus while the lower end estimate of IRE, which assumes perfect reabsorption, is still valid, the actual upper end estimate is likely somewhat lower.

As a result of this analysis there are two-fold conclusions to make. First is that optical design of the cell is important with CdSeTe as the absorber. Although this is true in the bi-layer as well since there was an increase in ERE due to increased escape probability, in the CdSeTe the IRE is high enough that re-absorption of photons provides additional increases in ERE and thus internal voltage, and these absorbers are therefore likely to see the greatest benefit from optical design. The second is that the CdSeTe bulk is far more desirable than the CdSeTe/CdTe bulk since the internal radiative efficiency is about an order of magnitude greater than the CdTe containing bulk. This is means that the bulk can produce performance much closer to the ideal case than the CdTe containing bulk since it is approaching or at the state where a majority of recombination in the cell occurs through radiative means.

4.4.5) Low Energy Emission and Resulting Implied Efficiency and Voltage

High ERE indicates that the deficit from the ideal voltage is very low. However, it is important to know what that ideal voltage is to determine the actual internal voltage. This starts with determination of the absorption behavior. Attempts to determine absorptance showed increasing values at low energy before the signal from the QE measurement tool became too low to measure and noise dominated the data. Ellipsometry determination of n and k data was difficult, due to the large roughness of the semiconductor films. Spectral photoluminescence measurements however, have been used with great precision to measure the absorptance at low energies [149]. Using calibrated spectral emission measurements of the absorbers with an InGaAs detector, the wavelength resolved luminescent emission was measured. The absorptance was calculated by a fitting routine on this data using the relationship in equation 18 [145]. This data can be found normalized to the maximum so both CdSeTe and CdSeTe/CdTe are visible in figure 48 and was

then used to determine $J_{0,rad}$ and J_{sc} for the detailed balance analysis of the absorptance limiting voltage.

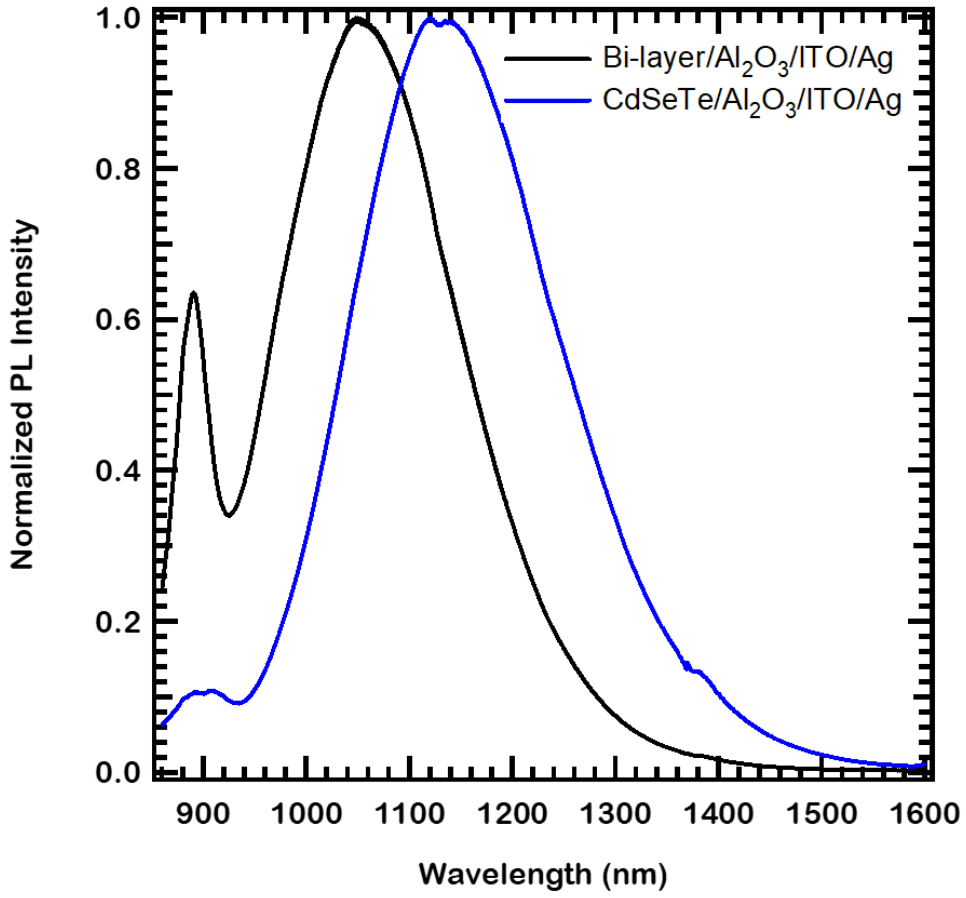

Figure 48: Normalized photon flux from photoluminescent emission measured with an InGaAs detector. Measured by Alex Bothwell and Darius Kuciauskas.

A large amount of low energy emission is observed in the spectral luminescence data, which indicates a dramatic decrease in the limiting voltage, despite the determined absorptance being very small. When applied to the calculation, the thermodynamic limiting voltage is determined to be below 1100 mV, around 1070 for the CdSeTe/CdTe structure and around 1050 for the CdSeTe structure. The 1 sun ERE numbers, meaningful for the implied V_{oc}, then place the implied voltages at ~910 and 970 mV respectively. This is only applicable if the emission is a

bulk phenomenon, as emission from interfaces is not indicative of the bulk quasi-Fermi level separation. The locality of the emission was measured by cathodoluminescence at Centre De Nanosciences et Nanotechnologies (C2N), seen in figure 49. This image very clearly shows low energy emission as a bulk phenomenon, as grain centers are brighter than grain boundaries, lending credibility to both the inclusion of this emission in the ERE and the absorptance derived limiting voltage.

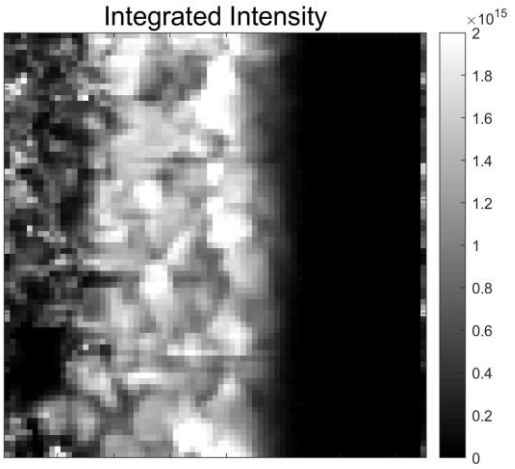

Figure 49: Cathodoluminescence measured centered at 1220 nm on CdSeTe Measured by Stephane Collin at C2N, Field of View is 13.075 μm.

Using the Suns – ERE technique and this absorptance data's $J_{0,rad}$ an implied JV curve was constructed using the principle of superposition. The implied voltage, now a function of both the changing ERE with injection and excitation current for the limiting voltage, was then plotted as a function of the pseudo-current density and found in figure 50. The implied efficiencies are 25.3% and 23% for well passivated CdSeTe and CdSeTe/CdTe structures (undoped) respectively. The dependence on injection observed in the ERE of the CdSeTe/CdTe cell causes the recombination

limit to fill factor to reduce that upper efficiency bound by a greater factor than the lower implied voltage alone would suggest.

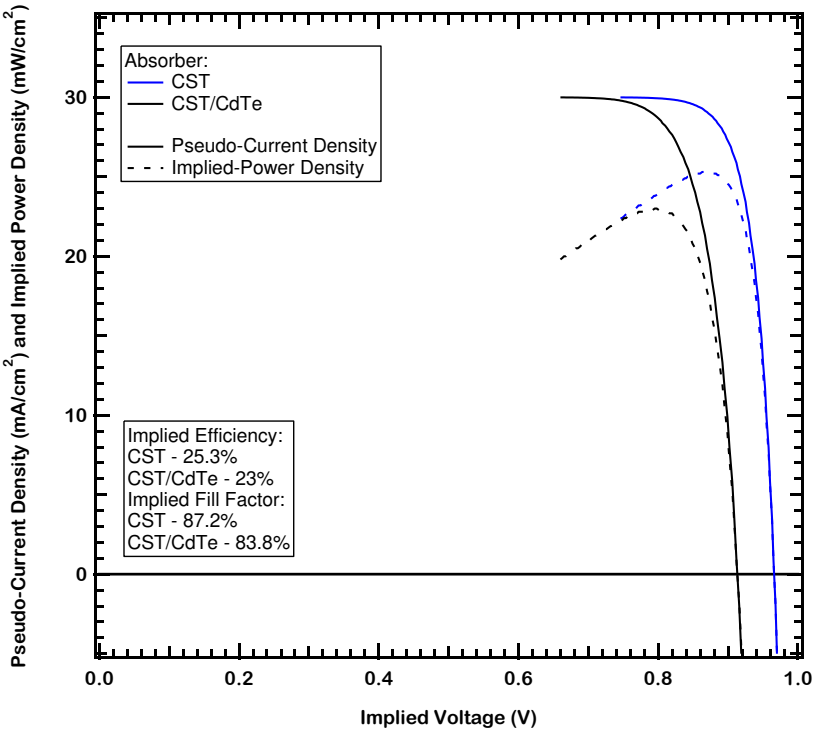

Figure 50: implied JV and power vs voltage curves calculated from suns-ERE data and accounting for sub-bandgap emission. Suns-ERE measured by Arthur Onno and Mason Mahaffey.

In addition to the measurement of suns ERE on well samples with well passivated surfaces to show the potential of the materials, a CdSeTe/CdTe/Te cell which measured 18.1% efficient was measured as well. Assuming the emission spectrum was the similar to the the CST/CdTe cell above, a recombination loss analysis for the JV was calculated – from absorptance/emissive losses to non-radiative recombination losses. The various JV curves can be found in figure 51, where it is clear that the non-radiative recombination losses are the largest limit to the cell, with the JV and implied JV being ~2% absolute different, primarily found in the difference of fill factor.

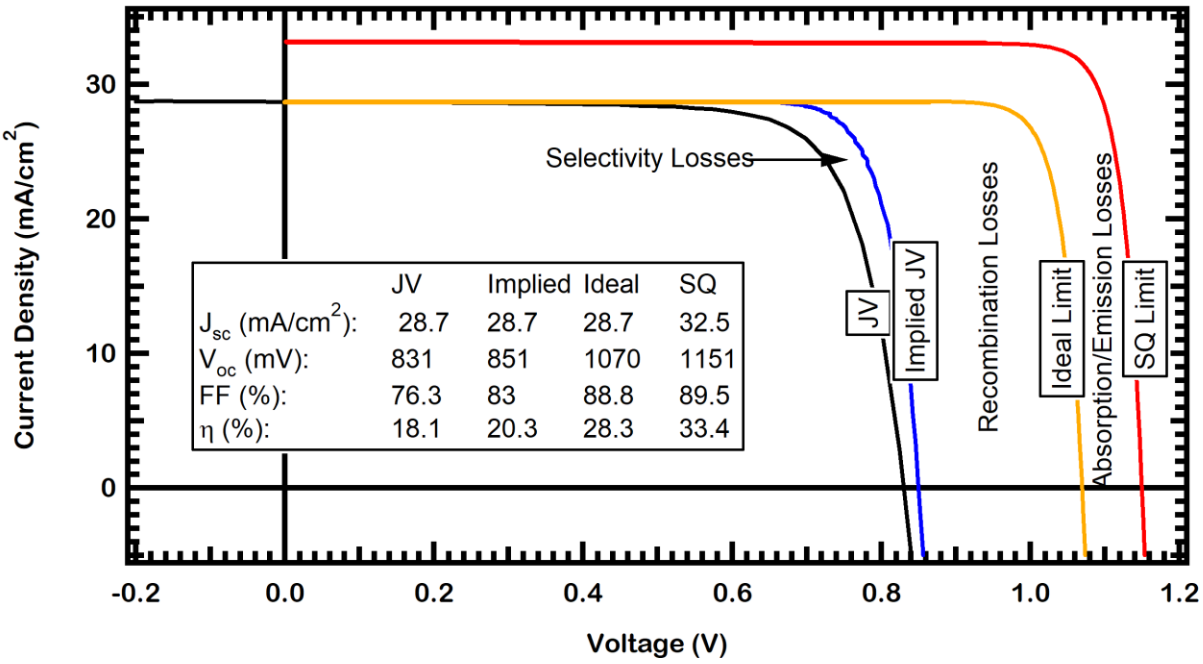

Figure 51: JV loss analysis from both absorption/emission and non-radiative recombination. ERE measured by Arthur Onno and Mason Mahaffey

CHAPTER 5: INVESTIGATION OF SELECTIVITY IN CADMIUM TELLURIDE SOLAR CELLS

It is easy to demonstrate that CSU's baseline CdSeTe/CdTe cells today are limited to a similar voltage by both selectivity and passivation. This is apparent in the data using co-sputtered MZO from Colorado School of mines, as the implied voltage and external voltage are similar in value, with the implied voltage ~20 mV greater than the external voltage. This implies that while the major losses are from passivation, the cell structure is not selective enough to support even that full voltage. However, it is necessary to understand where the selectivity that is present is coming from, and further, where the selectivity can be improved.

5.1) Electron Contact[3]

5.1.1) Status

The current Electron contact MgZnO has produced great benefits to CdTe solar cells. However, it is 100 nm of low electron mobility oxide, possibly inducing series resistance in the cells. It's band alignment however allows for transport of electrons and exclusion of holes so long as the recombination rate at the interface is low, which limits the available population of holes for recombination at the poor interface with FTO. Additionally, its wide bandgap allows for greater transmission of photons to the absorber. The combination of these two effects produced the Jsc and Voc increase first reported in CdTe cells [76-78].

[3] Results presented in this section related to co-sputtered undoped MZO are published in [78]. The rest is additional unpublished work.

Despite the clear benefits as is, MgZnO is a tunable oxide through alloying, and as such there is room for optimization. As with any film, the deposition technique and parameters can be optimized to produce films with the best possible properties for the application. With MZO, the most applicable properties are the alloying content and doping . In collaboration with Colorado School of Mines, we investigate MgZnO deposited by reactive co-sputtering, focusing on the alloying incorporation and dopants.

5.1.2) Co-Sputtered MgZnO

In addition to the passivation that the has been demonstrated in the previous chapter with co-sputtered MZO, an electron contact has to be conductive to electrons and resistive to holes. In the case of MZO, the selectivity appears to be due in a large part to the large energetic barrier to holes, as seen in the band diagrams from previous sections. This band offset dramatically reduces the probability of a hole entering the MZO and recombining at the electrode which ideally only exchanges electrons with the device. While the conduction band alignment is tunable with alloy content, at the optimum the offset is minimal which allows relatively easy exchange of electrons. This effect achieves selectivity by two effects: reducing the hole concentration in the MZO without reducing the electron concentration, thus increasing the relative conductivity of the MZO to electrons. Additionally, the small CBO acts to confine some electrons to the absorber near the interface, locally increasing the electron density and thus increasing the electron conductivity and reducing the hole concentration/conductivity through that portion of the film.

In spite of this, MgZnO is not believed by the community to be optimal. Numerous publications have recently called for increased doping of MgZnO, as the current MgZnO is believed to be low doped [76-78]. In addition to this, there has been literature showing that the relatively low series resistances measured in cells (~1 Ωcm^2) is in part possible only due to absorption of UV photons

increasing the conductivity of MZO similar to what was observed in similar structures with CIGS absorbers [78], with the conclusion that this is not an ideal situation, and the conductivity should be modulated by intentional doping. Further, it has been coupled with modelling showing that increased doping in MZO is necessary as the carrier concentration in the absorber is increased (as previously discussed this has been a push in the community) in order to maintain the benefits of the increased electron concentration relative to the hole concentration toward the interface to reduce recombination, although the same work shows this is less necessary if the interface recombination velocity is quite low [79].

Interestingly, the co-sputtered MZO appears to exhibit some of the beneficial traits that the increased doping have been theorized to. These cells again are prepared exactly as described in section 4.2 following the MZO deposition at Colorado School of Mines. Specifically, optimal O_2 sputter ambient influences this as the JV distortion increases with O_2 in the ambient (Figure 52), indicating that the conductivity of the MZO is high enough for the barrier not to be present without the UV illumination. This has been theorized to be related to the depletion of O from the MZO observed in the SIMS profiles previously presented, as oxygen vacancies are known to be donors in the material system [76-78].

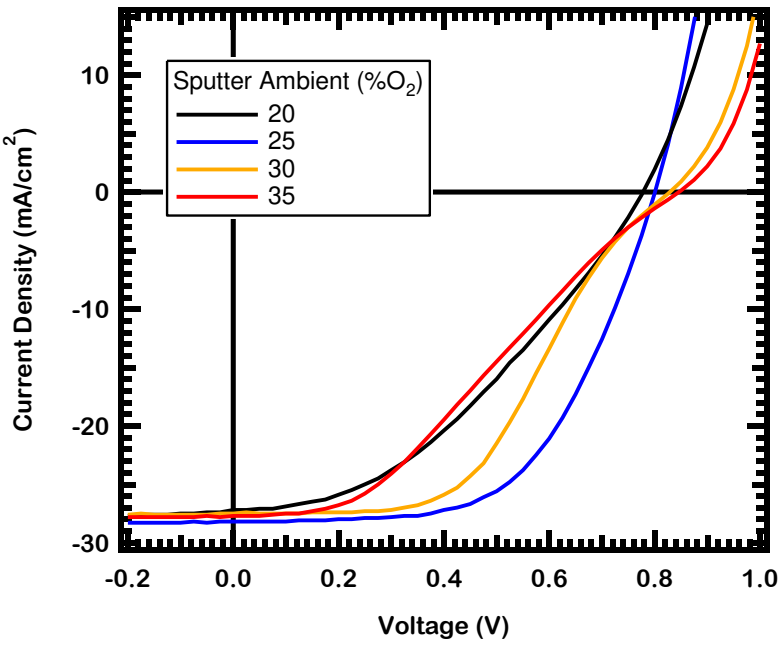

Figure 52: JV with a 400 nm – long pass filer from MZO/CdSeTe/CdTe solar cells with the MZO deposited under various oxygen ambient [78]

In addition to using an optimal ambient oxygen content to tune the MZO carrier concentration, investigation of Ga as a dopant has begun to be extensively researched. Taking advantage of the easy tuning of the co-sputtered MZO, a number of devices were made with different Ga contents, with the carrier concentration varying in kind as measured by Kelvin Probe measurement. Initial measurements of devices showed characteristic effects of large rates of recombination on FF and Voc, and trend with Ga content indicating an increase in the rate of recombination due to Ga defects. This high rate of recombination is confirmed by ERE too low to be detected using the standard measurement technique. A thin layer of intrinsic MZO to passivate the interface improved device performance, but devices with Ga-doped MZO remained well below their un-doped counterparts and the ERE remained below the detection limit. Boxplots of this data are found in figure 53.

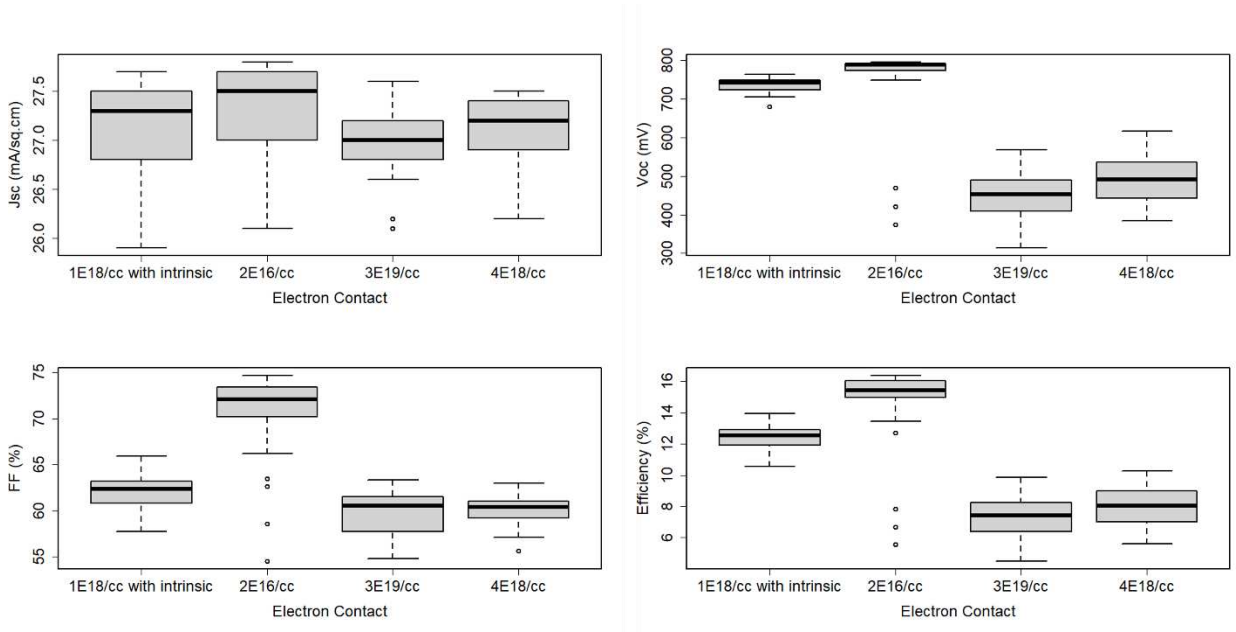

Figure 53: Boxplots of JV parameters for CdSeTe/CdTe devices using a Ga-doped MZO as the electron contact.

5.2) The Hole Contact[4]

5.2.1) Status

In CdTe, direct discussion of a hole contact is atypical, in favor of discussion of a p/n junction where the absorber is p-type and an ohmic "back contact" needs to be found to improve the FF by reducing the back barrier [81-84]. However, like any other solar cell, the technology is best discussed in terms of an absorber and an electron contact (traditionally the "n side of the p/n junction") and a hole contact which is conceptually separate from the absorber. In traditional CdTe cells with very short lifetimes and an equilibrium carrier concentration around $2x10^{14}$ cm^{-3} it is pretty easily demonstrated that the CdTe is acting as both the absorber (within the first 1-2 μm) and the hole contact through the remaining thickness. With a 2 - 10 ns lifetime and an

[4] Results in this section related to a-Si:H as a hole contact are published in part in [146]. The remainder are unpublished additional work.

approximate mobility of 100 cm^2/Vs, it is easily demonstrated that the diffusion length of electrons is less than 2 μm, forcing a dramatic reduction in electron conductivity through additional thickness of the CdTe. Cu doping of the back surface then acts to maintain the concentration of holes approaching the non-ohmic contact which depleted the majority carrier, preventing a dramatic reduction in hole conductivity which can be responsible for reducing the FF and causing s-shaped IV curves [55].

In CdSeTe/CdTe devices, the graded CdSeTe into CdTe again acts as a hole contact past the generation thickness of 1-2 μm. In part, this can be seen as the same effect – as the Se concentration decreases toward the back, the lifetime decreases and the diffusion length diminishes. This is easily demonstrated with TRPL measurement of lifetime from the front vs the back, and is further corroborated by the CL intensities declining dramatically from the front to back in cross-sectional profiles in literature [69-71]. In addition to this reduction in lifetime, the band structure forces some additional level of confinement of electrons to the lower bandgap region. At V_{oc}, the electron population shows no net current, and thus the gradient in the electro-chemical potential of the conduction band is minimal due to the natural inclination of electrons toward the lowest energy state available. The result of this is a relatively flat quasi-Fermi Level, at least through the graded region where lifetime is not as severely limiting diffusion length, while the CBM trends to higher energies. The effect of the population energetically normalizing while the CBM increases in energy is that the population of electrons decreases as a function of the CBM increased energy, which is easily demonstrated by calculation of electron population with increasing difference between the E_{CBM} and E_f using the the Fermi-Dirac distribution. Combined, this reduces the number of electrons entering the high recombination rate region at the back of the cell, the short lifetime of which then acts to further limit the number of electrons

exchanged at the electrode ideally only exchanging holes since this shorter lifetime reduces diffusion length and the QFLS but is still far slower than recombination at an interface which would thus have an outsized impact with a large concentration of excess carriers present. It is easy to demonstrate that an interface with a SRV of $1x10^4$ cm/s will produce a far larger rate of recombination than a bulk semiconductor with a lifetime in the 10s of ns for the same excess carrier concentration. Thus it is clear that a shorter lifetime CdTe at the back, while recombination prone, will assist in passivating the back surface despite it's overall high recombination placing a limit on the cell passivation. This has been modelled in the band diagram in figure 54, and the corresponding conductivities are proportional to the carrier concentration. It is clear that the concentration of electrons is reduced nearly 2 orders of magnitude by the graded region and another order of magnitude in the CdTe due to the short lifetime prior to the recombination active interface with Te.

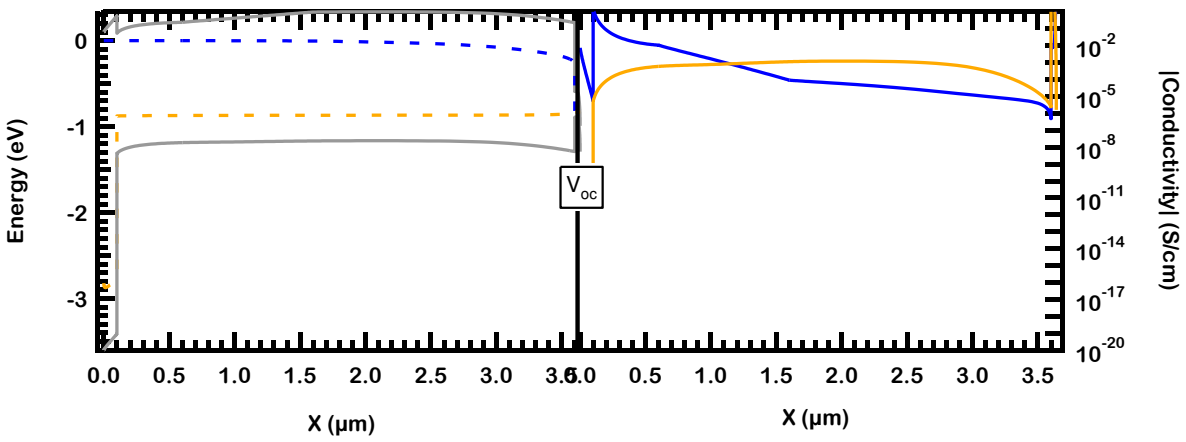

Figure 54: V_{oc} band diagram of a CdSeTe/CdTe cell with 500 nm CdSeTe and a 1 micron graded region.

It is notable however, that there is a deleterious effect to achieving hole selectivity through a short lifetime material at the back – the rate of recombination there introduces a gradient in the

electron qFL encouraging electrons to enter the short lifetime region and recombine, thus reducing the overall population of electrons through the absorber and reducing the qFLS as a result. A more ideal hole contact would limit the conduction of electrons through the hole contact into the electrode through other means than a reduced lifetime. This leaves two possibilities: the first is the effect that is accomplished only in part by the gradient in the CBM in CdSeTe/CdTe cells, an energetic barrier to electrons through engineering of the CBM relative to the absorber and the second is use of a material with extremely low electron mobility.

5.2.2) Routes to an Improvement

The concept of a large CBO to limit electron conduction to the rear terminal is not new, a plethora of literature has been published on the "electron reflector" [95, 127]. As such, it is well established that this effect can be accomplished through a few means. Similar to the Al-BSF structure in c-Si solar cells, a region of upward band bending will produce this effect and can be accomplished by both a high doping density in a small layer at the back of the cell and intimate contact with a material with an equilibrium fermi-level below that of the fermi-level of the absorber under illumination [27]. This effect increases the hole population through the absorber, necessarily moving the hole fermi-level closer to the valence band. As is known, the hole qFL is ideally flat at V_{oc} and as such, the reduced energetic difference between the hole qFL and the VBM induces upward band bending in the semiconductor, necessarily increasing the energetic difference between the CBM and the electron qFL (therefore reducing the electron population at the back to recombine at the hole contact's terminal). In the material system of CdTe it is extremely difficult to dope highly enough to produce the magnitude of band bending desired, and further, the deep fermi-level below vacuum, even with low carrier concentrations, creates difficulty in finding an appropriate material with an even deeper fermi-level.

A better approach to this would be to implement a large gradient or abrupt offset in CBM, similar to what CdTe already contributes in part. The larger this gradient or offset, the more effective at reducing the electron population, which is why the CdTe gradient at ~0.1 eV is not as effective as it could be and additional thickness of low lifetime CdTe is needed to further reduce the electron population via the shorter diffusion length [127]. An ideal gradient or offset would be large enough to force the electron population to near nothing without requiring the use of a recombination prone layer to further reduce the local diffusion length, which requires dramatic grading for $E_{f,e}$ to or a large enough abrupt offset to force the electron population to be dramatically reduced at the contact when, assuming carriers can equilibrate between the materials. Assuming that the minority electrons recombination rate is determined, an effective recombination velocity of the thermal velocity, even very small populations can lead to a forward current large enough to impact the external voltage, so it is best if the contacts are extremely effective at diminishing the minority carrier concentration at the contact.

If a material cannot be found with the appropriate band offset and doping is not possible, implementation of a low mobility material is the final option. In this manner, a low mobility reduces the diffusion length through the material, limiting the number of electrons which approach the hole contact terminal through the same mechanism as a shorter lifetime, but without causing excessive recombination. This however is plagued by the problem that materials with low mobility typically have low mobility for both carriers, and thus can induce resistive losses which affect fill factor, much the same as occurs with the formation of a non-ohmic back contact. Modelling of absorbers using a partial current density model for each contact however, show that when voltage is limiting the efficiency, gains can be made by introducing such a

material, as small reductions in the majority carrier exchange at the contact will not affect the power quadrant as much as the reduction in the current of the minority carrier [55].

Based on the work to date, it is apparent that CdSeTe is an excellent absorber. However, cells using this absorber are well below their maximum potential, with CdSeTe/CdTe structures out-performing CdSeTe only structures in production of useful work [73]. This, however, masks the greater potential of a CdSeTe-only absorber, as the superior CdSeTe/CdTe JV performance comes near the limit of that absorber's capability. This is apparent in the CdSeTe/CdTe absorber's ERE an often order of magnitude or more below that of the CdSeTe in any configuration measured to date, with the maximal V_{oc} being limited 10s of mV greater than current V_{oc} values.

This leaves the task of extracting the superior performance of CdSeTe devices, which currently suffer from quite low performance. In fact, since it is easy to show that CdTe in the CdSeTe/CdTe devices acts primarily as a poorly passivated hole contact, as discussed in the hole contact section, it would appear that the main difference between the CdSeTe/CdTe and CdSeTe only cells is that a large amount of recombination occurs at the Te contact, or essentially, that low or undoped CdSeTe is not effective as a hole contact for itself, and the long lifetimes allow for excessive recombination at the metal-like Te interface. It is likely that even if the extra recombination at that interface was not present a CdSeTe/Te cell would only show the same, or marginally increased V_{oc} as the bi-layer cells. This is apparent in that the measured V_{oc} of bi-layer cells is selectivity limited below the marginally higher implied voltage. It is possible that the selectivity is limited by the electron contact as well as the hole contact, but the deep valence band of CdTe and CdSeTe and estimated Fermi-level of Te would suggest that the major limit is the hole contact not being able to extract the majority carrier at the necessary rate [55]. In this

way, since the CdSeTe bulk does not limit the electron population at the back as part of the contact like CdTe does, the Te contact is poorly selective since it allows recombination of electrons and is non-ideal for hole extraction and needs to be replaced with a more appropriate contact.

The characteristics of such a contact in ideal cases are apparent from the discussion in the introduction. It should have a large conductivity to holes, with the energy at which it extracts this population matching the potential of holes in the absorber as to not induce resistive losses, a so-called “back barrier” or opposing Schottky diode. Additionally, it should have a low conductivity for electrons, so there are not excessive losses due to electron recombination at the hole contact’s metal or metal-like terminal. And finally, it should not induce a large amount of non-radiative recombination, as CdTe does in its bulk or at the interface as a metal would. Ideally this is using a material with a large CBO and a minimal VBO, allowing the potential barrier to electrons reduce the conductivity thereof and placing the allowed location of the fermi level to be as close as possible to the VBM of the absorber, providing its carrier concentration of holes is large enough, which is also needed for the large hole conductivity.

However, this is difficult to accomplish in practice, especially for CdTe since it’s valence band sits so deep below vacuum level [83, 84]. In the 1V V_{oc} MBE grown cell, doped CdMgTe was used at both electron and hole contacts to reduce the population of minority carriers since the band offset occurs in both directions [129]. However, use of this material has been extensively researched for poly-crystalline devices, and has generally been plagued by the loss of Mg during the $CdCl_2$ activation step resulting in the band offsets needed for effective reduction of electron population being diminished or eliminated [119]. Another option is CdZnTe or highly doped ZnTe, both of which offer potential barriers in the conduction band to electron conduction with

simultaneously small or negligible difference in the valence band maximum. These would appear ideal, but the ternary compound is prone to loss of Zn during $CdCl_2$ similar to CdMgTe [117, 118].

In the c-Si community, they have developed two methods for circumventing the need for a single material as a contact. This structure type requires a thin passivation layer to minimize recombination of the minority carrier, with a second layer with more ideal transport properties for the intended carrier immediately behind it. In so-called Silicon Hetero-Junction (SHJ) cells the materials used are intrinsic and doped amorphous silicon for the passivation and selective layers respectively [130]. In both Tunnel Oxide Passivated Contact (TOPCon) and Polycrystalline (silicon) on Oxide "PolO" cells, an oxide is used to accomplish the passivation while doped poly or micro-crystalline silicon is used to accomplish selectivity, with the difference between the two, if possible to distinguish, being the transport mechanism of the intended carrier (with TOPCon being tunnelling transport and PolO being traditional conduction through pinholes in the passivating oxide) [133, 134]. These structures inspired the Al_2O_3 layer when trying a-Si:H as a hole contact in the previously carried out work.

Al_2O_3, while known to produce excellent passivation for CdTe based materials, has an incredibly wide bandgap and further a large potential barrier for holes. This sets thickness requirements for tunnelling less than reasonable to control on a rough polycrystalline back surface. Luckily, other passivating materials are being discovered. In one report, NREL has shown that Cd-rich surfaces are less subject to non-radiative recombination than Te-rich surfaces, and as such could be advantageous to leverage as a passivation treatment, and recent work has shown that formation of TeO_x at interfaces with MgZnO and Al_2O_3 contribute to the passivation thereof, and now there is evidence of this TeO_x forming naturally on air-exposed surfaces [121, 126, 135]. Such effects

could be leveraged to render passive interfaces with materials most likely to produce other ideal hole contact effects, such as ZnTe.

Additionally, although this opens the door to re-trying some of the contacts previously attempted, there is room for other materials which could contribute the desired conduction behavior. One technology that has shown unimaginable progress in the last few years is that based on perovskite (PVK) materials. These materials leverage organic materials as contacts, and offer a number of options for use with CdSeTe.

5.2.3) Al_2O_3 and Amorphous Silicon

P-doped amorphous silicon has been demonstrated to be a highly effective hole contact for n-type single crystal CdTe solar cells [129]. Indeed, the only CdTe structure to consistently exceed 1 V measured V_{oc} is n-type sx-CdTe grown by MBE with CdMgTe passivation layers and a p-type a-Si:H/ITO/Ag contact and electrode structure for hole extraction [129].

a-Si:H highly doped with boron has numerous properties that make it an ideal candidate for a hole contact. It has a wider optical bandgap than CdSeTe or CdTe and can be doped heavily. While the effective work function and/or carrier concentration are difficult to ascertain and depend heavily on the hydrogenation of the layer, it is thought to be above 5.5 eV and $1x10^{18}$ cm^{-3} respectively [130]. While the 5.5 eV number is less than that of low doped p-CdTe (~5.7 eV) it's exact value is up for debate and the achieved 1V with an n-CdTe absorber would suggest it is high enough for efficient hole extraction [129, 130]. Additionally, the high carrier concentration would likely set the fermi-level so long as the holes are not depleted by the metal-like contact behind it [130]. In addition to the high work function and carrier concentration, it is a highly defective material. While that is usually *avoided* in solar cells due to the possibility of voltage

losses from non-radiative recombination, it has proven to be a benefit to the Si solar cells which use a-Si:H contacts. The key is that there is a passivating layer between the absorber and the highly doped a-Si:H, typically a-Si:H without dopants, which suppresses the recombination at the interface which would reduce the QFLS [130]. Additionally, its wide bandgap allows and high carrier concentration provide barriers to the incorrect carrier entering the contact by band offsets and band bending respectively [130]. As such, the quasi fermi levels converge within the material without causing large losses to the QFLS in the absorber [130]. However, the benefits of the defects are found primarily in the contact between the a-Si:H and the electrode. While the bands are bent unfavorably, which would result in a Schottky barrier to hole transport (essentially an opposing Schottky diode, as is typically thought to be an issue in CdTe cells), the plentiful defects allow for transport of holes to that electrode without major loss of energy by defect assisted tunnelling, maintaining the voltage despite the relatively smaller WF electrode's non-ideal nature [130].

In light of this, devices were made in various conditions – bi-layers with and without both As and Cu doping as well as CdSeTe with and without As-doping. Absorber deposition was carried out in the same manner as described in section 4.2, both with 420°C and 480°C substrate heater temperatures during CdSeTe deposition. The As-doped cells had As-doped layers deposited prior to $CdCl_2$ from both CdTe and CdSeTe with either $1x10^{20}$ cm^{-3} or $5x10^{17}$ cm^{-3} – the doped source was held at 560°C and the substrate heater was 450°C, and a Cd overpressure was supplied during the deposition by heating Cd to 211°C in a source that feeds the Cd vapor into the same pocket where the doped CdTe or CdSeTe are developed. Despite the ideal characteristics and demonstrated potential with MBE grown sx-n-CdTe, initial attempts for use with px-p-CdTe and

CdSeTe have shown poor voltages, around 250-350 mV below the CSU baseline structure as seen in figure 55. In the end it, it is likely that each structure had specific failure mechanisms.

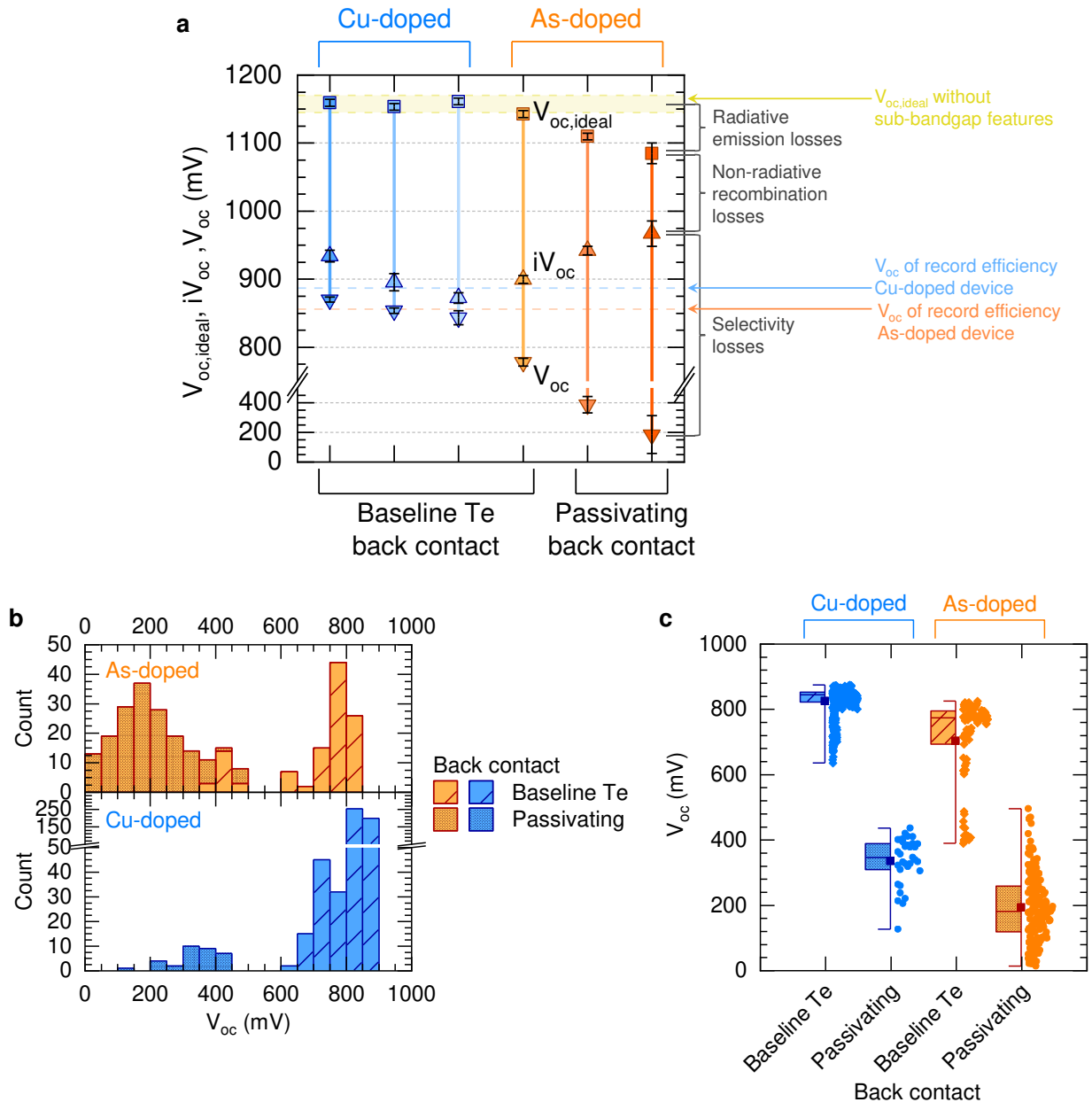

Figure 55: V_{oc} analysis of CdSeTe and CdSeTe/CdTe solar cells with Cu and As doping and the passivating contact containing Al_2O_3 and amorphous Silicon vs the Te contact [146]

Some of these structures underwent $CdCl_2$ and CuCl doping processes after deposition of all layers except the silver electrode used in these cells. In these cells, which typically produced better results that those that did these processes prior, it is likely that the doping of the absorber allowed for some small level of selectivity. This is however for a large part seemingly undone by a number of potential issues, some known and some unknown. First, it is known that high temperature processes are not "friendly" to amorphous silicon. While it is metastable in the amorphous phase, the kinetics suggest that full crystallization is unlikely to occur at the temperatures of the $CdCl_2$ treatment (~435 and 400°C) since extrapolation of crystallization time to these temperatures gives require times is 5-10 orders of magnitude longer than the duration of the $CdCl_2$ treatment [136]. The Cu doping process likewise is at a temperature ~200°C lower and would thus take exponentially longer and thus it is not a recrystallization which was likely the culprit. A process known to affect the material properties of a-Si is thermal dehydrogenation which has been documented to occur at the temperatures of the $CdCl_2$ treatment and alter both optical and electrical properties of the film, not the least of which are a reduction of both bandgap and effective carrier concentration [137]. These alone could account for a dramatice reduction of the properties which were hypothesized to provide selectivity – a reduction of bandgap would reduce any CBO to block the electron current, and a reduction of carrier concentration will simultaneously place the Fermi-Level in the a-Si:H above that of the valence band in the cell, and allow for further depletion of holes through the back portion of the device due to the non-ideal work-function of ITO for hole extraction from CdTe. In addition to this, the literature does not examine the effects of Cd, Cl, or Cu defects in either ITO or a-Si:H, which could further dramatically change the opto-electronic properties of these layers.

In samples which did not receive $CdCl_2$ or CuCl doping after deposition of the a-Si:H contact, selectivity was still poor. In this case, it is less clear what the cause might be. The best theory, since the current collection was close to ideal for a number of Al_2O_3 including structures, is that the a-SiH:B interface with Al_2O_3 pins the fermi level to a non-ideal value, as the estimated work function of p-doped a-Si:H is around 5.5 eV, approximately 1 eV below that of the SnO_2:F as typically modelled, which should allow for large voltages. This Fermi-level pinning, if present would force the hole collection at a lower potential than ideal for the structure, given the larger implied voltages. It was determined that significant efforts into determining the cause of these losses were best replaced with efforts to investigate novel materials that may provide the selectivity that a-Si failed to.

5.2.4) Organic Hole Transport Layers

With PVK technology's fast advance in efficiency following the "Passivation-Selectivity" framework, it is worth investigating materials they regularly use to select for holes. Although the band alignment is messy with organic materials, the "Highest Occupied Molecular Orbital" (HOMO) and "Lowest Unoccupied Molecular Orbital" (LUMO) are seen as analogous to the VBM and CBM respectively. Although the higher HOMO of many of these HTLs would appear non-ideal from a band alignment standpoint for CdTe-based materials since it is mid-gap, initial work with PTAA (HOMO: 5.25 eV) on CdTe from NREL/First Solar has shown that these materials may be useful despite these apparent non-ideal properties, likely due to the poor carrier mobility reducing the excess electron concentration rather than enabling more ideal hole transport properties [138]. As such, a number of these materials were used, and their HOMO and LUMO relative to the approximate CBM and VBM of CdSeTe can be found in figure 56. It appears that Me-4PACz should be able to supply the appropriate offset in the LUMO/CBO,

present in the rest of the candidate layers, while providing a better VB/HOMO alignment for hole extraction. However, MeO-2PACz and Me-4PACz are “self-assembled monolayers” (SAMs) and deposition of such layers on a semiconductor surface of the roughness observed in our devices is likely difficult to produce conformal coverage.

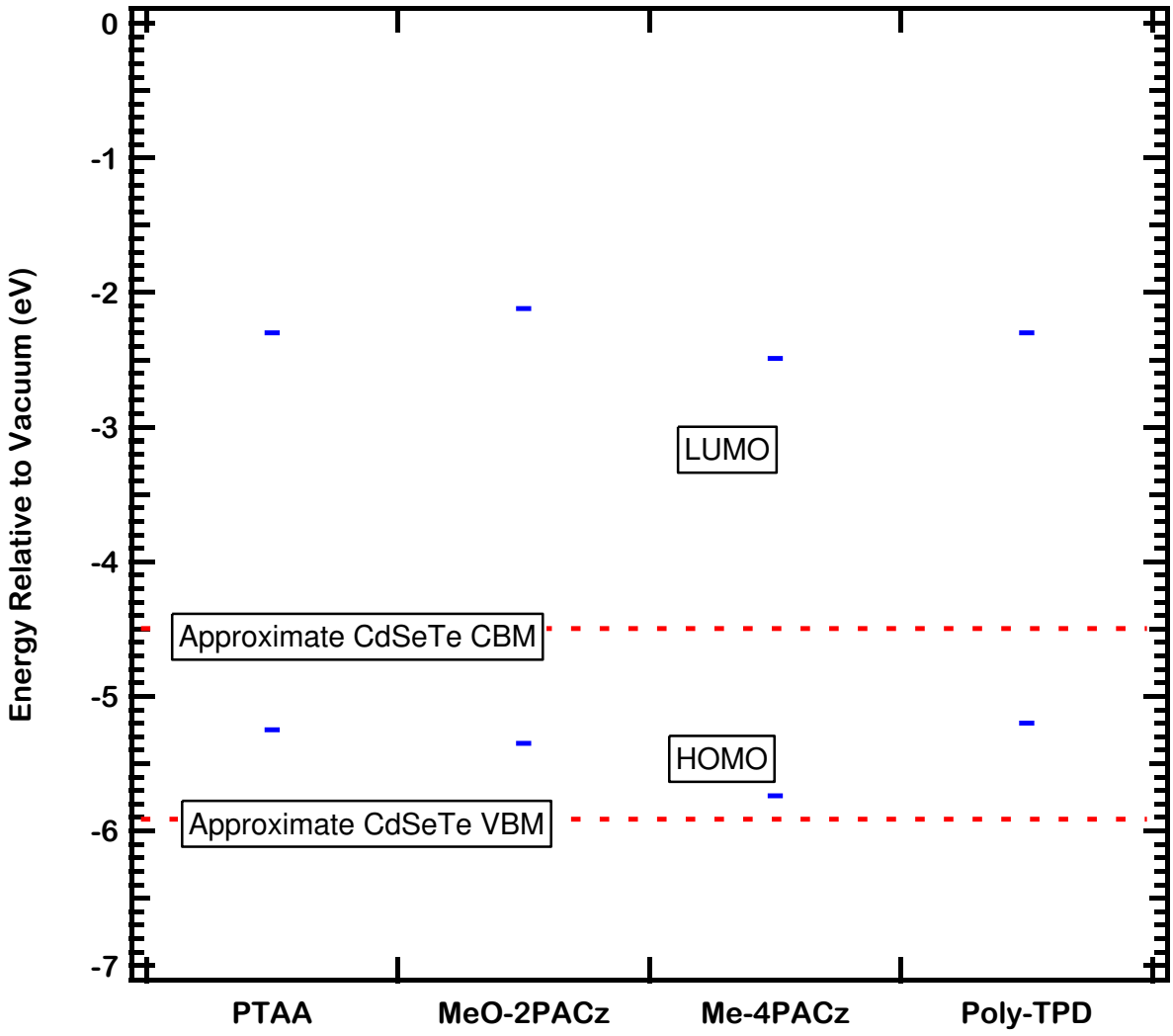

Figure 56: Highest Occupied Molecular Orbital (HOMO) and Lowest Unoccupied Molecular Orbital (LUMO) of hole contact candidates, data from [139, 140, 141, 142]

The first step for these layers was to measure the ERE before and after the deposition of them to ensure that their presence did not induce a large rate of recombination at the back surface, and then again after metallization to ensure that the films were sufficiently preventing recombination at the metal interface. HTLs were deposited by spin coating at Arizona State University on 1.5 μm CdSeTe films on the standard electron contact stack. MgZnO and CdSeTe were deposited using the method described in section 4.2, although the CdSeTe was deposited with a 540°C substrate heater temperature. The ERE results are found in figure 57. It is apparent that the ERE

and thus passivation was not hurt by the deposition of the organic HTL Layers, however, they did not remain passivating when Te and Cr were deposited.

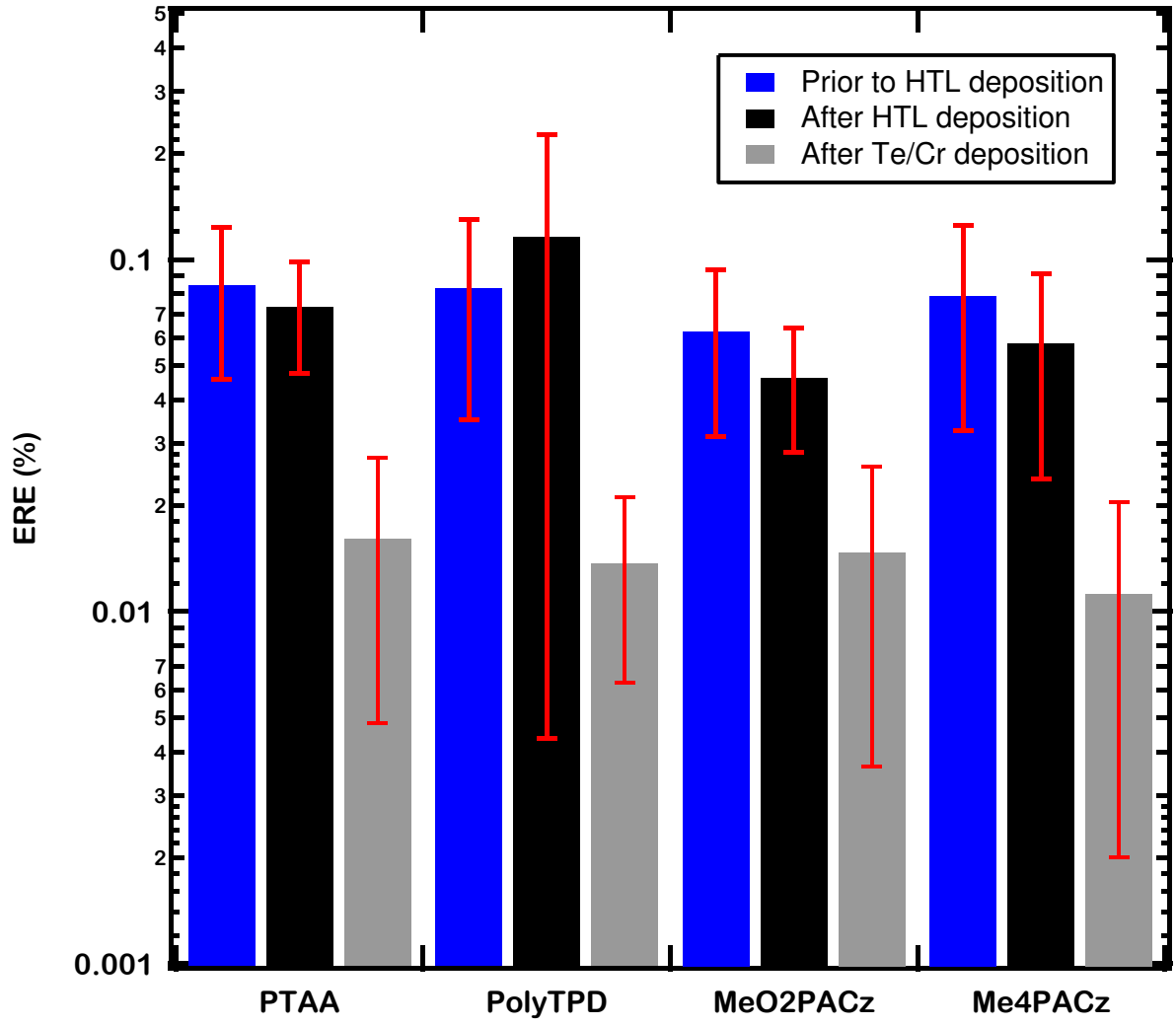

Figure 57: ERE of CdSeTe films measured at different stages in the device finishing process, ERE measured by Mason Mahaffey. Comparable samples with Te/Cr and Te/C/Ni directly deposited with no HTL were below detection limits.

It is likely that the very thin layers of these used in perovskite cells were unable to be conformally replicated on the rough CdSeTe surface. This is not an issue in the Perovskite community because the HTL is deposited on a relatively smooth ITO film prior to the deposition

of the perovskite absorber. This lack of conformality would allow for local formation of the CdSeTe/Te interface which is recombination prone and may act as a "sink" for excess electron concentration. Additionally, shunt paths through the cells after metallization, observed in many of the cell JV measurements, could be responsible for the reduction in ERE by essentially forcing the cells to short circuit despite the "open circuit" measurement conditions – thus extracting excess carriers and reducing their concentrations within the absorber. This is likely present in the samples, but the consistency of the ERE measurement for cells that were not as notably shunted would suggest other factors. A final possibility is then damage to the HTL or underlying CdSeTe from the Cr sputter deposition. This is again, less likely than the first option, since the Cr is deposited on a 40 nm layer of Te and the substrate is at a greater spacing from the dense plasma than our other sputter systems. Additionally, although it may not show in the bi-layer structure since the back surface with Te is already heavily recombination prone, the sputter deposition of electrodes from the same system has produced high performance devices.

Next, completed cells were delineated from the films and JV tested. They were compared to control samples with Te/Cr and the typical C/Ni paint. A number of the cells were entirely shunted, previously observed within the CSU laboratory in some cases with the sputtered metal electrode and not with the painted electrode. However, the Methyl-Ethyl Ketone solvent used in the painted electrode is not compatible with the organic compounds and thus the sputtered electrode was necessary. Despite the shunting problem, at least one cell from each contact group was not so thoroughly shunted as to pass through the origin of the JV plot and were used as closest to representative of the condition. The Open circuit voltages are found in figure 58 with the approximate iV_{oc} corresponding to the ERE measured after metallization. ERE was detection limited for all directly Te contacted samples, and thus iVoc is unknown and below that shown

for those samples. It is clear that the V_{oc} trails the iV_{oc} by a significant amount, suggesting that the selectivity in these cells remains an issue.

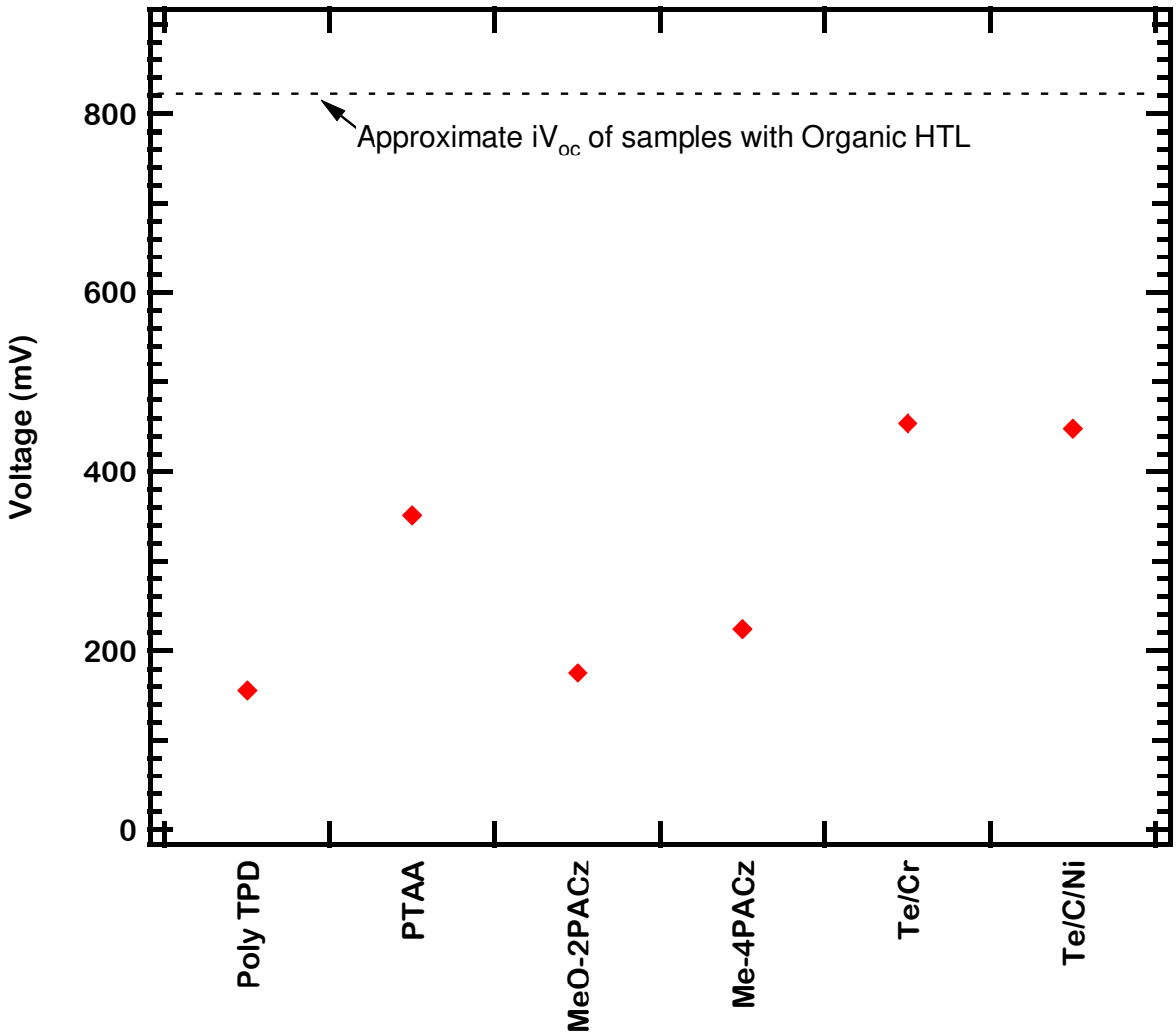

Figure 58: Open circuit voltage of CdSeTe cells with organic hole contact layers compared to their implied voltage as calculated from ERE assuming a ideal voltage of 1050 mV

5.2.5) Use of ZnTe with Passivating TeO_x

The use of ZnTe is currently the standard contact for the pre-eminent CdTe-based PV manufacturing company, First Solar. In spite of this, efforts have often fallen short at other institutions to demonstrate dramatic improvement in device performance with such a material as the hole contact. This is possibly due to the recombination prone CdTe layer that precedes it, but recombination at the interface has also been identified as a possible reason for the lack of expected device improvement from the hypothesized band structure [143, 144]. As such, it may produce the full expected benefits using a CdSeTe absorber with a local passivation of the interface rendering the CdSeTe/ZnTe interface more passive. The discovery of TeO_x as a passivation layer formed by air exposure provides a pathway to such a structure.

Sputter deposition of ZnTe at CSU is possible using an existing system, and has been used to deposit ZnTe films at the back of CdTe previously. ZnTe contacts were first evaluated in terms of their carrier concentration, deposited under conditions previously found to be optimal for device performance in the lab: an RF power of 60W across a 4 in diameter target, while the substrate is heated to 250°C. Next the passivation of the CdSeTe films upon which the ZnTe was deposited was checked via ERE measurement before and after the deposition, with varying deposition powers and substrate temperatures. This was then followed by metallization and measurement of the devices.

First, 900-1000 nm films of ZnTe were sputtered onto plain glass with an intrinsic SnO_2/SiO_2 barrier to sodium diffusion. Films deposited were from either an undoped source or a source with 8% Cu in the target. The undoped films were subjected to an anneal in a Cd_2As_3 vapor at 300°C (1. 280s, 2. 560 s, 3. 1120 s, and 4 2240 s) or a CSS CuCl doping process (1. 140s dose and 280 s anneal, 2. 240 s dose and 560 s anneal, 3. 140 s dose and 560 s anneal, and 4. 240 s dose and 280

s anneal), and one film was left undoped as a comparison. Films from the Cu doped target were annealed at 200°C for the same durations as the Cd_3As_2 anneals. Hall measurements were carried out on the films. The μA constant current setting was producing poor results, and NIST claims nA constant current during allows measurement up to ρ=1x10^7 Ωcm, thus a nA constant current setting was used for measurement of ZnTe films and results are assumed to be trustworthy for films with ρ=1x10^5 Ωcm [147]. Estimated carrier concentrations from the Hall measurements are found in figure 59. Te and TEC10 were measured to verify the system produced trustworthy results and carrier concentrations for these measurements match the estimated values in literature [83, 148].

Only the ZnTe deposited from the target containing Cu showed resistivities low enough for trustworthy results. These samples showed an increase in carrier concentration with post-deposition anneal time, as well as an increase due to additional copper from copper flakes on the target during deposition. All the sample with extrinsic Cu or As doping, as well as the intrinsic ZnTe reference samples, all showed high resistivities and with carrier concentrations of 1x10^{11} to 1x10^{12} cm^{-3} if the numbers can be trusted. While greater than n_i, which is low for ZnTe due to it's wide bandgap, such high resistivity and therefore low conductivity is non-ideal for producing selectivity without additional layers. This work suggests that ZnTe:Cu deposited from the ZnTe:Cu target with a long anneal should produce the best selectivity, and therefore voltage if sufficiently high ERE can be maintained in the absorber.

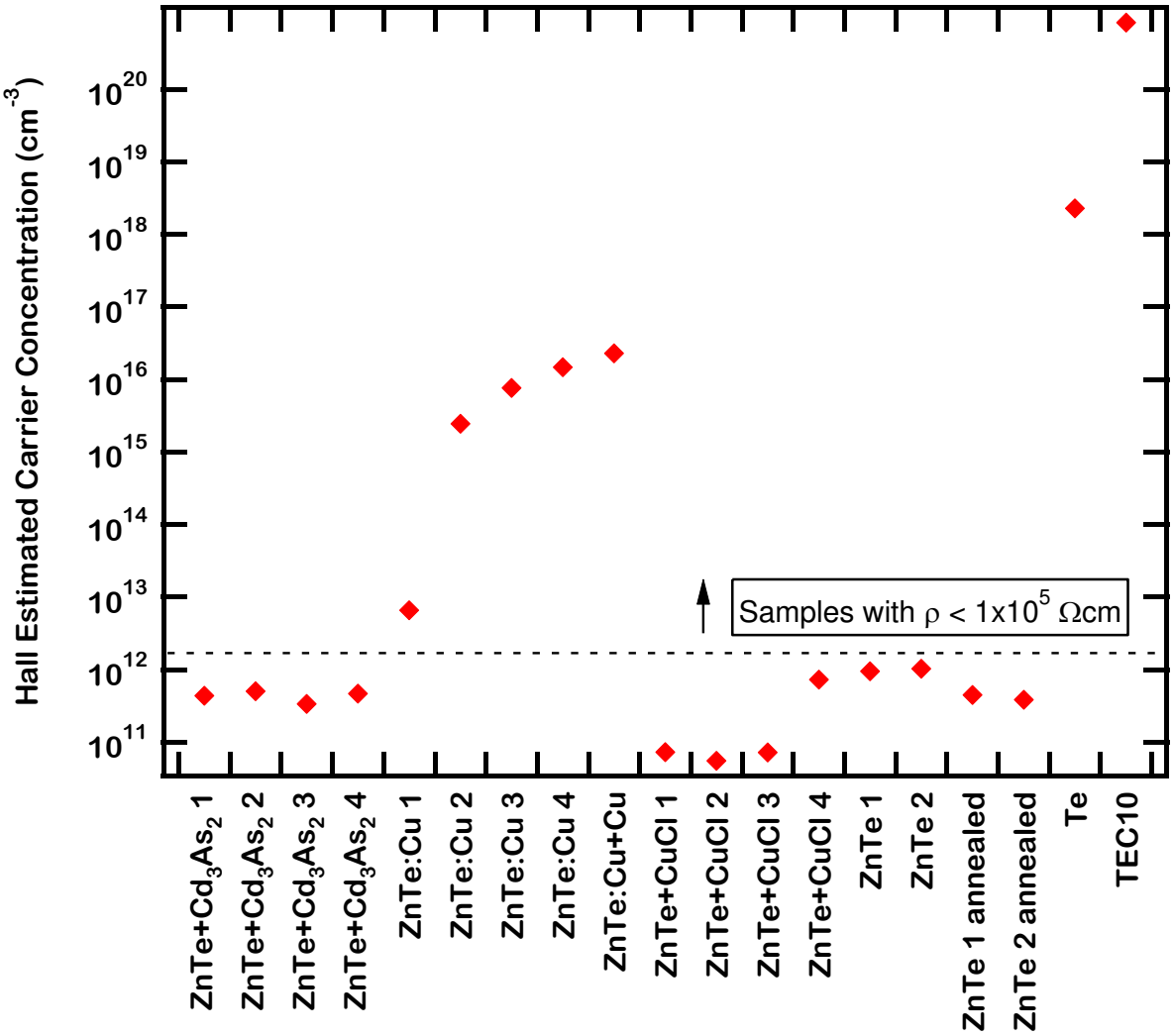

Figure 59: Calculated Carrier Concentrations in ZnTe from Hall Effect Measurement

Since doping of the ZnTe was unsuccessful in most cases and the successful case included Cu, known to hurt ERE in CdSeTe/CdTe structures, it was necessary to understand if undoped ZnTe might work. Another path to selectivity with ZnTe is also apparent: an intrinsic ZnTe layer to provide the desired CBO with Te or another high work function material behind it to provide the conductivity. Te's work function has been estimated to around 5.5-5.6 eV, approximately 0.3 eV above the VB of both CdSeTe and ZnTe. Assuming this pins the Fermi-level, this should allow approximately $1x10^{14}$ cm^{-3} hole density at the interface for both ZnTe and CdSeTe with Te.

Modelling of 1.5 micron CdSeTe cells (TCO WF = 4.5 ev,100 nm MZO ($2x10^{14}$ cm^{-3} n-type), S_{front} = 100 cm/s, CdSeTe with 1 microsecond lifetime (undoped), S_{back} = varied, 100 nm ZnTe (p-type doping varied), and Te WF = 5.6 eV) with a ZnTe hole contact show that while a very large carrier concentration is ideal, high voltage and efficiency can be achieved with a low carrier concentration in the ZnTe contact provided sufficiently low recombination at the interface, as seen in figure 60.

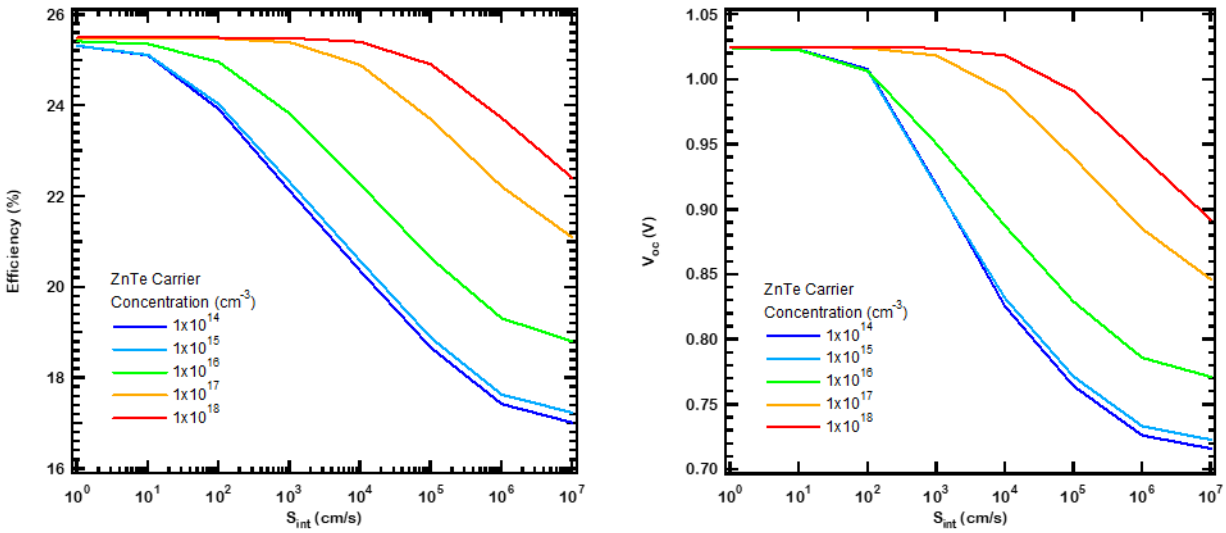

Figure 60: SCAPS 1-D modelled Efficiency for 1.5 micron thick CdSeTe cells with a ZnTe contact at various Carrier Concentrations and interface Recombination Velocities

Since ZnTe:Cu could provide sufficient conductivity and otherwise a lower doped ZnTe can still provide selectivity with a small rate of recombination at the interface, examination of this interface is essential. This was examined by ERE measurement at various stages in the device fabrication process. Similar to the work with the organic materials, ERE was measured after fabrication of the absorber films (identical process to the absorbers in that work) and a two week wait time in desiccated storage to allow TeO_x formation, then ERE was measured before and

after ZnTe deposition. ZnTe was deposited at all combinations of 60 or 100 W RF power across the target and 150 or 250°C substrate temperature. Additionally, a sample as fabricated with ZnTe:Cu was made to check if the Cu dopant which allowed for greater carrier concentration in the ZnTe would hinder the formation of a passivated contact with ZnTe. ERE measured before and after these depositions is found in figure 61. Demonstrating a reduction of ERE that is not correlated with the deposition conditions, although the lower starting ERE of CdSeTe was partially to blame since the ERE was pushed below detection limits in many cases. In the detection limited cases, assuming the same radiatively limited voltage calculated in previous sections, the implied voltage is below 813 mV and the one measurable sample shows 829 mV.

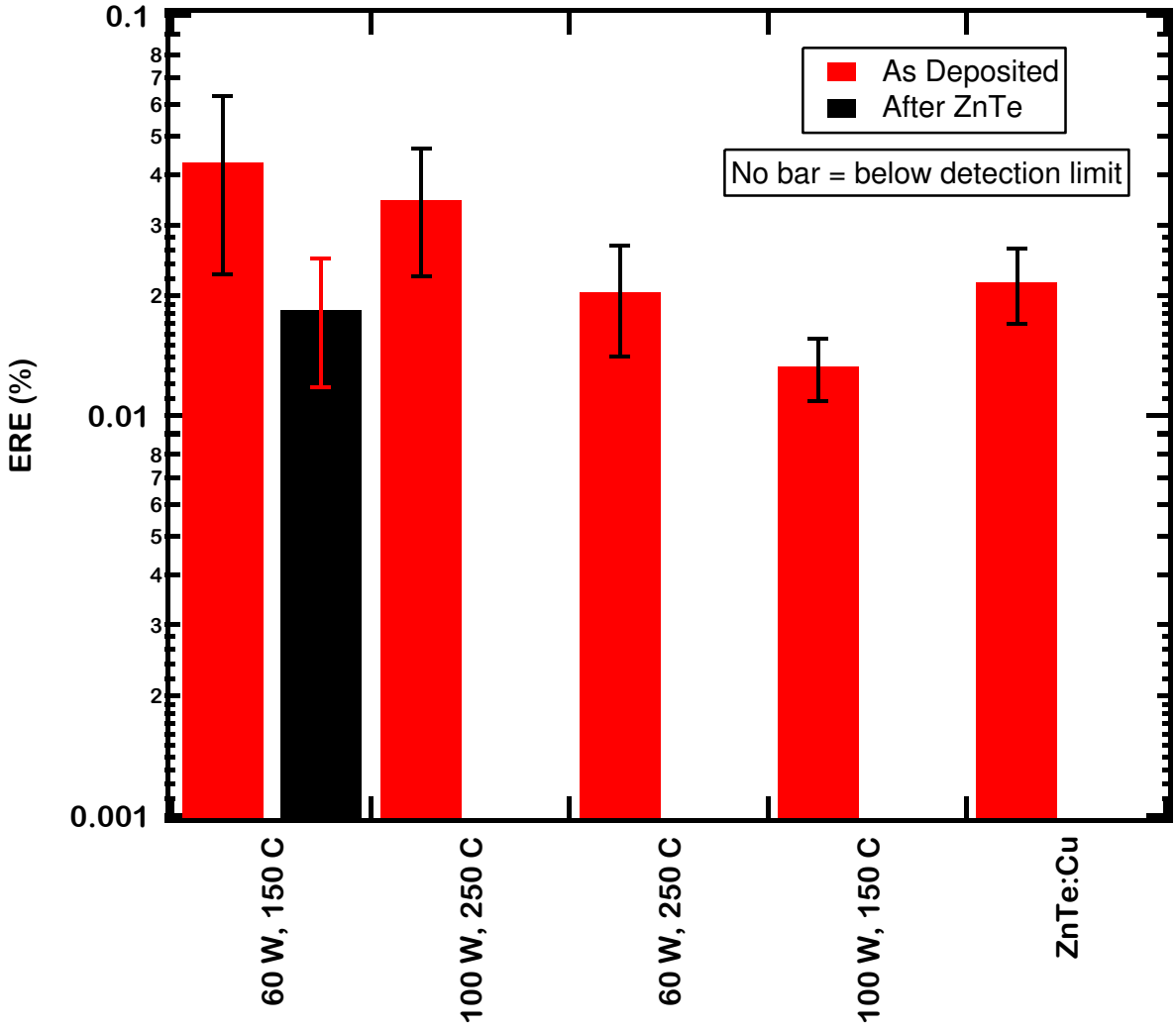

Figure 61: ERE measured on 1 micron CdSeTe films with ZnTe of different deposition or doping conditions. ERE measured by Mason Mahaffey.

ZnTe was again deposited at the back of 2 additional 1.5 micron CdSeTe absorbers with better ERE, both with the 60 W, 250 °C deposition conditions previously found to be optimal in CdSeTe/CdTe devices since the ERE decreased for all samples irrespective of deposition condition, this time to get a better idea of the extent of this reduction in passivation. One sample was subject to an As doping process, an Cd_3As_2 anneal, however the second was undoped like

the above samples, and both were subject to storage in dry air of over 2 weeks to allow TeO_x formation similar to the above samples. Here, the ERE is not below detection limit after the ZnTe deposition. The ERE did see a reduction of over 50% in both cases however, as seen in figure 62, confirming that the ZnTe interface is not passive, bringing the implied voltage from 923 and 910 mV to 889 and 885 mV for the undoped and As-doped CdSeTe film respectively.

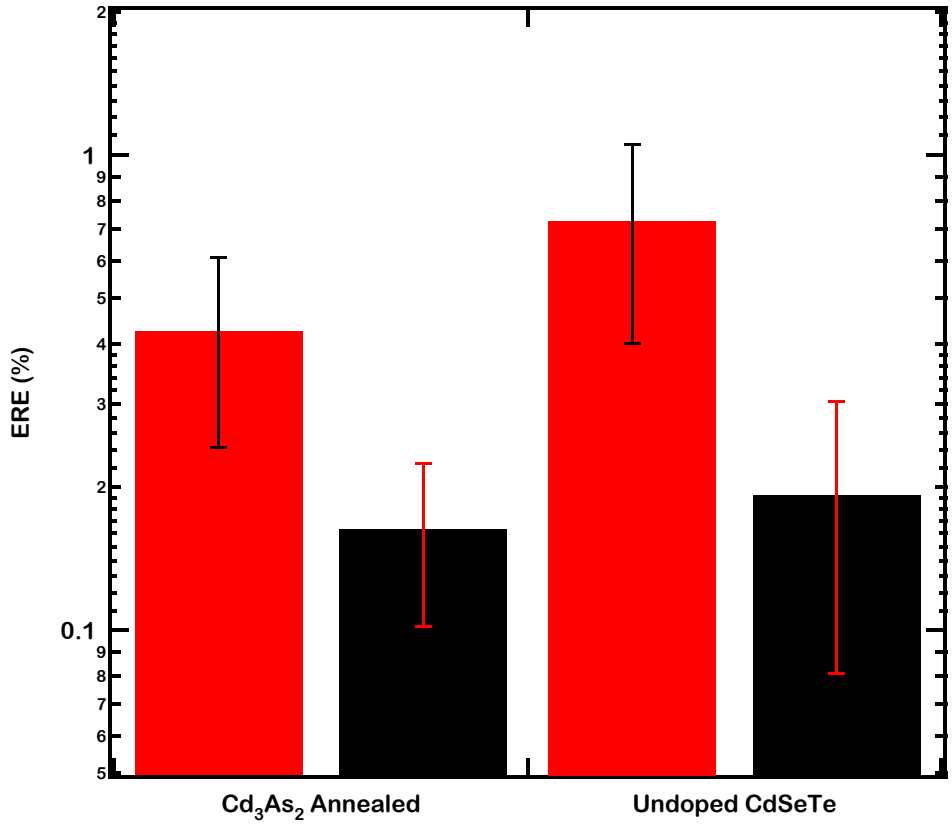

Figure 62: ERE of an As-doped and undoped micron CdSeTe film before and after ZnTe deposited at 60 W and 250C. ERE measured by Mason Mahaffey

It is apparent that the TeO_x formation at the surface is not sufficient to passivate the interface, since there was a decline in ERE in all cases. There are a number of possible factors. First, is sputter deposition places the surface of the absorber during deposition within the plasma since

the target to substrate spacing is only ~6", and high energy ion bombardment could damage the TeO_x that has formed. Additionally, it is possible that the thickness of TeO_x is not sufficient to prevent electron transport to the ZnTe interface, where they may recombine. Finally, following the DFT results there may be a number of states which remain near the CB, recombination of electrons through which would be mitigated by the band bending in the case presented in the DFT, but it is unclear if such band bending is present or remains after deposition of another material [new 127].

Devices were then made from the films in the passivation check and JV tested to determine the V_{oc}, along with a control sample with Te in direct contact with the CdSeTe absorber, which are found in figure 63. Although it is impossible to compare the cells which are ERE detection limited to their iVoc, it is clear that there is improvement in the device V_{oc} when 60 W is used rather than 100W. However, it is apparent that the high and low ERE cells with ZnTe deposited at 60 W and 250C, and those with and without As doping have very similar $V_{oc,}$, which indicates that the ZnTe is behaving in the same way, and limiting the V_{oc} in these cells by selectivity, likely due to large resistance to holes, since the implied voltages, when known, are approaching 900 mV. This is further exemplified by the ZnTe:Cu devices, with greater conductivity through the ZnTe, matching the control Te devices. It stands that the undoped ZnTe does produce selectivity losses, in addition to all conditions of ZnTe used here reducing the passivation.

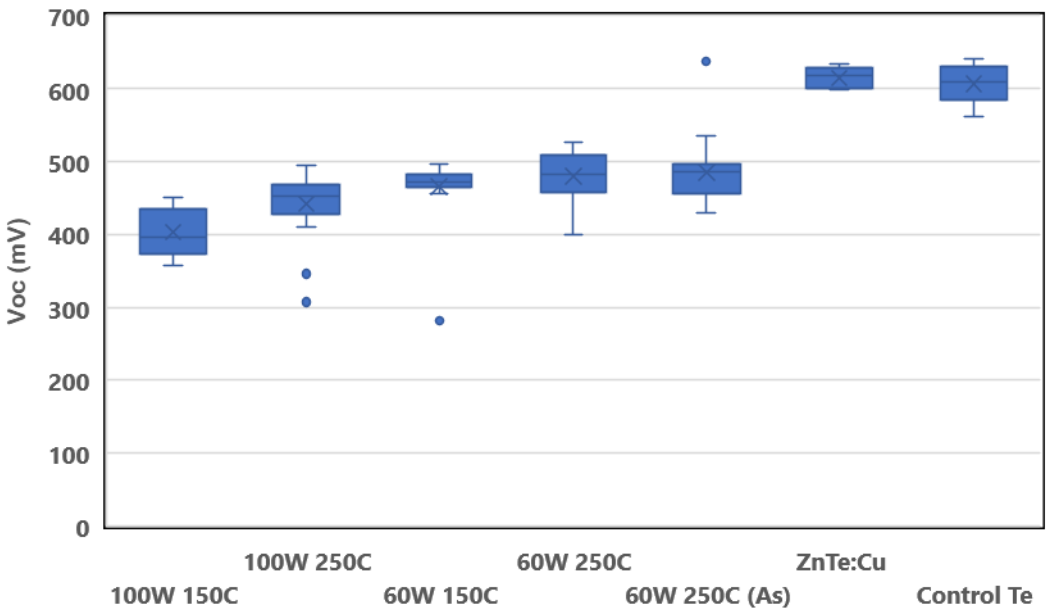

Figure 63: Open Circuit Voltage of cells made from 1 micron CdSeTe with a ZnTe contact

5.2.6) Al_2O_3 and Cu-doped CdTe

It is clear that the CdTe is limiting the internal voltage of CdSeTe/CdTe solar cells, but the CdTe:Cu is providing some appropriate level of selectivity for the current structure. In order to leverage the large QFLS and lifetime in CdSeTe samples with the selectivity provided by CdTe, a structure was devised to leverage both effects. This involves a layer of Al_2O_3 to passivate the interface and provide a diffusion barrier to dopants, followed by a thin Cu-doped CdTe layer to provide selectivity.

For these cells 1 nm Al_2O_3 was deposited by RF planar magnetron sputtering at 240 W across a 4" diameter target in 8% O_2/balance Ar at 5 mTorr behind a 2 micron CdSeTe film deposited by a similar process to that described in section 4.2. Films were then subjected to a CdTe deposition of 0, 50, or 100 nm and a $CdCl_2$ process. For each condition, a plate was made with the CuCl

doping process prior to or after the deposition of the Te electrode, with one sample without any Cu and a local control with no passivation layer and with Cu. Using ERE measurements, and assuming an ideal voltage of ~1150 mV (minimal losses due to sub-bandgap features), the voltage loss breakdown is found in figure 64 for the best cell in each structure, with the distribution showing the maximum only slightly higher than the mean for each condition.

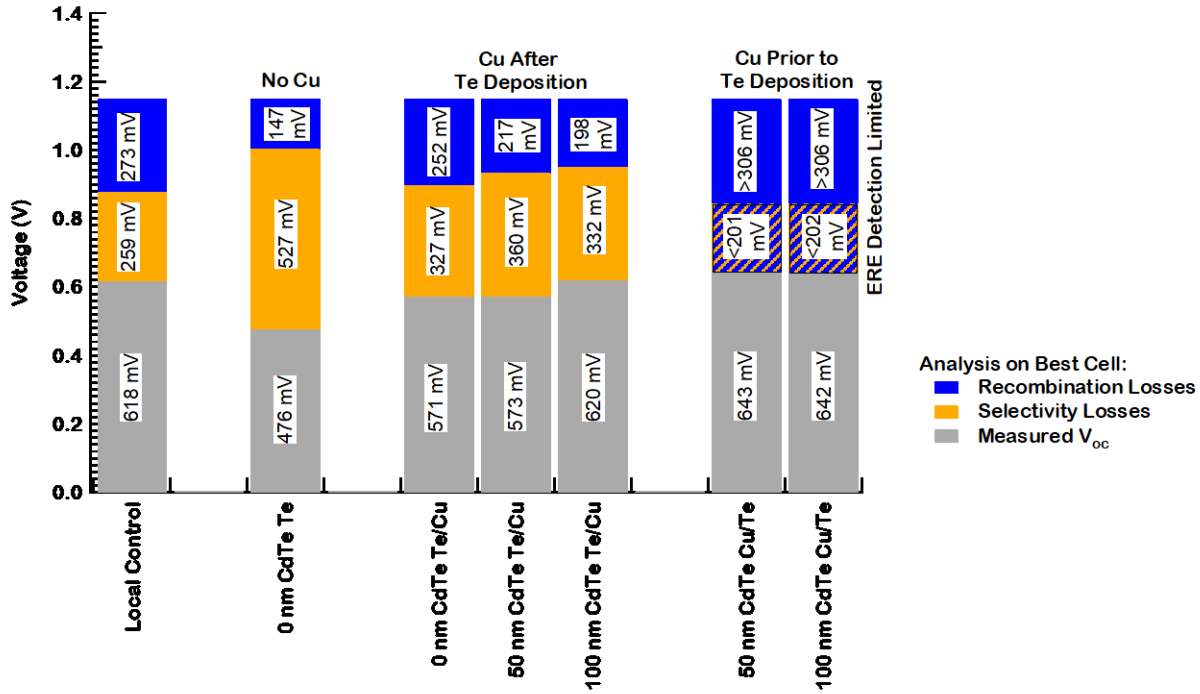

Figure 64: V_{oc} loss analysis for 2 micron thick CdSeTe cells with 1 nm Al_2O_3 passivation and CdTe:Cu as a contact. ERE measured by Mason Mahaffey

It becomes apparent that the recombination losses in the cell trend directly with the number and overall thickness of layers the Cu was required to diffuse through, other than the Cu-doped control sample. Additionally, it is clear that the Cu dopant making it into the absorber is likely the reason for the reduced passivation, since that increase passivation comes at the cost of the selectivity. This is observed in the higher measured Voc data but smaller implied Voc with a

smaller required diffusion thickness for Cu. A thicker CdTe layer may produce a better barrier to Cu diffusion, and allow for overall better selectivity provided the Al_2O_3 passivation keeps the ERE high with the thick, lower lifetime material behind it. While exact selectivity losses are unknown for the cases where the ERE is below detection limits, it is clear that they are subject to the smallest selectivity losses. This indicates that the selectivity in this structure is inherently at the cost of the passivation, which is required to advance the voltage and efficiency.

5.2.7) Issues in the Bulk

Through the work in developing a hetero-junction contact for hole extraction, it became clear that not only was the contact an issue, but so was the bulk. This became apparent first in a loss of J_{sc} present in devices made of CdSeTe only that were greater than 1-2 microns in thickness. In the modelling of a CdSeTe-only device that matches the thicknesses and lifetimes of those measured with CdSeTe and a Te contact, a small hole mobility was required to reproduce the majority of the measurements on the cell.

First, this was proposed as the mechanism for low J_{sc}, as equal currents of holes and electrons in opposite directions are needed for current to flow. In keeping with the relation that the partial current of electrons or holes is related to the conductivity and the gradient in the quasi-Fermi level thereof, it makes sense that a reduced mobility to the carrier traversing the greater thickness would, provided sufficient reduction, limit the overall extracted current. As such, modification of the electron mobility did little in modelling, other than improve the open circuit voltage by reducing the electron concentration at the back interface since the photo-carriers are excited in close proximity to the electron contact. On the other hand, a reduction in the hole mobility alone produced a reduction in Jsc, specifically when the hole mobility dipped below 0.1 cm^2/Vs did this come close to the measured J_{sc}. Indeed, comparing CdSeTe/Te cells vs those modelled at

comparable thicknesses with a 0.05 cm^2/Vs hole mobility showed a comparable trend with thickness in both J_{sc} and V_{oc}. The simulated and measured JV curves can be found in figure 65. Table 1 provides model details.

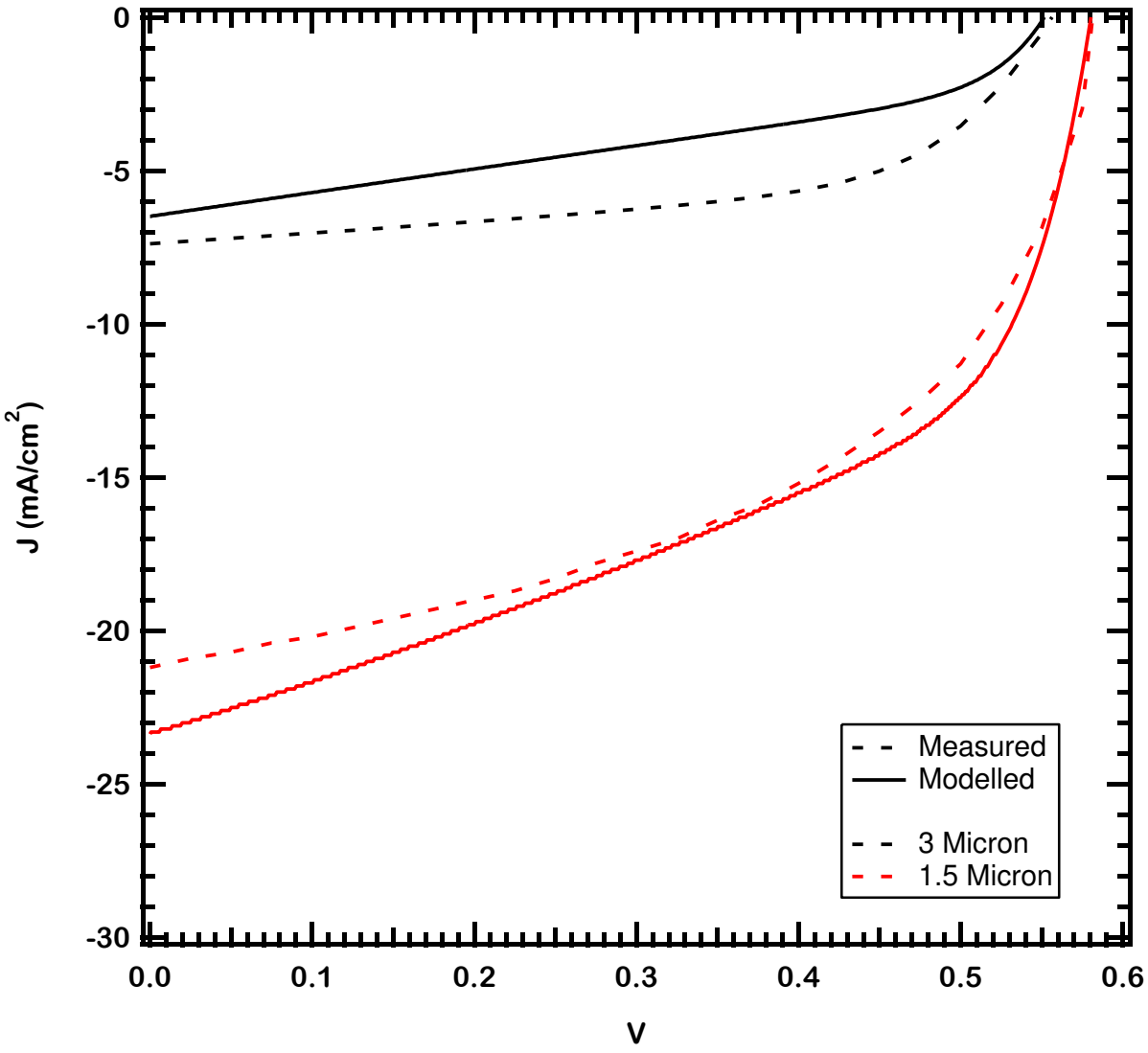

Figure 65: SCAPS Simulated JV and measured JV for cells with properties approximately the same as found in table 1.

Next, this same simulation which produced the low current was using the measured lifetime in the bulk of ~1 microsecond for this structure. This allowed for a large implied voltage at the

front of the device as modelled, while producing a voltage within the range of the measured cell – dramatic selectivity losses through the bulk of the semiconductor as depicted in figure 66. In fact, the modelled implied voltage, matches the external voltage closely if the device is modelled with a higher hole mobility.

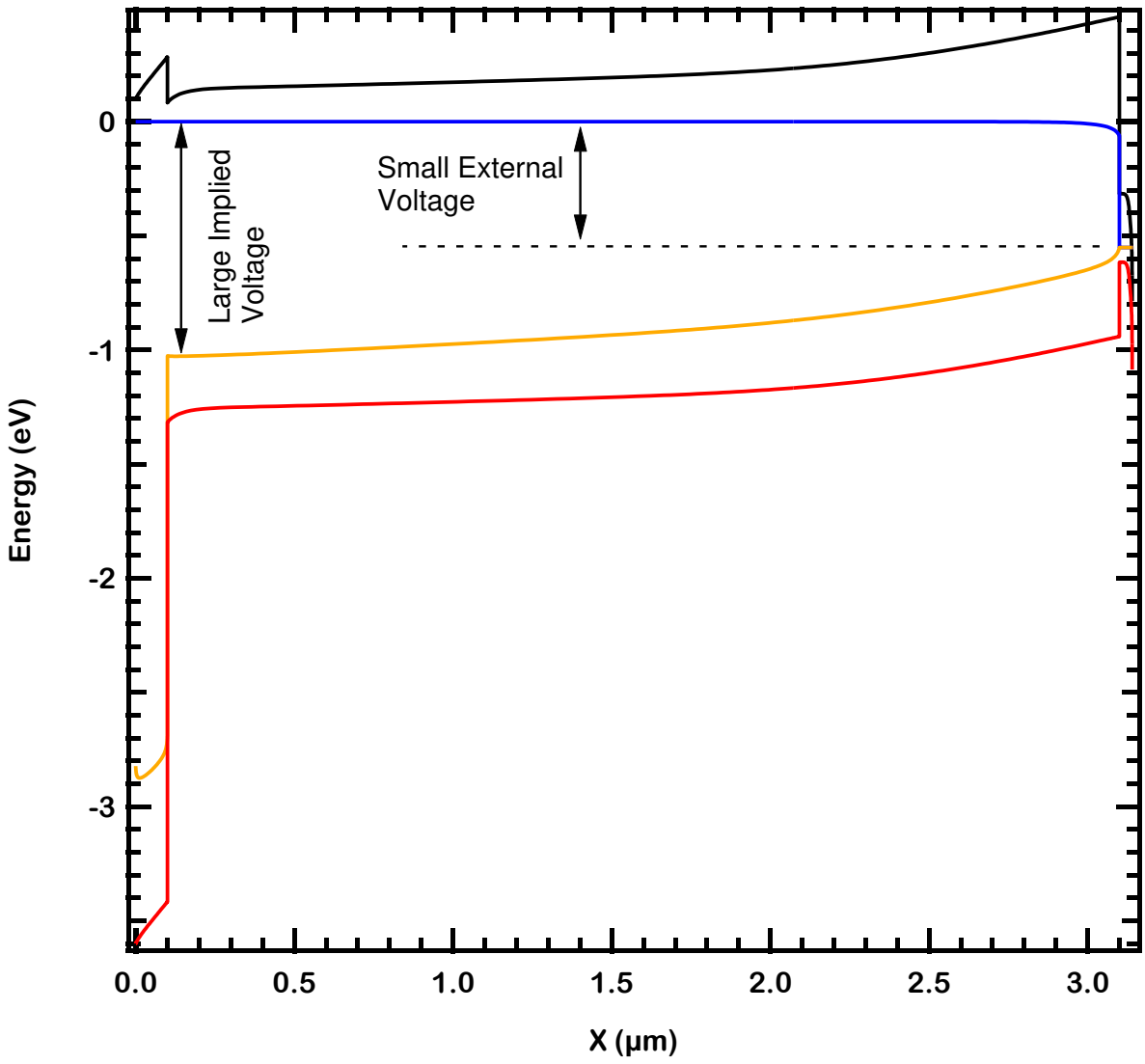

Figure 66: V_{oc} band diagram for the SCAPS simulated cell with low hole mobility

TABLE 1: PARAMETERS FOR SCAPS MODEL

Property	Front Electrode	MgZnO	CdSeTe	Te	Rear Electrode
Electron Affinity (eV)	-	4.3	4.5	5.275	-
Bandgap (eV)	-	3.7	1.4	0.3	-
Work Function (eV)	4.5	-	-	-	5.04
Carrier Concentration (cm^{-3})	-	$2.00x10^{14}$ (n-type)	intrinsic	$1.00x10^{18}$ (p-type)	-
Lifetime (ns)	-	1	1000	0.1	-
Hole Mobility (cm^2/Vs)	-	25	0.05	50	-
Electron Mobility (cm^2/Vs)	-	1	320	50	-
Thickness (μm)	-	0.1	1.5 and 3	0.04	-
SRV with CdSeTe (cm/s)	-	100	-	1.00E+04	-

Next, the possible source of poor hole transport: the very emissive defects that reduced the detailed balance limiting voltage of the cells as discussed in the passivation section. Because the black body spectrum is quasi-exponential in the NIR, a very small absorptance and therefore minuscule density of defects at these states would be necessary to produce the emission observed. The low DOS would suggest that carriers in these states do not have available states at similar energy to transition between as they traverse the material, and thus such states act to trap

carriers. Indeed, injection dependent TRPL supports this. As found in figure 67 injection dependent TRPL shows short-decay dependence on injection for the emission centered around the primary band edge, but low energy emission did not, suggesting that carrier movement which defines the speed of the initial decay due to carrier separation along gradients in the quasi Fermi Levels is not present, and thus carriers in these states where they eventually recombine radiatively are immobile. A list of hole traps with energies less than 0.5 eV into the bandgap are listed in table 2 from [150]. As is obvious, a number of native defects, defect complexes, and defects due to impurities expected in the undoped cells that act as hole traps are possible, although it is unknown if their position within the bandgap remains the same in the CdSeTe alloy vs the binary CdTe compound in which they were measured for. If the relative positions are the same, few give perfect matches to the low energy emission observed in Figure 48. It is likely that a number of these exist, and all contribute, as the low energy emission is found in a broad peak.

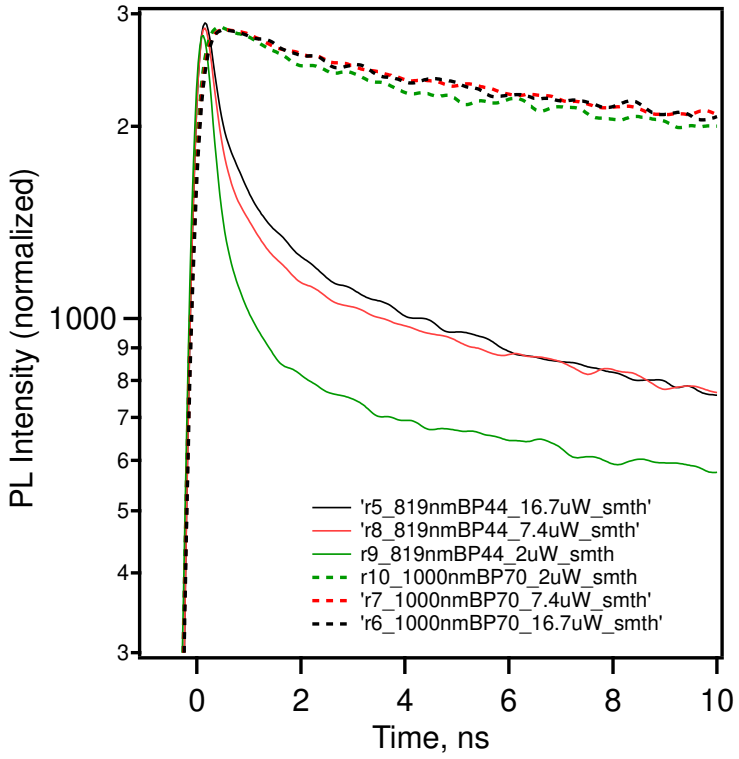

Figure 67: TRPL early time decays of band to band (solid) and sub-bandgap (dotted) emission. Measured by Darius Kuciauskas.

The implication is that there are losses to selectivity by the reduction of conductivity to holes approaching the hole contact through the bulk material. Such losses to selectivity would not be dramatically improved by a hetero-contact alone. In order to overcome such losses, addressing the causes of the loss of conductivity are a good first order of business, and otherwise increasing the carrier concentration will help in any case and reduction of absorber thickness will reduce the required distance the carriers need to travel to be extracted. Such improvements are modelled in SCAPS and the simulated JV results are found in figure 68, which demonstrate that thinner cells perform better and higher carrier concentrations in the absorber separately can also produce an improvement, although there is an optimum. It would be easy to attribute the improvement by increased carrier concentration to an increased electric field magnitude, however, the hole

extraction would still require traversal of the bulk with low hole mobility – the driving force being further on the side of diffusion since the stronger field would also be associated with a narrower depletion width and thus leave the majority of the bulk quasi-neutral. Instead, hole transport through the bulk is assisted by the larger conductivity afforded by orders of magnitude larger carrier concentration. Additionally, there is a clear improvement in the cell's behavior with use of a more ideal hole contact, showing that just addressing bulk conductivity issues is not sufficient to produce high performing cells. In this case the more ideal hole contact is modelled as ZnTe with a $1x10^{18}$ cm^{-3} carrier concentration and a very passive interface with the CdSeTe of S = 10 cm/s and Te with the same interface recombination velocity and bulk properties was used as a rear layer, and this ideal contact is required to improve the V_{oc} and thus attainable efficiency This effect is attributed to the CBO and large hole concentration in the modelled ideal contact reducing the electron population at the Te interface.

TABLE 2: HOLE TRAPS IN CDTE AND THEIR ENERGIES [150]

Defect level relative to the bands (eV)	Defect Identification
0.2	Unspecified
0.32	Te_{Cd} complex
0.2	Au and Ag impurities
0.23	Te Vacancies
0.35	Native defects, Te precipitates
0.2	Unspecified
0.23	Complex defect
0.3	Unspecified

0.3	Cu
0.35	Unspecified
0.42	Complex defect
0.49	V_{Cd}^{2-}
0.36	Cu
0.46	Complex defect
0.2	Complex defect
0.34	Cu
0.22	Shallow impurities
0.22	Impurities
0.38	Te vacancy
0.45	Native Defects
0.2	Cd vacancy
0.35	Unspecified
0.25	Unspecified
0.35	Cu impurities
0.43	Unspecified
0.14	Cl A center
0.16	Cl A center
0.13	$V_{Cd}Cl_{Te}$
0.02	Li, Na, P, N
0.06	$Te_i^{2-}/2Cl_{Te}^{+}$
0.11	Unspecified, V_{Cd}^{2-}/Cl_{Te}^{+}, Ag

0.12	Unspecified
0.15	Unspecified, Complex Defect, Cu
0.17	Unspecified
0.19	Complex Defect
0.06	Te_i^{2-}/Cl_{Te}^{+}, Li, Na, P, N, O
0.09	$V_{Cd}^{2-}/2Cl_{Te}^{+}$, Ag
0.06	Te_i^{2-}/Cl_{Te}^{+}
0.12	Ag, V_{Cd}^{2-}/Cl_{Te}^{+}
0.16	Unspecified
0.19	Unspecified
0.18	Unspecified
0.095	Cd vacancy, anti-site Cd_{Te}
0.115	Cd vacancy, anti-site Cd_{Te}
0.135	$V_{Cd}Cl_{Te}$
0.084	Unspecified
0.086	Unspecified
0.11	Unspecified

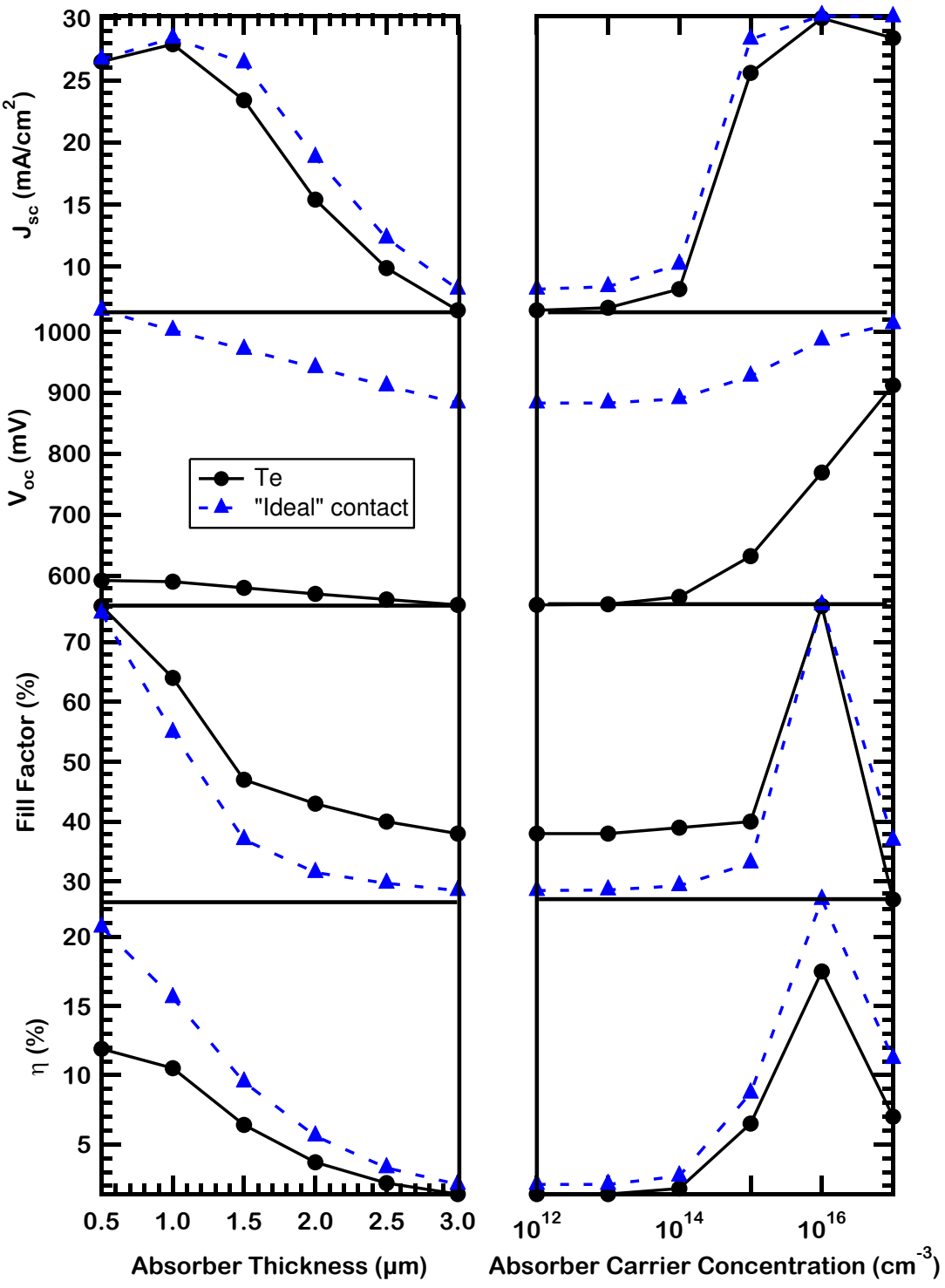

Figure 68: SCAPS modelled JV parameters of CdSeTe solar cells with 0.05 cm^2/Vs hole mobility.

CHAPTER 6: SUMMARY AND FUTURE WORK

There are a number of key results in this work that are meaningful to the future of CdTe-based solar cells and can be categorized into two main categories: findings that show a path to higher voltage and efficiency and findings that revealed challenges to the

technology which need to be overcome to realize that potential. These findings are the result of an estimated 131 experimental runs, over 495 distinct experimental structures, and an estimated 11850 small area devices.

6.1) The Potential of CdTe-based PV

A framework is presented that describes a solar cell as functioning in the result of cumulative effects of generation, recombination, and conductivity informed by both equilibrium and excess carriers and the electric fields which may be present as a result of this distribution. The use of this framework as an engineering tool has been applied to CdTe-based solar cells enabled by the development of novel characterization techniques by collaborators. First, this allowed analysis of recombination losses to the open circuit voltage and efficiency, and then examination of losses due to inadequate asymmetry in conductivity – known as selectivity. It should be noted that because selectivity involves modification of the electronic structure or absorber interfaces, which can affect the passivation, recombination losses were re-evaluated during the examination of selectivity losses.

Through this work it is demonstrated that CdTe-based photovoltaics have great unrealized potential via measurement and loss analysis of physical films rather than only virtual models which require idealized behaviors for cell phenomena. A path to overcome the present limits to

TABLE 3: KEY FINDINGS

Passivation	**Selectivity**
MgZnO interface is quite passive with CdSeTe, limiting recombination is now elsewhere in the device	MgZnO, especially deposited under appropriate conditions, provides good electron selectivity
Cu-doped absorbers are passivation limited due to Cu-defect induced recombination	CdTe provides hole selectivity in current undoped CdSeTe/CdTe scructures.
CdSeTe/CdTe devices are limited by recombination with ERE below 0.1% in functional devices and ~0.1% in well passivated structures, corresponding to lifetimes in the 100s of ns at best	Organic layers may be deposited without harming passivation, but appear not to maintain passivation after metallization
undoped CdSeTe only devices are capable of lifetimes approaching 10 microseconds, and ERE >1% in well passivated structures	Deposition of ZnTe under various conditions leads to a reduction of passivation (ERE< 50% of initial) even after native TeOx growth
undoped CdSeTe/CdTe devices are limited to ~23% by recombination in their current form, where CdSeTe only provides an upper limit of ~25% from recombination	Neither organic hole transport layers nor ZnTe produced increased selectivity relative to the current Te contact (Voc < 700 mV), as the Voc of CdSeTe only devices trail their iVoc by large margins
native TeOx forms in dry air storage and its presence as measured by XPS is correlated with increased ERE, suggesting surface passivation	Bulk conductivity issues may limit hole selectivity - SCAPS modelled devices with low hole mobility (<0.1 cm^2/Vs) reproduce measured iVoc and JV curves well.
low energy emission is reducing the detailed balance limit to open circuit voltage and efficiency in CdSeTe cells	Bulk conductivity issues may be caused by the same defects that cause low energy emission in the PL spectrum, TRPL finds they do not change with injection at early times in the decay associated with carrier movement

cells is made apparent through the removal of the Cu dopant and the use of the very long lifetime CdSeTe material in the bulk, which was found to be approaching 10 μs in well passivated cases.

In the best case measured in this work, this brings the recombination limit of the cells to approximately 25.3% with an open circuit voltage limited at around 970 mV, 70-100 mV above the current baseline structure at CSU which is similar to the structures produced throughout the community. Additionally, it was shown that the MgZnO interface is both passive and can be tuned to produce excellent selectivity.

A significant finding is that TeO_x, a layer which is found to be formed at interfaces with MgZnO and Al_2O_3 and correlated to the lifetime in literature, can form with exposure to dry air and is similarly capable of passivating the interface. This opens the possibility of a chemical passivation for interfaces if a contact layer can be applied without damaging or removing the oxide. Such passivating layers are difficult to find, and natively grown oxides are shown in c-Si technology to be an excellent pathway to highly passivated contacts.

6.2) New challenges to progressing CdTe based photovoltaics and future work

The primary discovery in this work that will need to be overcome is the presence of states within the bandgap. These states appear to be detrimental to both the upper limit to device performance by reduction of their detailed balance limiting voltages, and the performance of devices currently made with the undoped material likely due to reduction of carrier mobility as suggested by SCAPS modelling. Identification of these defects and the mitigation of their formation during deposition and post-deposition processing will be essential to realizing the full potential promised by the long lifetimes and large radiative efficiencies measured in CdSeTe only cells.

This effect will be noted first in allowing the detailed balance limiting voltage to increase by a reduction in the absorbed black body photon flux without a corresponding reduction in the excitation current under illumination. This effect will allow for greater implied voltages at comparable levels of external radiative efficiency. Second, in line with the TRPL results measured on this long wavelength emission, it will likely allow for recovery of carrier mobility. This cannot come at the expense of ERE however, as it is observed that these states are present to a far smaller extent in Cu-doped cells, but the reduction in ERE is more than sufficient to cause the implied voltage to be below that of the undoped case when accounting for the reduction in ideal voltage. This is likely due to the filling of the bandgap with additional states that change the relative probability of recombination via emission of a photon vs thermalization, and thus is more detrimental to the overall rate of recombination. That said – if the small mobility is unable to be overcome, there is a narrow pathway to improved performance via the increase of carrier concentration or thinning of the absorber. These pathways alone are not sufficient and require a good hetero-junction contact for hole selectivity in addition to overcome bulk conductivity issues.

Recommended future work is also regarding the hole contact layers, as use of a variety of schemes did not produce high efficiency devices. It is unfortunately the case that any benefits of these layers may have been masked by the detrimental effects within the bulk, and many of these layers may be worth revisiting if or when such defects are mitigated without loss in ERE. Modelling of CdSeTe absorbers shows that without a passivating and selective hole contact, the CdSeTe will not be able to produce the full potential that is promised by its long lifetimes. The parameters for such a contact are known and laid out in this document. Using these guiding

principles, it should be possible to produce very highly efficient CdTe-based PV, although further development certainly faces non-trivial challenges.

REFERENCES

[1] M. Moran, H. Shapiro, D. Boettner, and M. Bailey, Fundamentals of Engineering Thermodynamics, Wiley, 7th edition, 2010.

[2] "Solar Variability: Striking a Balance with Climate Change," NASA, Website: https://www.nasa.gov/topics/solarsystem/features/solar_variability.html#:~:text=%3E%20Larger%20image%20%22The%20fluctuations%20in,University%20of%20Colorado%20in%20Boulder 2021.

[3] "Framing and Context," IPCC, website: https://www.ipcc.ch/sr15/chapter/chapter-1/ 2021.

[4] "Energy Flow in an Ecosystem", Byju's, website: https://byjus.com/biology/energy-flow-in-ecosystem/ 2021.

[5] "Goldilocks Zone," NASA, website: https://exoplanets.nasa.gov/resources/323/goldilocks-zone/ 2021.

[6] M. G. Mlyknczak, R. P. Cageao, H. Latvakoski, D. Kratz, D. Johnson, J. Mast, "The Far-Infrared Spectroscopy of the Troposphere (FIRST) Instrument: New Technology for Measuring the Earth's Energy Balance and Climate Change," Earthzine, website: https://earthzine.org/the-far-infrared-spectroscopy-of-the-troposphere-first-instrument-new-technology-for-measuring-earths-energy-balance-and-climate-change-2013-earth-science-technology-showcase/ 2013.

[7] M. Planck, "On the Law of Distribution of Energy in the Normal Spectrum," *Annalen der Physik*, vol. 4, p553, 1901.

[8] "Temperature Change and Carbon Dioxide Change," NOAA, Website: https://www.ncdc.noaa.gov/global-warming/temperature-

change#:~:text=When%20the%20carbon%20dioxide%20concentration,goes%20down%2C%20temperature%20goes%20down. 2021.

[9] IPCC, "Summary for Policy Makers," *Contribution of Working Gorup 1 to the Sixth Assessment Report of the Intergovernmental Panel on Climate Change,* 2021.

[10] R. Lindsey, "Climate Change: Atmospheric Carbon Dioxide," Website: https://www.climate.gov/news-features/understanding-climate/climate-change-atmospheric-carbon-dioxide 2021.

[11] "Monthy Average Mauna Loa CO_2," NOAA, Website: https://gml.noaa.gov/ccgg/trends/mlo.html 2020.

[12] "Global Temperature Report for 2020" Berkely Earth, website: http://berkeleyearth.org/global-temperature-report-for-2020/ 2021.

[13] "The Effects of Climate Change," NASA, Website: https://climate.nasa.gov/effects/ 2021.

[14] R. Perez, "Richard Perez - ASRC - U Albany," Website: http://asrc.albany.edu/people/faculty/perez/

[15]"Weather and Climate Basics," NOAA, website: https://oceanservice.noaa.gov/education/pd/oceans_weather_climate/weather_and_climate_basics.html 2021.

[16] "Benefits of Hydropower," US Government Office of Energy Efficiency and Renewable Energy, Website: https://www.energy.gov/eere/water/benefits-hydropower#:~:text=Because%20hydropower%20plants%20can%20generate,%2C%20irrigation%2C%20and%20water%20supply. 2021.

[17] “Hydropower Resource Assessment and Characterization,” US Government Office of Energy Efficiency and Renewable Energy: Water Power Technologies Office, website: https://www.energy.gov/eere/water/hydropower-resource-assessment-and-characterization 2021.

[18] “Environmental Impacts of Dams,” International Rivers, Website: https://archive.internationalrivers.org/environmental-impacts-of-dams 2021.

[19] “Electricity Explained: Use of Electricity” US Energy Information Administration, website: https://www.eia.gov/energyexplained/electricity/use-of-electricity.php#:~:text=Total%20U.S.%20electricity%20consumption%20in,and%20used%20by%20the%20consumer. 2021.

[20] “Radioactive Waste Management,” World Nuclear Association, website: https://world-nuclear.org/information-library/nuclear-fuel-cycle/nuclear-wastes/radioactive-waste-management.aspx 2021.

[21] “How much Waste to Nuclear Reactors Produce per kWh?” https://www.quora.com/How-much-waste-do-nuclear-reactors-produce-per-kilowatt-hour 2021.

[22] “Fossil,” US Department of Energy, website: https://www.energy.gov/science-innovation/energy-sources/fossil 2021.

[23] C. Honsberg and S. Bowden, “Properties of Sunlight,” PV Education, website: https://www.pveducation.org/pvcdrom/properties-of-sunlight/ 2021.

[24] D. Guenther, “Age of the Sun,” *Astrophysical Journal*¸ vol 339, p. 1156-1159, 1989.

[25] I. Juliana-Sackmann et al., “Our Sun: III. Present and Future,” *Astrophysical Journal,* vol 418, p. 457-468, 1993.

[26] M. Green, “Solar Cells: Operating Principles, Technology, and System Applications,” Prentice-Hall, 1982.

[27] P. Wurfel and U. Wurfel, “Physics of Solar Cells,” *Wiley-VCH,* 3rd edition, 2016.

[28] Cecilia Payne-Gaposchkin, “Stellar Atmospheres: A contribution to the observational study of high temperatures in the reversing layers of stars,” Thesis, University of Michigan, 1925.

[29] Andrew A. Lacis, James E. Hansen, “A Parameterization for the Absorption of Solar Radiation in the Earth’s Atmosphere,” *Journal of the Atmospheric Sciences*, vol 31, p. 118, 1973.

[30] “Reference Air Mass 1.5 Spectra” National Renewable Energy Laboratory, https://www.nrel.gov/grid/solar-resource/spectra-am1.5.html

[31] P. Wurfel, “The Chemical Potential of Radiation,” *J. Physics C: Solid State Physics*, vol. 15, 1982.

[32] J. Tauc, “Optical Properties and Electrical Structure of Amorphous Ge and Si,” *Materials Research Bulletin,* vol 3, 1968.

[33] N. Bohr and P. Copenhagen, “On the Constitution of Atoms and Molecules,” *Philosophical Magazine*, Vol. 26, 1913.

[34] “Silicon Crystal Structure” Website: http://hyperphysics.phy-astr.gsu.edu/hbase/Solids/sili2.html 2021.

[35] “CdTe,” Materials Project, website: https://materialsproject.org/materials/mp-406/ 2021.

[36] S. Kayali, “GaAs Material Properties,” website: chrome-extension://efaidnbmnnnibpcajpcglclefindmkaj/viewer.html?pdfurl=https%3A%2F%2Fparts.jpl.nasa.gov%2Fmmic%2F3-I.PDF&chunk=true 2021.

[37] C. Honsberg and S. Bowden, "$CuInSe_2$," PV0Education.org Website: https://www.pveducation.org/pvcdrom/materials/cuinse2 2021.

[38] "Band Theory Of Solids" Website: *https://www.examfear.com/notes/Class-12/Physics/Semiconductor-Electronics/1909/Band-theory-of-solids.htm 2022.*

[39] "CdTe (Zinc-Blende) DFT Study" Website: https://www.bragitoff.com/2017/12/cdte-zinc-blende-dft-study/ 2022.

[40] Thomas P. Weiss, Benjamin Bissig, Thomas Feurer, Romain Carron, Stephan Beucheler, Ayodhya N. Tiwari, "Bulk and Surface Recombination Properties in Thin Film Semiconductors with Different Surface Treatments from Time-Resolved Photoluminescence Measurements," *Scientific Reports,* 2019.

[41] Fermi, E. Zur Quantelung des idealen einatomigen Gases. *Z. Physik* **36,** 902–912 (1926).

[42] P. Dirac, "On the Theory of Quantum Mechanics," Proceedings of the Royal Society A, 1926.

[43] "Boltzmann Approximation," Website: http://lampx.tugraz.at/~hadley/ss1/semiconductors/boltzmann.php 2021.

[44] U. Wurfel, A. Cuevas, "Charge Carrier Separation in Solar Cells," *IEEE J. Photovolt.* Vol. 5, 2015.

[45] A. Onno, et. Al., "Passivation, Conductivity, and Selectivity in Solar Cell Contacts: Concepts and Simulations Based on a Unified Partial-Resistances Framework," *J. Appl. Phys.* Vol. 126, 2019.

[46] C. Honsberg and S. Bowden, “Optical Properties of Silicon,” PVeducation.org, website: https://www.pveducation.org/pvcdrom/materials/optical-properties-of-silicon 2021.

[47] Kunta Yoshikawa, Wataru Yoshida, Toru Irie, Hayato Kawasaki, Katsunori Konishi, Hirotaka Ishibashi, Tsuyoshi Asatani, Daisuke Adachi, Masanori Kanematsu, Hisashi Uzu, Kenji Yamamoto, “Exceeding conversion efficiency of 26% by heterojunction interdititated back contact solar cell with think film Si technology,” Solar Energy Materials and Solar Cells, Vol. 173, p. 37-42, 2017.

[48] W. Shockley and H. Queisser, “Detailed Balance limit of efficiency of p-n junction solar cells,” *Journal of Applied Physics*, 1961.

[49] Sven Rhule, “Tabluated values of the Shockley-Queisser limit for single junction solar cells,” *Solar Energy*, vol. 130, 2016.

[50] Jean-Francois Guillemoles, Thomas Kirchartz, David Cahen, Uwe Rau, “Guide to the perplexed to the Shockley-Queisser Model for Solar Cells,” *Nature Photonics,* vol 13, p. 501-508, 2019.

[51] A. Onno et. Al., “Calculation of the Thermodynamic Voltage Limit of CdSeTe Solar Cells,” *47th IEEE Photovolt. Specialist Conference*, 2020.

[52] A. Shah et. Al. “Understanding the Role of CdTe in Polycrystalline $CdSe_xTe_{1-x}$/CdTe-graded Bilayer Photovoltaic Devices,” *Solar RRL*, Vol. 5, 2021.

[53] X. Zheng et. Al., “Roles of Bandgrading, Lifetime, Band Alignment, and Carrier Concentration in High-Efficiency CdSeTe Solar Cells,” *J. Appl. Phys.,* Vol.. 128, 2020.

[54] Arturo Morales-Acevedo, “A Simple Model of Graded Band-gap $CuInGaSe_2$ Solar Cells,” *Energy Procedia,* 2010.

[55] E. T. Roe et al., “Exchange Current Density Model for the Contact Determined Current-Voltage Behavior of Solar Cells,” *J. Appl. Phys.,* Vol. 125, 2019.

[56] “Cadmium Telluride,” US Government Office of Energy Efficiency and Renewable Energy, website: https://www.energy.gov/eere/solar/cadmium-telluride 2021.

[57] Drew E. Swanson, James R. Sites, and Walajabad S. Sampath, ”Co-Sublimation of $CdSe_xTe_{1-x}$ layers for CdTe Solar Cells,” *Solar Energy Materials and Solar Cells*, 2016.

[58] L. Hannachi and N. Bouarissa, “Electronic structure and Optical Properties of $CdSe_xTe_{1-x}$ mixed crystals,” *Superlattices and Microstructures,* Vol. 44, 2008.

[59] Sadao Adachi, Toshifumi Kimura and Norihiro Suzuki, “Optical Properties of CdTe: Experiment and Modelling,” *Journal of Applied Physics*, Vol. 74, 1993.

[60] A. Abbas et al., “Cadium Chloride Assisted Re-Crystallization of CdTe: The Effect of Annealing Over-Treatment,” *IEEE 40th Photovoltaic Specialists Conference,* 2014.

[61] P. Hatton et al., “Chlorine Activated Stacking Fault Removal Mechanism in Thin Film CdTe Solar Cells: The Missing Piece,” *Nature Communications,* Vol. 12, 2021.

[62] A. Abbas, “The Effect of Cadmium Chloride Treatment on Close Spaced Sublimated Cadmium Telluride Thin Film Solar Cells,” *IEEE 38th Photovoltaic Specialists Conference,* 2012.

[63] A. Munshi et al., "Effect of $CdCl_2$ Passivation Treatment on Microstructure and Performance of CdSeTe/CdTe Thin-Film Photovoltaic Devices," *Sol. Energ. Mat. And Sol. Cells,* Vol. 186, 2018.

[64] Hideo Tai, Shigenori Hori, "CdTe-$CdCl_2$ and CdTe-$CdBr_2$ System Equilibrium Phase Diagram," *Jounral of the Japan Institute of Metals*, 1976.

[65] Ce Sun, Tadas Paulauskas, Faith G. Sen, Guoda Lian, Jinguo Wang, Christopher Buurma, Maria K. Y. Chan, Robert F. Klie, Moon J. Kim, "Atomic and Electric Structure of Lomer Dislocations at CdTe Bicrystal Interface," *Scientific Reports,* 2016.

[66] J. D. Major, "Grain Boundaries in CdTe Thin Film Solar Cells: a Review," *Semiconductor Science and Technology,* Vol. 31, 2016.

[67] Yu Jin, Scott T. Dunham, "The Impact of Charged Grain Boundaries on CdTe Solar Cell: EBIC Measurements Not Predictive of Device Performance," *IEEE Journal of Photovoltaics,* Vol. 7, 2017.

[68] Chen Li, Yelong Wu, Jonathan Poplawsky, Timothy J. Pennycook, Naba Paudel, Wanjian Yin, Sarah J. Haigh, Mark P. Oxley, Andrew R. Lupini, Mowafak Al-Jassim, Stephen J. Pennycook, Yanfa Yan, "Grain-Boundary-Enhanced Carrier Collection in CdTe Solar Cells," *Physical Review Letters,* 2014.

[69] J. Kephart et al., "Sputter-Deposited Oxides for Interface Passivation of CdTe Photovoltaics," *IEEE J. Photovolt.,* Vol. 8, 2018.

[70] X. Zheng et. Al., "Recombination and Bandgap Engineering in CdSeTe/CdTe Solar Cells," *APL Materials,* Vol. 7, 2019.

[71] T. Ablekim et. Al., “Exceeding 200 ns Lifetimes in Polycrystalline CdTe Solar Cells,” *Solar RRL*, Vol. 5, 2021.

[72] Faith G. Sen, Arun Mannodi-Kanakkithodi, Tadas Paulauskas, Jinglong Guo, Luhua Wang, Angus Rockett, Moon J. Kim, Robert F. Klie, Maria K. Y. Chan, “Computational Design of Passivants for CdTe Grain Boundaries,” *Solar Energy Materials and Solar Cells,* vol. 232, 2021

[73] A. Shah et. Al. “Understanding the Role of CdTe in Polycrystalline $CdSe_xTe_{1-x}$/CdTe-graded Bilayer Photovoltaic Devices,” *Solar RRL*, Vol. 5, 2021.

[74] J. Kephart et. Al., “Optimization of CdTe Thin-Film Solar Cell Efficiency Using a Sputtered, Oxygenated CdS Window Layer,” *Prog. In Photovolt.,* Vol. 23, 2015.

[75] X. Wu et al., “Interdiffusion of CdS and Zn_2SnO_4 Layers and its Application in CdS/CdTe Polycrystalline Thin-Film Solar Cells,” *J. Appl. Phys.,* Vol. 89, 2001.

[76] J. Kephart et al., “Band Alignment of Front Contact Layers for High-Efficiency CdTe Solar Cells,” *Sol. Energ, Mat. And Sol. Cells,* Vol. 157, 2016.

[77] B. B. Li et al, “Eliminating S-Kink to Maximize the Performance of MgZnO/CdTe Solar Cells,” *ACS Appl. Energ. Mater.* 2019.

[78] G. Yeung at al., “Robust Passsivation of CdSeTe Based Solar Cells Using Reactively Sputtered Magnesium Zinc Oxide,” *Sol. Energ. Mat. And Sol. Cells,* vol. 233, 2021.

[79] R. Pandey et al., Mitigation of JV Distortion in CdTe Solar Cells by Ga-doping of MgZnO emitter,” *Sol. Energ. Mater. And Sol. Cells.,* Vol. 232, 2021.

[80] J. Pan et al., “Hole Current Impedance and Electron Current Enhancement by Back-Contact Barriers in CdTe Thin-Film Solar Cells,” *J. Appl. Phys.,* Vol. 100, 2006.

[81] S. H. Demtsu and J. R. Sites, “Effect of Back-Contact Barrier on Thin-Film CdTe Solar Cells,” *Thin Solid Films,* Vol. 510, 2006.

[82] J. H. Yang et al., “Review on First Principles Study of Defect Properties of CdTe as a Solar Cell Absorber,” *Semicond. Sci. Technol.,* Vol. 31, 2016.

[83] T. Song et. Al. , ”Te Layer to Reduce the CdTe Back-Contact Barrier,” *IEEE J. Photovol.,* vol. 8, 2017.

[84] S. Du et al., “Bilayered ZnTe/$Cu_{1.4}$Te Alloy Thin Films as a Back Contact for CdTe Solar Cells,” *Solar Energy,* Vol. 185, 2019.

[85] R. Geisthardt et al., “Status and Potential of CdTe Solar Cell Efficiency,” *IEEE J. Photovolt.,* Vol. 5, 2015.

[86] M. Green et al., “Solar Cell Efficiency Tables (Version 57),” *Prog. In Photovolt.,* Vol. 29, 2021.

[87] S. Hegedus and W. Shafarman, “Thin Film Solar Cells: Device Measurements and Analysis,” *Prog. In Photovolt.: Res. And App.,* Vol. 12, 2004.

[88] J. Li et al, Theoretical Analysis of Effects of Deep Level, Back Contact, and Absorber Thickness of Capacitance-Voltage Profiling of CdTe Thin-Film Solar Cells,” *Sol. Energ. Mater. And Sol. Cells,* Vol. 100, 2012.

[89] W. Becker et al., “Fluorescence Lifetime Imaging by Time-Correlated Single-Photon Counting,” *Microscopy Research and Technique*, Vol. 63, 2004.

[90] D. Kuciauskas et al., "Optical-Fiber-Based, Time-Resolved-Photoluminescence Spectrometer for Thin-Film Absorber Characterization and Analysis of TRPL Data for CdS/CdTe Interface," *38th IEEE Photovoltaics Specialist Conference Proceedings*, 2012.

[91] T. Weiss et al., "Bulk and Surface Recombination Properties in Thin Film Semiconductors with Difference Surface Treatments from Time-Resolved Photoluminescence," *Scientific Reports*, 2019.

[92] A. Kanevce et al., "The role of drift, diffusion, and recombination in time-resolved photoluminescence of CdTe solar cells determined through numerical simulation," *Prog. In Photovolt.: Res. and App.,* Vol. 22, 2014.

[93] J. Mosley et al., "Diverse Simulations of time-resolved photoluminescence in thin- film solar cells: a $SnO_2/CdSe_yTe_{1-y}$ a case study," *J. Appl. Phys.,* Vol. 130, 2021.

[94] P. Jundt et al., "Simulating the Effect of p-n Junction Fields on TRPL Transients of Thin-Film CdTe Solar Cells," *47th IEEE Photovoltaic Specialists Conference,* 2020.

[95] M. Green, "Radiative Efficiency of State-of-the-Art Photovoltaic Cells," *Prog. In Photovolt,* vol. 20, 2012.

[96] M. Green and A. Ho-Baillie, "Pushing to the Limit: Radiative Efficiencies of Recent Mainstream and Emerging Solar Cells," *ACS Energy Lett.*, 2019.

[97] H. Park et al., "Passivation Quality Control in Poly-Si/SiO_x/c-Si Passivated Contact Solar Cells with 734 mV Implied Open Circuit Voltage," *Sol. Energ. Mater. And Sol. Cells,* vol. 189, 2019.

[98] I. Braly et al., “Hybrid Perovskite Films Approaching the Radiative Limit with Over 90% Photoluminescence Quantum Efficiency,” *Nature Photonics*, Vol. 12, 2018.

[99] W. Tress, “Perovskite Solar Cells on the Way to Their Radiative Efficiency Limit – Insights into a Success Story of High Open-Circuit Voltage and Low Recombination,” *Adv. Energ. Mater.,* Vol. 7, 2017.

[100] P. Balaji et al., “Improving Surface Passivation on Very Thin Substrates for High Efficiency Silicon Heterojunction Solar Cells,” *Sol. Energ. Mater. And Sol. Cells,* Vol. 216, 2020.

[101] M. Green, “Limits on the Open-Circuit Voltage and Efficiency of Silicon Solar Cells Imposed by Intrinsic Auger Processes,” *IEEE Transactions on Electron Devices,* Vol. 31, 1984.

[102] M. Kerr et al., “Limiting Efficiency of Crystalline Silicon Solar Cells Due to Coulomb-Enhanced Auger Recombination,” *Prog. In Photovolt.,* Vol. 11, 2003.

[103] O. Miller et al., “Strong Internal and External Luminescence as Solar Cells Approach the Shockley-Queisser Limit,” *IEEE J. Photovolt.,* Vol. 2, 2012.

[104] M. Steiner et al., “Optical Enhancement of the Open-Circuit Voltage in High Quality GaAs Solar Cells,” *J. Appl. Phys.,* Vol. 113, 2013.

[105] V. Ganapati et al., “The Voltage Boost Enabled by Luminescence Extraction in Solar Cells,” *IEEE J. Photovolt.,* Vol 6, 2016.

[106] A. Kavence et al., “The roles of carrier concentration and interface, bulk, and grain-boundary recombination for 25% efficient CdTe solar cells,” *J. Appl. Phys.* Vol. 121, 2017.

[107] J. Duenow and W. Metzger, “Back-surface recombination, electron reflectors, and paths to 28% efficiency for thin film photovoltaics: a CdTe case study,” *J. Appl. Phys.* Vol. 125, 2019.

[108] J. N. Duenow et al. “Relationship of Open-Circuit Voltage to CdTe Hole Concentration and Lifetime,” *IEEE J. Photovolt.,* Vol 6, 2016.

[109] J. Sites and J. Pan, “Strategies to increase CdTe solar-cell voltage,” *Thin Solid Films,* vol. 515, 2007.

[110] D. Kuciauskas et al., “Spectrally and time resolved photoluminescence analysis of CdS/CdTe interface in thin-film photovoltaic solar cells,” *Appl. Phys. Lett.,* vol. 102, 2013.

[111] D. Swanson et al., “Single Vacuum Chamber with Multiple Close Space Sublimation Sources to Fabricate CdTe Solar Cells,” *J. Vac. Sci. and Technol. A.*, Vol 34, 2016.

[112] T. Fiducia et. al, “Understanding the Role of Selenium in Defect Passivation for Highly Efficient Selenium-Alloyed Cadmium Telluride Solar Cells,” *Nature Energy,* vol. 4, 2019.

[113] M. Ohring, “Materials Science of Thin Films, Deposition and Structure,” second edition, 2002.

[114] D. Swanson et al., “$CdCl_2$ passivation of polycrystalline CdMgTe and CdZnTe absorbers for tandem photovoltaic cells,” *J. Appl. Phys.,* Vol. 123, 2018.

[115] C. Reich et al., “Optical Characterization of Ternary Element Loss during Co-Chloride Passivation of Polycrystalline of II-VI Wide-Bandgap Alloys,” *46th IEEE Photovoltaic Specialists Conference*, 2019.

[116] C. Reich et al., “Passivation of a $Cd_{1-x}Mg_xTe$ absorber for application in a tandem cell,” *IEEE 43rd Photovoltaic Specialists Conference*, 2016.

[117] T. Shimpi et al., “Effect of the Cadmium Chloride Treatment on RF Sputtered $Cd_{0.6}Zn_{0.4}Te$ films for application in Multi-junction Solar Cells,” *J. Vac. Sci. Technol. A*, Vol. 34, 2016.

[118] T. Shimpi et al., “CdS barrier to minimize Zn loss during $CdCl_2$ treatment of CdZnTe Absorbers,” *Solar Energy,* Vol. 173, 2018

[119] P. Kobyakov, “Development of $Cd_{1-x}Mg_xTe$ thin films for application as an electron reflector in CdS/CdTe solar cells,” Dissertation, 2014.

[120] J. Poplaysky et al., “Structural and Compositional Dependence of the $CdSe_xTe_{1-x}$ Alloy Layer Photoactivity in CdTe-Based Solar Cells,” *Nature Comm.,* vol. 7, 2016.

[121] T. Ablekim et al., “Exceeding 200 ns Lifetimes in Polycrystalline CdTe Solar Cells,” *Solar RRL,* Vol. 5, 2021.

[122] J. Rangel-Cardenas and H. Sobral, “Optical Absorption Enhancement in CdTe Thin Films by Microstructuration of the Silicon Substrate,” *Materials,* 2017.

[123] J. Yang, “Carrier providers or killers: the case of Cu Defects,” *Appl. Phys. Lett.,* vol. 111, 2017.

[124] S. H. Demtsu et al., “Cu-Related Recombination in CdS/CdTe solar cells,” *Thin Solid Films,* vol. 516, 2008.

[125] R. Watanabe et al., “Film Properties of Alumina Passivation Layer for Silicon Solar Cells Prepared by Spin-Coating Method,” *Thin Solid Films,* Vol. 590, 2015.

[126] C. Perkins et al., “Interfaces between CdTe and ALD Al_2O_3,” *IEEE J. Photovolt.,* Vol. 8, 2018.

[127] A. Nicholson, “Density Functional Theory and Green’s Function Approach to Investigate Cadmium Telluride Based Thin Film Photovoltaics,” Dissertation, Colorado State University, 2020.

[128] K. Hsiao and J. Sites, “Electron Reflector to Enhance Photovoltaic Efficiency: Application to Thin-Film CdTe Solar Cells,” *Prog. In Photovolt.: Res. And App.*, vol. 20, p. 486-489, 2012.

[129] Y. Zhao et al., “Monocrystalline CdTe Solar Cells with Open-Circuit Voltage over 1V and Efficiency over 17%,” *Nature Energy*, Vol. 1, 2016.

[130] W. Van Sark, L. Korte, and F. Roca, “Physics and Technology of Amorphous-Crystalline Heterostructure Silicon Solar Cells,” *Springer: Engineering Materials,* 2012.

[131] T. Shimpi et al., “Effect of the Cadmium Chloride Treatment on RF Sputtered $Cd_{0.6}Zn_{0.4}Te$ films for application in Multi-junction Solar Cells,” *J. Vac. Sci. Technol. A*, Vol. 34, 2016.

[132] T. Shimpi et al., “CdS barrier to minimize Zn loss during $CdCl_2$ treatment of CdZnTe Absorbers,” *Solar Energy,* Vol. 173, 2018.

[133] J. Krugener et al., “Improvement of the SRH Bulk Lifetime Upon Formation of n-type POLO Junctions for 25% Efficient Solar Cells,” *Sol. Energ. Mater. And Sol. Cells,* Vol. 173, 2017.

[134] Y. Zeng et al., “Theoretical Explanation Towards High-Efficiency Tunnel Oxide Passivated Carrier-Selective Contacts (TOPCon) Solar Cells,” *Sol. Energ.,* vol. 155, 2017.

[135] M. O. Reese, “Intrinsic Surface Passivation of CdTe,” *J. Appl. Phys.* Vol. 118, 2015.

[136] G. L. Olson and J. A. Roth, “Kinetics of Solid Phase Crystallization in Amorphous Silicon,” *Mat. Sci. Rep.* Vol. 3, 1988.

[137] A. de Calhieros Velozo, G. Lavareda, C. Nunes de Carvalho, A. Amaral, "Thermal Dehydrogenation of Amorphous Silicon Deposited on c-Si: Effect of the Substrate Temperature During Deposition," *Current Topics in Solid State Physics,* 2012.

[138] J. Hack et al., "Hole Transport Material for Passivated Back Contacts on CdTe Solar Cells," *2021 IEEE 48th Photovolt. Spec. Conf. (PVSC),* 2021.

[139] "PTAA for Perovskite Applications," Website: https://www.ossila.com/products/ptaa-perovskites 2021.

[140] "PolyTPD," Website: https://www.ossila.com/products/polytpd 2021.

[141] "Me-4PACz" Luminescence Technology Group, website: https://www.lumtec.com.tw/products-view.php?ID=8990 2020.

[142] Y. Lin et al., "18.4% Organic Solar Cells Using a High Ionization Energy Self-Assembled Monolayer as a Hole-Extraction Interlayer," *ChemSusChem,* Vol. 14, 2021.

[143] D. Rioux et al., "ZnTe: A Potential Interlayer to Form Low Resistance Back Contacts in CdS/CdTe Solar Cells," *J. Appl. Phys.,* Vol. 73, 1993.

[144] D. Kuciauskas et al., "Charge-Carrier Transport and Recombination in Heteroepitaxial CdTe," *J. Appl. Phys.,* Vol. 116, 2014.

[145] M. Amarasinghe et al., "Mechanisms for long carrier lifetime in Cd(Se)Te double heterostructures," *Appl. Phys. Let.,* vol 118, 2021.

[146] A. Onno et al., "Understanding What Limits the Voltage of Polycrystalline CdSeTe Solar Cells," *Nature Energy* 2022.

[147] “Resistivity and Hall Measurements” NIST, website: https://www.nist.gov/pml/nanoscale-device-characterization-division/popular-links/hall-effect/resistivity-and-hall 2022.

[148] H. Zare Asl and S. Mohammed Rozati, “High Quality Spray-deposited Fluorine-Doped Tin Oxide: Effect of Film Thickness on Structural, Morphological, Electrical, and Optical Properties,” *Appl. Phys. A: Mat. Sci. and Processing*, 2019.

[149] G.Rey, C. Spindler, F. Babbe, W. Rachad, S. Siebentritt, M. Nuys, R. Carius, S. Li and C. Platzer-Bjorkman, “Absorption Coefficient of a Semiconductor Thin Film from Photoluminescence,” *Phys. Rev. Appl.*, Vol 9, 2018.

[150] X. Matthew, “Photo-induced Current Transient Spectroscopic Study of the Traps in CdTe,” *Sol. Ener. Mat. And Sol. Cells*, Vol 76, 2003.

[151] J. Guo, A. Mnnodi-Kanakkithodi, F. G. Sen, E. Schwenker, E. S. Barnard, A. Munshi, W. Sampath, M. K. Y. Chan, and R. F. Klie, “Effect of Selenium and Chlorine So-Passivation in Polycrystalline CdSeTe Devices,” *Appl. Phys. Lett.* Vol. 115, 2019.

[152] J. Guo, F. G., Sen, L. Wang, S. Nam, M. Kim, Y. Chan, R. F. Klie, “Atomic Resolution Study of Grain Boundaries in CdTe using Scanning Transmission Electron Microscopy,” *Microscopy and Analysis Supplement S1: Proceedings of Microscopy and Analysis 2018*, 2018.

[153] F. G. Sen, C. Buurma, T. Paulauskas, C. Sun, M. Kim, S. Sivananthan, R. F. Klie, M. K. Y., Chan, “Atomistic Simulations of Grain Boundaries in CdTe,” *IEEE 42nd Photovoltaic Specialists Conference,* 2015.

[154] F. G. Sen, A. M. Mannodi-Kanakkithodi, T. Paulauskas, C. Sun, J. Guo, L. Wang, J. Wands, A. Rockett, M. J. Kim, R. F. Klie, M. K. Y. Chan, “Efficient CdTe Photovoltaics by Co-Passivating Grain Boundaries,” *IEEE 7th World Conference on Photovoltaic Energy Conversion,* 2018.

[155] A. Shah, A. P. Nicholson, T. A. M. Fiducia, A. Abbas, R. Pandey, J. Liu, C. Grovenor, J. M. Walls, W. S. Sampath, A. H. Munshi, "Understanding the Copassivation Effect of Cl and Se for CdTe Grain Boundaries," *ACS Appl. Mater. Interfaces,* 2021.

[156] F. G. Sen, A. Mannodi-Kanakkithodi, T. Paulauskas, J. Guo, L. Wang, A. Rockett, M. J. Kim, R. F. Klie, M. K. Y. Chang, "Computational Design of Passivants for CdTe Grain Boundaries," *Sol. Energy Mat. And Sol. Cells,* 2021.

[157] S. H. Wei, and S. B. Zhang, "First Principles Study of Doping Limits of CdTe", *Phys. State. Sol. B.* vol 299, 2002.

[158] D. P. Halliday, M. D. G. Potter, J. T. Mullins, A. W. Brinkman, "Photoluminescence Study of a Bulk Vapour Grown CdTe Crystal," *J. Crystal Growth,* vol. 220, 2000.

[159] D. Kuciauskas, P. Dippo, A. Kanevce, Z. Zhao, L. Cheng, A. Los, M. Gloeckler, W. Metzger, "The Impact of Cu on Recombination in High Voltage CdTe Solar Cells," *Appl. Phys. Lett.,* vol 107, 2015.

[160] M. H. Du, H. Takenaka, D. J. Singh, "Native Defects and Oxygen and Hydrogen-related Defect Complexes in CdTe: Density Functional Calculations," *J. Appl. Phys*, vol. 104, 2008.

PUBLICATIONS

Journal:

T. Ablekim, C. Perkins, X. Zheng, **C. Reich**, D. Swanson, E. Colegrove, J. Duenow, D. Albin, S. Nanayakkara, M. Reese, T. Shimpi, W. Sampath, W. Metzger, Tailoring MgZnO/CdSeTe Interfaces for Photovoltaics. *IEEE Journal of Photovoltaics* (2019)

D. Swanson, **C. Reich**, A. Abbas, T. Shimpi, H. Fernando, A. Ponce, J. Walls, Y. Zhang, W. Metzger, W. Sampath, Z. Holman, $CdCl_2$ Passivation of Polycrystalline CdMgTe and CdZnTe Absorbers for Tandem Photovoltaic Cells, *Journal of Applied Physics*. (2018)

Y. Samoilenko, G. Yeung, A. Munshi, A. Abbas, **C. Reich**, M. Walker, M. Reese, A. Zakutayev, J. Walls, W. Sampath, C. Wolden, Stable Magnesium Zinc Oxide by Reactive Co-Sputtering for CdTe-Based Solar Cells. *Solar Energy Materials and Solar Cells* (2020)

J. Guo, A. Sharma, A. Munshi, **C. Reich**, A. Danielson, W. Sampath, S. Swain, R. Klie, Study of Arsenic Doped CdSeTe Solar Cells using Transmission Electron Microscopy, *Microscopy and Analysis* (2020)

*Yeung, G., ***Reich, C.,** Onno, A., Bothwell, A., Danielson, A., Holman, Z., Sampath, W.S., & Walden, C. Robust passivation of CdSeTe based solar cells using reactively sputtered magnesium zinc oxide. *Solar Energy Materials and Solar Cells.* (2021) *Co-First Author Onno, A., **Reich, C.,** Li, S., Danielson, A., Weigand, W., Bothwell, A., Grover, S., Bailey, J., Xiong, G., Kuciauskas, D., Sampath, W.S., Holman, Z.C., Understanding what Limits the Voltage of Polycrystalline CdSeTe Solar Cells, *Nature Energy* (2022)

Torabi, A., Sullivan, J., **Reich, C.,** Wunch, M. A., Garcia, J. A., Beck, C., Munshi, A. H., Shimpi, T., Roberts, M., Sampath, W., Harvey, T., Quantitative Cathodoluminescence Mapping: A CdMgSeTe Thin-Film Case Study, *ACS Omega*, Accepted for Publication, (2022)

Danielson, A., **Reich, C.**, Bothwell, A., Drayton, J., Shimpi, T., Sites, J., & Sampath. W.S. A Comprehensive Material Study of CdSeTe Films Deposited with Differing Selenium Compositions. *Thin Solid Films*, (Under Review)

Danielson, A., **Reich, C.,** Munshi, A., Pandey, R., Onno, A., Weigand, W., Kuciauskas, D., Li, S., Bothwell, A., Guo, J., Murugeson, M., MCCloy, J., Klie, R., Holman, Z., & Sampath, W.S. Electro-optical Characterization of Arsenic-doped CdSeTe and CdTe Solar Cell Absorbers doped In-Situ During Close Space Sublimation, *Solar Energy Materials and Solar Cells,* (under review)

Bothwell, A., **Reich, C.**, Danielson, A., Onno, A., Holman, A., Sampath, W. S., Kuciauskas, D., Charge Carrier Lifetime Determination in Graded Absorber Solar Cells Using Time-Resolved Photoluminescence Simulations and Measurements. Under Preparation – expected submission *Solar RRL.*

Reich, C., A. Onno, A. Danielson, A. Bothwell, C. Wu, D. Kuciauskas, Z. Holman, W. Sampath, High Efficiency Un-doped CdSeTe Solar Cells Enabled by Long Lifetimes. Under Preparation.

Reich, C., Onno, A., Danielson, A., Mahaffey, M., Holman, Z., Sampath, W. S., Optical Considerations to Maximize Photovoltage in CdSeTe Solar Cells with Long Lifetimes. Under Preparation

Conference:

C. Reich, D. Swanson, T. Shimpi, J. Drayton, A. Munshi, A. Abbas, W. Sampath, Passivation of a $Cd_{1-x}Mg_xTe$ Absorber for Appplication in a Tandem Cell. *IEEE 2016 PVSC Conference Proceedings*

C. Reich, D. Swanson, A. Onno, T. Shimpi, W. Metzger, W. Sampath, Z. Holman, Alloy Loss Mitigation Through Use of Barrier Layers During $CdCl_2$ Processing of $Cd_{0.60}Zn_{0.40}Te$ and $Cd_{0.87}Mg_{0.13}Te$. *7th World Conference on Photovoltaic Energy Conversion, The joint 2018 PVSC, PVSEC and EU PVSEC Conference Proceedings*

T. Shimpi, D. Swanson, **C. Reich**, J. Kephart, A. Kindvall, R. Pandey, Z. Holman, K. Barth, W. Sampath, Co-Sublimated Polycrystalline $Cd_{1-x}Zn_xTe$ Filmes for Multi-junction Solar Cells. *7th World Conference on Photovoltaic Energy Conversion, The joint 2018 PVSC, PVSEC and EU PVSEC Conference Proceedings*

Z. Holman, A. Onno, W. Weigand, **C. Reich**, A. Danielson, A. Munshi, W. Sampath, D. Kuciauskas, Polycrystalline CdSeTe Solar Cells with Implied Open-Circuit Voltage of 965 mV. *Asia-Pacific Solar Research Conference*

Munshi, J. Kephart, **C. Reich**, D. Hemenway, T. Shimpi, A. Abbas, K. Cameron, A. Danielson, K. Barth, J. Walls, W. Sampath, Advanced Co-Sublimation Hardware for Deposition of Graded

Ternary Alloys in Thin-Film Applications. *7th World Conference on Photovoltaic Energy Conversion, The joint 2018 PVSC, PVSEC and EU PVSEC Conference Proceedings*

A. Onno, A. Danielson, **C. Reich,** A. Kindvall, W. Weigand, A. Munshi, S. Li, D. Kuciauskas, W. Sampath, Z. Holman, Calculation of the Thermodynamic Voltage Limit of CdSeTe Solar Cells. *2020 IEEE PVSC Conference Proceedings*

D. Kuciauskas, D. Albin, J. Mosley, S. Li, P. Scajev, **C. Reich**, A. Munshi, A. Danielson, W. Sampath, C. Lee, Microsecond Carrier Lifetimes in Polycrystalline CdSeTe Heterostructures and in CdSeTe Thin Film Solar Cells. *2020 IEEE PVSC Conference Proceedings*

C. Reich, A. Onno, A. Bothwell, A. Kindvall, Z. Holman, W. Sampath, Determination of Series Resistance in CdSeTe/CdTe Solar Cells by the J_{sc}-V_{oc} Method. *2020 IEEE PVSC Conference Proceedings*

A. Torabi, C. Beck, A. Munshi, **C. Reich**, W. Sampath, T. Harvey, Cathodoluminescence Measurement of High Bandgap CdTe-based Devices. *Bulletin of the American Physical Society* (2020)

C. Reich, A. Onno, W. Sampath, Z. Holman, Optical Characterizationof Ternary Element Loss During Co-Chloride Passivation of Polycrystalline II-VI Wide-Bandgap Alloys. *2019 IEEE PVSC Conference Proceedings*

Danielson, A., Munshi, A., Onno, A., Weigand, W., Kindvall, A., **Reich, C.,** Yu, Z., Shi, J., Kuciasuskas, D., Abbas, A., Walls, J., Holman, Z, & Sampath, W.S. Sputtered Aluminum Oxide and *p*+ Amorphous Silicon Back-Contact for Improved Hole Extraction in Polycrystalline $CdSe_xTe_{1-x}$ and CdTe Photovoltaics. *IEEE 2019 PVSC Conference Proceedings*

Munshi, A., Danielson, A., Swain, S., **Reich, C.,** Shimpi, T., McPherson, S., Lynn, K., Kuciauskas, D., Ferguson, A., Guo, J., Klie, R., & Sampath, W.S. Doping $CdSe_xTe_{1-x}$/CdTe Graded Absorber Films with Arsenic for Thin-Film Photovoltaics. *IEEE 2019 PVSC Conference Proceedings*

Danielson, A., **Reich, C.,** Weigand, W., & Holman, Z. $CdSe_xTe_{1-x}$/CdTe Devices with Reduced Interface Recombination Through Novel Back Contacts and Group-V Doping. *IEEE 2020 PVSC Conference Proceedings*.

Munshi, A., **Reich, C.,** Danielson, A., Pandey, R., Kuciauskas, D., Li, S., Shah, A., Swain, S., Lynn, K., Sites, J., & Sampath, W.S. Arsenic Doping of CdSeTe Device for Microsecond Recombination Life-time and High Carrier Concentration. *IEEE 2020 PVSC Conference Proceedings*

Shimpi, T., **Reich, C.,** Danielson, A., Munshi, A., Kindvall, A., Pandey, R., Barth, K., & Sampath, W.S. Influence of Process Parameters and Absorber Thickness on Efficiency of Polycrystalline CdSeTe/CdTe Thin Film Solar Cells. *IEEE 2020 PVSC Conference Proceedings*

Onno, A., Li, S., **Reich, C.,** Danielson, A., Weigand, W., Sampath, W.S., Kuciauskas, D., Holman, Z., Sub-Bandgap Features in CdSeTe Solar Cells: Parsing the Roles of Material Properties and Cell Optics, *IEEE 2021 48th Photovoltaic Specialists Conference.*

Reich, C., Yeung, G., Onno, A., Danielson, A., Holman, Z.C., Wolden, C., Sampath, W.S., Photoluminescence Study of the $Mg_xZn_{1-x}O/CdSe_yTe_{1-y}$ Interface: The Effect of Oxide Bandgap and Resulting Band Alignment, *IEEE 2021 48th Photovoltaic Specialists Conference*

Reich, C., Onno, A., Sampath, W.S., Holman, Z.C., Optical Characterization of Ternary Element Loss during Co-Chloride Passivation of Polycrystalline II-VI Wide-Bandgap Alloys, *IEEE 2019 46th Photovoltaic Specialists Conference*

Munshi, A., Kephart, J., Abbas, A., Fiducia, T., Danielson, A., **Reich, C.,** Shimpi, T., Walls, J., Sampath, W.S., Progress and Challenges in Absorber and Interface Fabrication of Polycrystalline CdTe Photovoltaics, *Material Research Society Spring Meeting* (2019)

Reich, C., Swanson, D., Shimpi, T., Abbas, A., Holman, Z., Sampath, W.S., $MgCl_2$ Passivation for 1.7 eV $Cd_{1-x}Mg_xTe$ Solar Cells, *Material Research Society Spring Meeting* (2018)

Reich, C., Onno, A., Carpenter, J., Shimpi, T., Kindvall, A., Munshi A., Metzger, W.K., Sampath, W.S., Holman, Z.C., Co-Sublimation of $Cd_xZn_{1-x}Se_yTe_{1-y}$ Alloys for Application in Tandem PV, *Material Research Society Spring Meeting* (2019)

Reich, C., Onno, A., Danielson, A., Bothwell, A., Kuciauskas, D., Holman, Z., Sampath, W.S., Assessing and Overcoming Recombination Limits on Open Circuit Voltage in CdTe-based Solar Cells, *Hands On Photovoltaic Experience* (2021)